POLITECNICO DI MILANO

Scuola di Ingegneria Industriale e dell'Informazione

Corso di Laurea Magistrale in Ingegneria Aeronautica

An optimization procedure to refine the optimal design of morphing devices

Relatore: Prof. Sergio RICCI

Correlatore: Ing. Alessandro DE GASPARI

Tesi di Laurea di:

Vittorio CAVALIERI Matr. 863275

Anno Accademico 2017 - 2018

Abstract

Morphing devices for aircraft wings represent a promising technology to improve the performances, enabling the achievement of more efficient aircraft. However the design of morphing wings is a complex problem due to the conflicting requirements that must be handled. Therefore specific procedures must be developed in order to adequately face the challenging morphing problem. Optimization analysis is the main tool that can help the designer in finding solutions that are optimal from both the aerodynamic and the structural point of view. In the present work an optimization procedure is proposed for the improvement of the optimal design of morphing devices based on the distributed compliance concept. The integration of a mathematical toolbox with a finite element solver allows to refine morphing solutions but also to adapt existing topologies to different materials and geometries. Another tool is employed to get the numerical solution closer to the manufacturing process. The new procedure is applied to the design of a morphing droop nose to be installed on a reference regional aircraft. The same steps are repeated using a superelastic material as an alternative to the aluminium alloy. The results show a significant improvement of shape quality, but only the superelastic material allows to completely satisfy stress requirements. Moreover the preliminary design of a scaled wind tunnel model aimed at operational tests is performed. All the results validate each aspect of this optimization procedure which can assist the engineer up to the definition of a virtual prototype.

Keywords: morphing, optimization procedure, compliant mechanisms, droop nose, superelastic material

Sommario

I dispositivi morphing per le ali dei velivoli rappresentano una tecnologia promettente per migliorare le prestazioni, consentendo di realizzare velivoli più efficienti. Tuttavia il progetto di ali morphing è un problema complesso a causa dei requisiti conflittuali che occorre gestire. Pertanto apposite procedure devono essere sviluppate per affrontare in maniera adeguata l'impegnativo problema del morphing. L'ottimizzazione è il principale strumento che può aiutare il progettista nel trovare soluzioni che siano ottime sia dal punto di vista aerodinamico che strutturale. In questo lavoro viene proposta una procedura di ottimizzazione per il miglioramento del progetto ottimo di dispositivi morphing basati sul'idea di flessibilità distribuita. L'integrazione di strumenti matematici con un solutore a elementi finiti permette di perfezionare soluzioni morphing ma anche di adattare topologie esistenti a materiali e geometrie diversi. Un altro strumento è utilizzato per avvicinare la soluzione numerica al processo produttivo. La nuova procedura è applicata al progetto di un droop nose morphing da installare su un velivolo regionale di riferimento. Gli stessi passi sono ripetuti usando un materiale superelastico come alternativa alla lega di alluminio. I risultati mostrano un miglioramento significativo della qualità della forma, ma solo il materiale superelastico permette di soddisfare completamente i vincoli sugli sforzi. Inoltre è stato eseguito il progetto preliminare di un modello in scala destinato a prove di funzionalità in galleria del vento. Tutti i risultati validano ogni aspetto di questa procedura di ottimizzazione che può assistere l'ingegnere fino alla definizione di prototipi virtuali.

Parole chiave: morphing, procedura di ottimizzazione, meccanismi compliant, droop nose, materiale superelastico

Ringraziamenti

Desidero ringraziare il Professor Ricci per avermi dato la possibilità di intraprendere questo lavoro di tesi e per la sua supervisione durante tutto il percorso.
Vorrei poi ringraziare Alessandro De Gaspari per il suo costante supporto, per avermi seguito con la sua esperienza e con la grande passione che mette nel suo lavoro.
Ringrazio inoltre tutti quei docenti che nel corso degli anni hanno contribuito ad accrescere la mia preparazione e le mie competenze.
Ringrazio tutta la mia famiglia, i miei genitori per il loro affetto e per avere sempre appoggiato le mie scelte di vita anche quando non potevano comprenderle a fondo, mio fratello Riccardo per il suo essere continuamente fonte di ispirazione e motivazione e per ricordarmi sempre di analizzare ogni situazione da punti di vista diversi. Ringrazio inoltre tutti gli altri parenti che mi sono stati vicini.
Ringrazio Emanuele per tutte le esperienze che abbiamo condiviso sin da quando eravamo piccoli, per riempire i miei silenzi nelle nostre conversazioni e per aiutarmi a trovare una direzione quando ne ho bisogno.
Ringrazio tutti quei colleghi universitari con cui ho trascorso le giornate di lezione, affrontato lo studio per gli esami e le stimolanti collaborazioni nei progetti grazie ai quali ho imparato divertendomi.
Ringrazio tutti gli amici che mi sono stati vicini nel corso degli anni, anche quelli con cui le strade ora si sono divise. Tutti hanno contribuito in un modo o nell'altro a farmi diventare la persona che sono e al raggiungimento dei miei traguardi.
Infine ringrazio Ornella per essermi vicina nei momenti di gioia e in quelli di difficoltà, per tutto ciò che amiamo condividere, per i suoi stimoli a ricercare sempre nuove sfide e per sognare ogni giorno insieme a me ad occhi aperti.

Milano, Dicembre 2018 V. C.

Contents

List of Figures

List of Tables

Chapter 1

Introduction

1.1 General overview of morphing aircraft

The design of conventional aircraft wings is the result of an optimization process based on a single flight condition, typically the cruise, at a given speed and altitude. Regarding the other conditions the performances of the aircraft are sub-optimal. For example, low cambered thin airfoils are suitable for high speed flight while highly cambered thick airfoils are better for low speed high angle of attack flights such as take-off and landing.This specific problem is tipically addressed with the adoption of high lift devices. If there was the possibility of changing on demand the wing shape during the mission, near-optimal performances for different conditions could be achieved. This potentiality is the idea behind the morphing concept.

Nowadays, increased awareness of environmental issues like those in the ACARE Flightpath 2050, concerning emissions and noise, in combination with growing passenger volumes determine the request for more efficient aircraft. For these reasons aircraft manufacturers have to take into account novel configurations and technologies in order to achieve substancial improvements in aircraft efficiency, in terms of both fuel consumption and acoustic emissions. Morphing aircraft can be the solution to overcome the future challenges in aviation.

Morphing is a bio-inspired concept. Looking at the wings of birds and insects it is evident their ability of adaptation depending on the required aerodynamic characteristics in a specific flight condition [39]. It can be stated that in nature mission adaptive and flight control capabilities are naturally implemented. These lessons learned push the research in the direction of trying to emulate such adaptability features, aiming at achieving

the related benefits.

Many definitions of morphing aircraft there exist. According to the NATO RTO Technical Team on Morphing Vehicles morphing is "real-time adaptation to enable multi-point optimized performance" [37]. Weisshaar [63] suggested that "morphing aircraft are multi-role aircraft that change their external shape substantially to adapt to a changing mission environment during flight".
Although morphing has been acquiring great visibility in the last years, it is far from being a recent idea. Even the Wright brothers' first biplane was provided with morphing flight control. Indeed, roll control was performed by changing the twist of the wing using cables actuated by the pilot [5]. Moreover the usual conventional aircraft are equipped with many classical examples of morphing, like slats, flaps and retractable landing gear.
According to the wing parameters involved a classification of morphing is possible: planform alteration, out-of-plane transformation and airfoil adjustment [5]. Each transformation can be due to different parameters, as shown in Figure 1.1. Wing planform morphing can concern span, sweep or chord changes. Wing out-of-plane transformation is mainly affected by twist, dihedral, and span-wise bending. Airfoil adjustment is tipically achieved via camber variation, although thickness change has also been considered. Airfoil modification by means of camber variation will be the

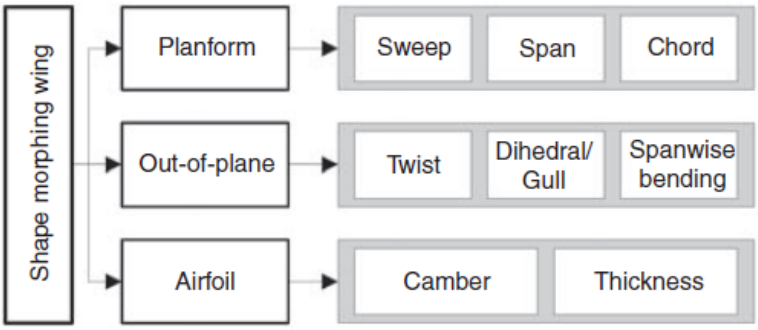

Figure 1.1: Classification of shape morphing wings

morphing strategy discussed in this thesis work. An in-depth overview of the related solutions considered over the years is reported in section 1.2.

Morphing solutions can provide many benefits. The possibility, in subsonic regime, to modify the airfoil geometry depending on the flight conditions, allows to increase the lift/drag ratio. [5] Regarding the replacement of

classical high lift devices with smart ones, the major advantage lies in the resulting aerodynamic efficiency, the low drag and also the airframe noise reduction. Other advantages of morphing concern the integration between structure and functionality, the possibility of embedding smart material actuation into the structure with a reduced mechanical complexity [39], the natural redundancy provided by distributed actuation [5].
Unfortunately the design of morphing structures is not an easy task. Specific tools are needed to assist the engineers in the many design phases encountered when dealing with this kind of structures. The reason behind this complexity lies in the morphing paradox: the same structure has to be stiff enough to withstand the external aerodynamic loads without suffering appreciable deformations and it has to be fairly flexible to change its shape into the required one [3]. In this sense many authors talk about the morphing challenge. In general lots of key disciplines may be involved in the aforementioned design process. According to [64], they are: advanced materials, smart structures, flow control, acoustics, controls, integration, multidisciplinary design optimization.
Careful attention must be devoted to skin design. Indeed, in order to properly apply the morphing wing concept, flexible or sliding aerodynamic surfaces are needed. The design of flexible skins requires trade-off studies since they are subjected to the usual conflicting requirements of morphing structures [5]. The main problem is related to the high strains in the skin. Moreover the external surface must be smooth in order to not compromise the aerodynamic efficiency. Many skin solutions have been proposed, for instance the use of a composite corrugated structure [61] and elastomeric matrix composites [41, 45]. Being part of a semi-monocoque structure, the skin plays a role in sustaining the aerodynamic loads, hence it is subjected to tensile, compression and shear stresses. This explains the need for compromise between its stiffness and its flexibility [3]. A suitable morphing skin must possess a high curvature at rupture. Moreover, the stiffness has to be maximized in the spanwise direction in order to withstand the aerodynamic loads without requiring an excessive number of kinematic ribs. The typical solution to satisfy these requirements is the adoption of extremely anisotropic skin structures [51].
In addition to the design complexity, many other issues are related to morphing technology and they must be carefully assessed before a wider application of morphing structures could take place.
First of all "large shape change concepts usually have associated design penalties such as added weight or complexity" [5]. Therefore sound estimations have to state if overall system-level benefits overcome the abovementioned drawback. Another problem concerns the unconventional nature

of morphing devices that makes their certification an open issue. This is mainly due to the typically low Technology Readiness Level (TRL) of morphing solutions. With this in mind it is clear that a transition period to bring the current technology to an high maturity level is required. In order to do that, technology programs shoud flank the research activities.

To sum up, morphing wings have the potential to revolutionize future designs of next-generation aircraft, improving significantly their performances [4, 5, 8]. However, a lot of work is needed to adequately face the challenging morphing problem and to overcome the widespread skepticism about morphing so that morphing aircraft can be seen filling the skies in the near future.

1.2 Active camber morphing

One of the most promising morphing concepts is the active camber morphing, whose aim is the variation of the airfoil camber in order to increase the aerodynamic performances, especially in take-off and landing phases. Different implementing solutions of this concept have been thought and evaluated during the years. In 1973, at the NASA Ames 14-ft transonic wind tunnel, Boeing tested an advanced variable camber wing, having some smooth and curved variable camber flaps in addition to the usual hinged leading and trailing-edge flaps [22]. The performance improvement was meaningful, however the required internal design was too complex. Later Boeing research [7, 17] focused on wing camber control for military aircraft performed through an automated control system. The first significant program was the Advanced Fighter Technology Integration (AFTI)/F-111 (Figure 1.2 [12]), promoted by NASA in collaboration with the USAF. The adopted solution for the wing modification consisted in sliding panels and flexible glass fiber panels for the trailing edge surfaces, while the leading edge surfaces were made of flexible composite panels (Figure 1.3). Camber control was provided by an internal rods and linkages arrangement driven by electro-hydraulic actuators. The flight tests assessed valuable performance increase in terms of range, efficiency and loads withstanding [56, 57].
In the field of civil transport aircraft, Szodruch and Hilbig [59, 60] demonstrated the benefits provided by a variable camber wing concept.
In the framework of the ADIF project carried out by EADS-Airbus, DaimlerChrysler F&T and DLR, Monner [40] worked at the replacement of the usual rigid ribs with a flexible solution able to guarantee at the same

Figure 1.2: F-111 Advanced Fighter Technology Integration

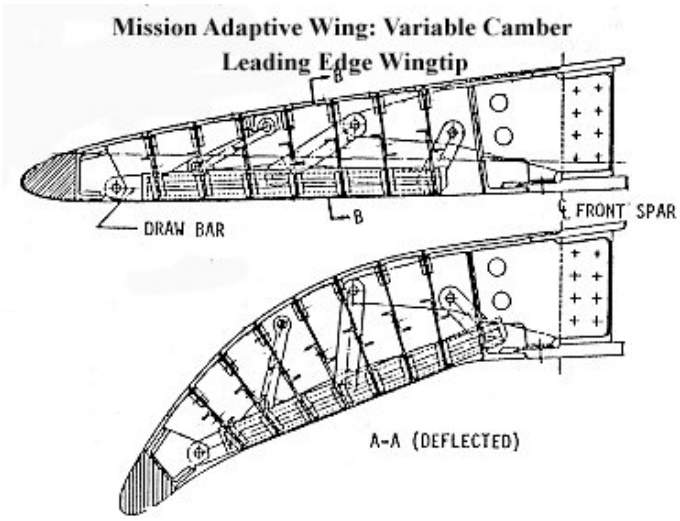

Figure 1.3: Mission Adaptive Wing: variable camber leading edge

time the required high stiffness. The proposed finger concept consisted of ribs made of several plates linked by revolute joints. The skin relative movement was allowed by including slide joints. The focus of the research was an optimization aimed at the minimization of the joint stress while achieving the desired camber. The leading idea of the developed concept is that introducing a chordwise and spanwise differential camber variation with a smooth contour and no gaps can provide many advantages from both the aerodynamic and the structural points of view. For instance higher aerodynamic efficiency with the related saving in fuel, higher operational flexibility and reduction of bending moment at the wing root can be achieved.
The subsequent work of Monner within the SmartLED project, based on a collaboration between DLR and EADS, concerned the development of a smart leading edge as an alternative to the conventional droop nose device used for the A380. The starting point of the new smart device was the Dornier Patent DE 2907912 (Figure 1.4) and an optimization process for the design of the overall system was performed. The main purpose of the device was to achieve a smooth leading surface to be deflected for high lift application. The seamless and gapless design for the high lift leading egde device aimed at the reduction of airframe noise and drag and also to promote the introduction of laminar wing technology.

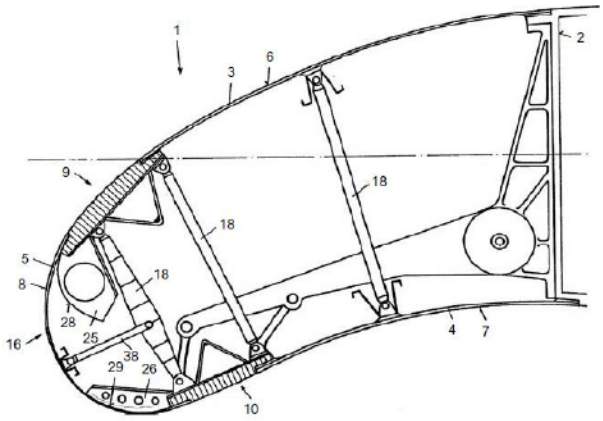

Figure 1.4: Dornier patent (1979)

Many other EU projects included the design of smart leading-edge devices. SADE project focused on the design, manufacturing, and ground testing of a seamless smart leading-edge device, which was enabler for laminar wings and offered great benefits in reducing the acoustic emissions [25, 32]. The proposed concept for the internal structure design were the eccentric

beam and a kinematic chain. Subsequently the SARISTU project dealt with the integration of typical leading-edge functions like de-icing, erosion protection, impact protection, bird strike protection and lightning strike protection [27]. The major challenge was due to the limited design space and the large curvature at the wing leading edge. In both cases, wind tunnel tests assessed the performances.
The described concepts of droop nose device are based on a flexible skin coupled to a rigid mechanism having rigid levers and kinematic joints. An alternative to the rigid kinematics approach for the realization of variable camber wings has been developed by Flexsys Inc. [30] based on compliant structures, which are discussed in section 1.3.
In this thesis an optimization procedure for the design of morphing wings is proposed following the active camber concept, but limited to leading and trailing-edge deflections, with an internal structure designed with compliant structures.

1.3 Compliant structures

"Compliant mechanism are mechanical devices that achieve motion via elastic deformation". They are designed to be flexible and this flexibility, efficiently implemented into the structure, allows the desired motion [20, 42]. A force acts as input, the structure deforms and a desired motion or shape is obtained as output. The input energy is stored as strain energy in the structure, and most of that strain energy is transformed into controlled displacements of the output points in order to obtain the requested shape [52]. This concept of distributed compliance was originally proposed by Kota [30] as an alternative to the distributed actuation one. Compliant structures are optimized to deform in such a way to produce the desired shape change. Instead of using hinges and rigid links, an efficient use of the material provides the achievement of the required shape. An example of compliant structure is shown in Figure 1.5 [29].

The major issue when dealing with the design of compliant structures is that conflicting requirements must be simultaneously satisfied: the structure must be flexible enough to accomplish the desired motion (kinematic requirement), moreover it must be stiff enough to withstand the external loads (structural requirement). In order to achieve a feasible design according to these requirements, dedicated design procedures have to be developed and specific tools like multiobjective optimization are required for them. Due to the peculiar characteristic of compliant structures, they

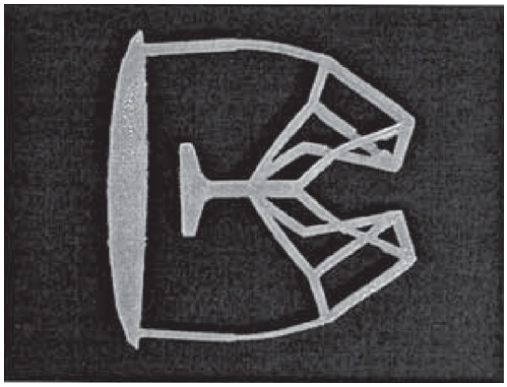

Figure 1.5: Two-dimensional compliant gripper

can be considered having the features of both structures and mechanisms: they are structures with imposed deformation, they are mechanisms without kinematic joints [36].

The great interest in compliant structures lies in the numerous advantages they can give. Indeed, unlike rigid mechanisms, they are built in a single-piece without joints, hence they don't require assembly and are less subjected to wear, noise and backlash [38]. The absence of flexural joints reduces high stress concentration. Moreover compliant structures exhibit higher fatigue life and reliability. The easier manufacture can also lead to time and cost savings [29].
In addition to the above-mentioned advantages, compliant mechanisms are suitable to be used in aircraft wings in order to realize seamless and gapless high lift devices. Indeed, replacing flaps and slats with morphing leading and trailing–edge surfaces eliminates the discontinuities. The result is that these camber variations allow the optimization of low speed performances without the drawback of conventional high lift systems.

FlexSys Inc., the company founded by Professor Sridhar Kota in 2001, exploits material elasticity to design variable geometry trailing edge control surfaces, based on the distributed compliance concept [24]. Moreover, in collaboration with the Air Force Research Laboratory and NASA, FlexSys team has successfully flight tested the developed structure on a Glufstream III aircraft. The flight tests have demonstrated the structural feasibility and robustness of the FlexFoil^{TM} Adaptive Compliant Trailing Edge (ACTE) [28]. This technology can improve aerodynamic efficiency and reduce noise during takeoffs and landings. Estimated fuel savings between 2% to 11% have encouraged further research, also related to different

variable geometry technologies, like trim tabs, leading–edges, winglets and engine inlets.

As far as the design of compliant mechanisms is concerned, according to [23], the synthesis procedure must consider different criteria: required kinematic motion, available design space, required stiffness under external loads, material properties, stress limits, buckling, weight limitations. It is evident that the design is a complex problem, and must be the result of many trade-offs between different objective functions, subjected to many constraints.
Possible objective functions are: structural weight, required energy to accomplish the shape change, aerodynamic characteristics, control effort [32]. The design variables can be classified in shape variables and structural variables. The optimization methods can be classified in topology optimization algorithms and parameter optimization (gradient-based optimization algorithms).
In this context, topology synthesis assumes a fundamental role for the definition of the overall structural configuration able to give the desired behaviour. Genetic algorithms can be adopted for the initial searching over the optimization region to determine a suitable topology, but they must be followed by an additional search, at a local level, performed through a gradient-based optimization, to determine a more accurate sizing of the mechanism in order to improve the previously found optimal solution [36]. Therefore suitable tools must be developed in order to face the challenging design of compliant structures. Among the others, attention should be paid to avoid permanent deformation or fatigue failure of the material [53].

1.4 Aims of the work

In this thesis an approach for the optimal design of morphing structures is presented. The main focus of the work is on the internal structure design by means of compliant mechanisms. The choice of the distributed compliance concept is led by the need to avoid the high stresses due to the adoption of rigid mechanisms.
The proposed procedure is general for the application to leading and trailing–edge morphing devices. However, since the criticalities concerning the leading–edge morphing solutions are higher, only application to droop nose will be shown. The main difference between leading and trailing edge is the different chord extension that is lower in the first case, hence it requires a more complex effort to achieve the desired deflection.

Many difficulties are encountered when dealing with the design of a droop nose and also compliant structures can be characterized by an high stress level. In this thesis the problem is overcome by the adoption of Nitinol as the material for the internal mechanism. Nitinol is here used in a passive way, by exploiting its superelastic behaviour instead of the shape memory effect.

The working environment for the examples of application of the procedure is the contribution of POLIMI in the framework of the EU funded Clean Sky 2 REG-IADP AG2 project [55].

Some important preliminary considerations about the selected morphing solution follow. The idea of design addressed in this thesis is based on the concept of a wing composed by a central wing-box with morphing leading and trailing edges attached to it. This choice is based on the belief that the traditional central wing-box must be left unchanged by morphing, both for strength-to-weight ratio considerations and for functionality issues, such as the need for fuel storage in the wing. As a consequence, the concept here considered is that of hybrid wings. The traditional wing-box is the same of conventional fixed-wing aircraft and also the approach for its design doesn't change. Leading and trailing edges become morphing devices, with the role of conformable and gapless control surfaces. This partially morphing solution have the potential to be worth of consideration from industries and certification bodies and can represent the intermediate step in the transition from conventional aircraft wings to more futuristic fully-morphing wings.
Another issue to be considered is the impact of aeroelasticity on the functionality of morphing devices, in terms of deployment capability and accuracy of the target deformed shape. Concerning this point, the idea is that a compliant solution instead of a rigid one has the advantage to introduce a degree of freedom into the structure. This should avoid further stress concentrations and also the appearance of unwanted coupling effects between the morphing device and the rest of the structure. Indeed, a problem encountered when using rigid kinematics is that the resulting structure is overdetermined. This may represent a problem, in particular in these times of more and more flexible aircraft. Moreover no one has tested so far rigid kinematics-based mechanisms attached to a wing-box structure. Conversely, as an activity related to the design of the Clean Sky 2 droop nose, FEM simulations have virtually assessed the suitability of the coupling between wing-box and morphing devices realized with compliant mechanisms: the presence of morphing device doesn't modify the wing

deflection under loads neither the wing deflection compromises droop nose deployment.

1.4.1 Thesis outline

An overview of the chapters content is reported:

Chapter 1 has described the concept of morphing aircraft, focusing on the potential benefits but also on the intrinsic complexity. Particular attention has been given to the active camber morphing technology and its application to the design of high lift devices based on compliant structures. Finally the aims of the work have been reported.

Chapter 2 introduces the proposed procedure for the refinement of the design of morphing devices, its potentialities and the background on which it is located.

Chapter 3 describes the optimal solution that will be improved by means of the optimization procedure. Moreover it contains a review of the material superelastic behaviour that will be exploited in the applications.

Chapter 4 focuses on the new optimization tools, showing their working principles as well as the reasons that have led to their development.

Chapter 5 reports the results of the application of the procedure and analyzes the obtained improvement.

Chapter 6 is devoted to additional examples and their results.

Chapter 7 draws the conclusions of the whole thesis and outlines possible future works.

Chapter 2

Design procedure

The aim of this thesis is the development of a procedure for the optimal design of morphing wings. A schematic representation of this procedure is shown in Figure 2.1.
The general framework can be outlined in four phases:

1. An aerodynamic shape optimization with structural constraints. The objective is the definition of the optimal morphing shape according to the requirements in terms of performances. At the same time, a constraint on the strain computed as a function of curvature assures the feasibility of the skin solution from a structural point of view.

2. A multi-objective genetic algorithm optimization for the definition of the topology of the internal compliant structure. In this phase a fictitious material is used for the compliant structure.

3. A gradient-based optimization to optimize the sizing variables of the selected topology when the actual material of the compliant structure is included. The objective is the improvement of the morphing shape obtained when the mechanism is actuated, while limiting the stress inside the structure.

4. A shape optimization of the compliant mechanism to reduce local peaks of stress and finalize the design details.

At the end of the procedure, the designed solution has to be verified from both the morphing shape quality and the structural points of view. If the result is acceptable, the mechanism is ready for the manufacturing.

The background of the suggested procedure is the two-levels optimization approach proposed by De Gaspari [13], whose capabilities are expanded here developing dedicated tools. Their main potentialities are:

- the possibility of postponing the choice of the material and the geometric scaling factor, after the definition of an optimal topology;
- the versatility of the FEM simulations, in terms of material constitutive laws and modeling;
- the high-level refinement of the final solution, which brings it nearer to the step of manufacturing process.

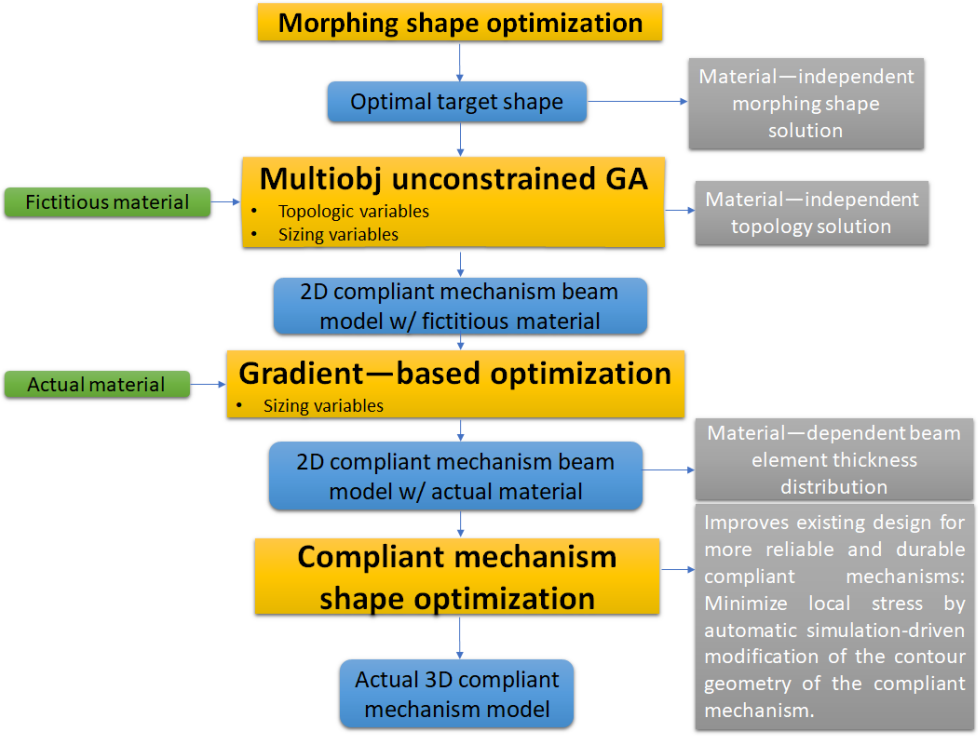

Figure 2.1: Optimization procedure for the design of morphing wings

The following sections focus on the description of the existing optimization procedure, also introducing the main differences for its use in the new approach. The detailed description of the new tools is reported in chapter 4.

The scheme of the two-levels approach for the design of compliant structure is shown in Figure 2.2.
The first level of the procedure consists in an aero–structural optimization of the morphing shape. The objective is to obtain the most efficient aerodynamic shape, but minimizing the axial and bending strains in the skin. This aspect is very relevant since the skin plays an important role in

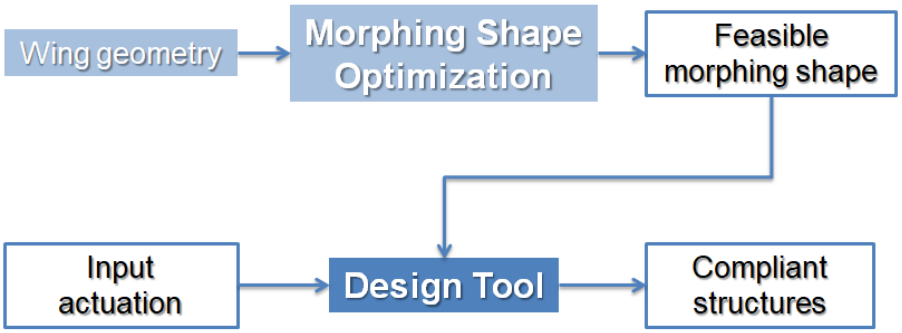

Figure 2.2: Two-levels approach

the whole morphing solution. Therefore taking into account its structural behaviour from the begininning helps in finding feasible structural solutions at the later stage.
The aerodynamic shape needs a suitable geometric representation to be described. The approach here adopted is the compact airfoil representation technique (CST), based on the method proposed by Kulfan in [31] and extended to leading and trailing edge continuous control surfaces. The advantages of this fully analytical description of the airfoil shape are the reduced number of parameters needed and the straightforward calculation of the stresses into the skin.
After the completion of the first level, the topological synthesis of the internal compliant mechanism takes place. This design is based on the Load Path Representation method [34] and aims at obtaining the best internal structural configuration able to achieve the target optimal shape previously found.

2.1 Morphing shape optimization

The morphing shape optimization is performed by means of a Knowledge-Based Engineering (KBE) framework that revolves around an object oriented code named PHORMA (Parametric sHapes for aerOdynamic and stRuctural Modelling of Aircraft) [15]. At this stage, the objective is the design of morphing shapes which are optimal from the aerodynamic point of view, under skin structural requirements. The aerodynamic optimality can concern the efficiency, in order to reduce the fuel consumption, but also the improvement of the performances over a wide range of different flight conditions. An overview of the framework is shown in Figure 2.3. It is able

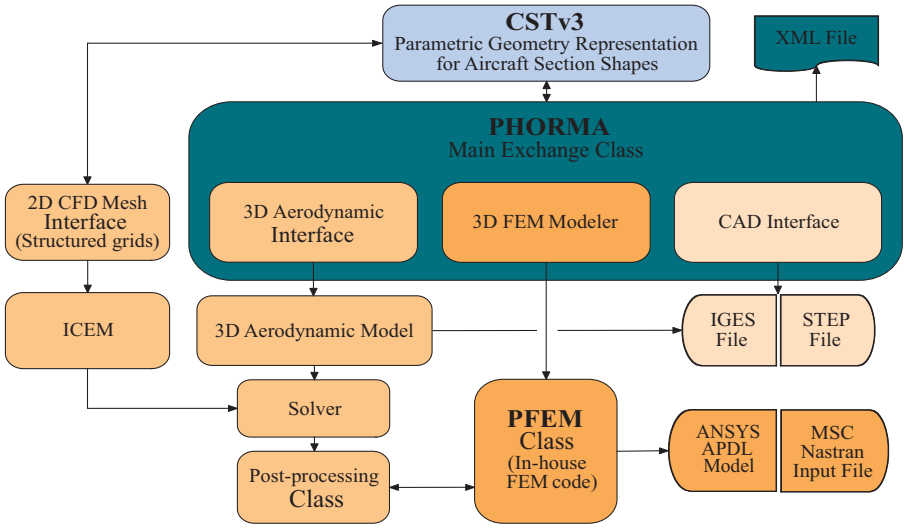

Figure 2.3: Parametric framework

to provide advanced parametric capabilities for the aircraft description. Moreover it can couple the parametric geometry representation with aerodynamic and structural solvers, enabling the computation of aerodynamic performances and the prediction of the skin structural response. Thanks to the second aspect, there is the guarantee that only feasible shapes are considered in the optimization problem; these shapes must satisfy wing–box volume constraints and morphing skin structural requirements.

2.1.1 Airfoil geometry representation

In order to describe aerodynamic shapes to be efficiently included in an optimization algorithm, it is essential to represent adequately the admissible continuous geometry changes. The adopted parameterization technique has a direct effect on the number of design variables and the accuracy of the optimal shape.
According to the morphing application, the chosen technique must allow to deform the global shape properties without, however, affecting the local regularity of the airfoil. Therefore the analytical approach is used to introduce a compact formulation that combines a baseline shape and a shape function.
The starting point of the presented technique is the analytically function transformation technique, proposed by Kulfan. However, in order to properly represent leading and trailing-edges morphing, a particular

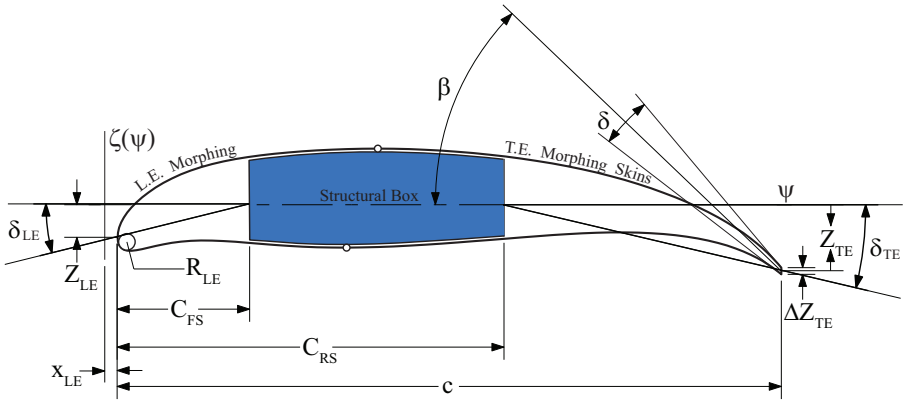

Figure 2.4: CST geometric parameters for airfoil sections

modification of the basic technique has been performed.
Bezier curves can be used to model smooth curves. The Class function/Shape function Transformation (CST) geometry representation method is an application of the generalized Bezier curve definition to represent aircraft geometries. The class function defines fundamental classes and the shape function defines unique geometric shapes within each class. The shape function is represented with a Bernstein polynomial, thus eliminating slope or curvature discontinuities.
The CST parameterization is based on merging four terms: a Shape Function, a Class Function and two additional terms related to the airfoil leading–edge and trailing–edge shapes. The general mathematical expression representing the airfoil geometry is:

$$\zeta(\psi) = C_{N2}^{N1}(\psi)\mathbf{a} \cdot \mathbf{b}_n^T(\psi) + \psi\zeta_{TE} + (1-\psi)\zeta_{LE} \tag{2.1}$$

where, $\psi = x/c$, $\zeta = z/c$ are the non–dimensional coordinates with respect to airfoil chord c, $\zeta_{TE} = Z_{TE}/c$ and $\zeta_{LE} = Z_{LE}/c$. Other significant parameters are the airfoil leading–edge nose radius R_{LE}, the trailing–edge boat–tail angle β, the thickness ΔZ_{TE} and the angular thickness δ. All these "CST parameters" are shown in Figure 2.4. Starting from these parameters, more definitions follow. The leading edge deflection and the trailing edge equivalent deflection are respectively:

$$\delta_{LE} = \arctan\left(Z_{LE}/(C_{FS} - x_{LE})\right) \tag{2.2}$$

$$\delta_{TE} = \arctan\left(Z_{TE}/(c - C_{RS})\right)$$

where C_{FS} and C_{RS} are the front and rear spar positions.

The first term of Equation 2.1 is the Class function, that affects both the leading and the trailing edge shape. Its general form is:

$$C_{N2}^{N1}(\psi) \triangleq \psi^{N1}\,(1-\psi)^{N2} \tag{2.3}$$

By varying the exponents ($N1$ and $N2$) in the class function, it is possible to obtain different basic general shapes.
The second term of Equation 2.1 is the Shape function. It is defined using a set of $(n+1)$ Bernstein polynomial components $B_i(\psi)$, of selected order n, arranged in the function array $\mathbf{b}_n(\psi)$ and scaled by the unknown extra–coefficients A_i in vector $\mathbf{a}$.
The *i–th* shape function component is defined as the product between the *i–th* Bernstein polynomial component and the *i–th* associated binomial coefficient. Each Bernstein polynomial component is multiplied by the Class function defining the systematic decomposition of the airfoil shapes into corresponding scalable *airfoil components*. Consequently, the constant coefficient A_i can be used to scale the entire airfoil function which is a smooth function that eliminates local discontinuities.
The first and last terms of vector $\mathbf{a}$ are related to the leading and trailing edge boundary conditions and are equal to the Shape function evaluated in $x/c = 0$ and $x/c = 1$. In particular:

$$\mathbf{a}(1) = \sqrt{2R_{LE}/c}, \qquad \mathbf{a}(n+1) = \tan\beta + Z_{TE}/c - Z_{LE}/c \tag{2.4}$$

The other $n-1$ terms have no effect neither on the leading–edge radius nor on the trailing–edge angle and can be used to scale the individual Bernstein components.
Thanks to the analytical nature of the CST parameterization technique it is also possible to describe the structural behavior of the skin. The calculation of the first and second order derivatives can be used to compute the length and curvature of airfoil upper and lower surfaces:

$$\mathrm{L}(x) = \int_0^c \sqrt{1 + \left(\frac{d\zeta}{dx}\right)^2}\, dx \tag{2.5}$$

$$\kappa(x) = \frac{\zeta''(x)}{\left(1+\zeta'^2\right)^{3/2}}, \tag{2.6}$$

These geometrical quantities allow the computation of the stress (or strain) inside the skin. This stress is the sum of two contributes: the axial stress σ_{axial} and the bending stress σ_{bend}. The former is related to the variation

of length between the undeformed shape and final morphing shape. The bending stress is related to the curvature difference between the initial and the final airfoil shape:

$$\Delta\kappa(l) = \kappa_m\left(x(l)\right) - \kappa_u\left(x(l)\right) \tag{2.7}$$

where κ_u and κ_m are the curvature functions of the undeformed and morphing airfoil, $x(l)$ is the inverse of normalized arc length function $nal(x)$. According to Euler–Bernoulli beam theory, the maximum bending stress along the skin can be computed from the curvature difference function as:

$$\sigma_{bend} = \frac{Et}{2}\,\Delta\kappa(l) \tag{2.8}$$

where E is the Young's Modulus and t is the minimum skin thickness to be assigned to the morphing skin.
The stress in the skin calculated in this way can be used as constraint in the morphing shape optimization procedure.

A parametric identification is required to provide a CST identification of preexisting CAD models. The detailed mathematical description of this identification process is beyond the scope of this discussion on CST and it can be found in [15]. The identified models are then ready to be modified in order to introduce the morphing shape changes.

2.1.2 Optimization problem definition

This first level shape optimization aims at defining the best airfoil change that satisfies specific mission requirements. As already mentioned, in order to take into account the structural limitations of the skin, the optimization must obtain the best morphing shape that is optimal according to the aerodynamic performances, but at the same time assuring limited deformation energy of the skin itself and limited actuation power required for the shape change. Moreover, a Constant Cross–section Length (CCL) strategy is adopted in order to limit the axial stresses in the skin. It consists in minimizing the maximum axial stress along the skin in the morphing configuration.
The aerodynamic models of the physically acceptable shapes are generated by means of parametric meshing capabilities. The wing structural box constraint is implemented in an implicit way into the the shape optimization.
A possible formulation of the optimization problem is:

$$\begin{aligned} \text{Minimize} \quad & C_d \\ \text{such that} \quad & \Delta\psi_{wing-box} \equiv (C_{FS},\, C_{RS}) \\ & C_l \geq \bar{C}_l \\ & \mid \Delta L_{LE,skin} \mid = 0 \\ & \max\left(\Delta\kappa(x)\right) \leq \Delta\bar{\kappa} \end{aligned} \tag{2.9}$$

The objective function to be minimized is the drag coefficient C_d. The first constraint is the wing box constraint, which imposes that the wing region between the front spar position C_{FS} and the rear spar position C_{RS} isn't affected by morphing changes. The second constraint assures that the lift coeffient C_l is at least equal to $\bar{C}_l$. The third constraint doesn't allow any length variation of the morphing leading edge skin. The fourth constraint limits the maximum curvature variation $\Delta\kappa(x)$ to a value $\Delta\bar{\kappa}$. The optimization variables are the geometric parameters used in the CST formulation to affect the camber morphing. A Genetic algorithm is used to solve the optimization problem.
It is important to note that this optimization problem does not depend on the material of the compliant mechanism that will be designed in the next level.

What described until now represents an older version of the first level optimization. After that the geometric representation tools have been updated and today the state of the art consists in a tool able to directly deals with three dimensional aerodynamic shapes. In other words, instead of focusing on few airfoils and then interpolating between them in order to obtain the 3D solution, it is possible to generate three dimensional parametric shapes and use them in the optimization loop.
This upgrade represents a noteworthy improvement at this level of the process, but doesn't change the general meaning of the design procedure.

2.2 Multi-objective Genetic Algorithm

The second level optimization makes use of the target aerodynamic shape that is the result of the morphing shape optimization problem described in section 2.1. Given this shape, the current step aims at designing a suitable internal compliant structure able to match once actuated the desired morphing shape according to PHORMA.
The already described CST tool is useful also in the second level. It provides the target curve, analytically imposes the structure internal

point boundaries for the the optimization constraints, allows to find the optimal position of the active output points and to compute the external aerodynamic loads.
The main tool used in the second level is SPHERA (Synthesis of comPliant mecHanisms for EngineeRing Applications) [13, 14]. Its purpose is the design of morphing airfoils, taking into account the presence of the skin, a structure and a mechanism, in such a way to satisfy the conflicting requirements of deformability, load–carrying capability and low weight. As already said, the approach here adopted for the synthesis of compliant mechanisms is based on the distributed compliance concept.

2.2.1 Load path representation

SPHERA is based on the load path representation. It is a design parameterization of the stiffness tensor that makes use of load paths in order to represent different structural topologies, cross–sectional beam areas and the position of the points of interest for the shape problem. The presented approach is based on beam element models and it is able to provide solutions according to the distributed compliance concept. The approach is intended for the synthesis of Single–Input Single–Output (SISO) compliant mechanisms [19, 54] but it can be also used for the design of Single–Input Multi–Output (SIMO) compliant mechanisms for the structural shape control [35].
Load path representation application to morphing airfoils is suitable to optimize a compliant structure and make it able to transfer the input actuator force to a set of active output points along the boundary in order to obtain a target shape.
Load paths are physical connection sequences between points. The three types of points are input actuation, structure constraints and active output points. The possible load paths connect respectively load input and active output points (InOut paths), load input and constraint points (InSpc paths), and constraint points and active output points (SpcOut paths). Another type of characteristic points is that of the structure internal points at the intermediate connections between the load paths.
An example of load path representation is shown in Figure 2.5
In the application of the load path representation to shape control problems, the design variables are: path sequence (Seq), binary path existence variable (Top), internal point coordinates (InterLoc) and cross sectional load path

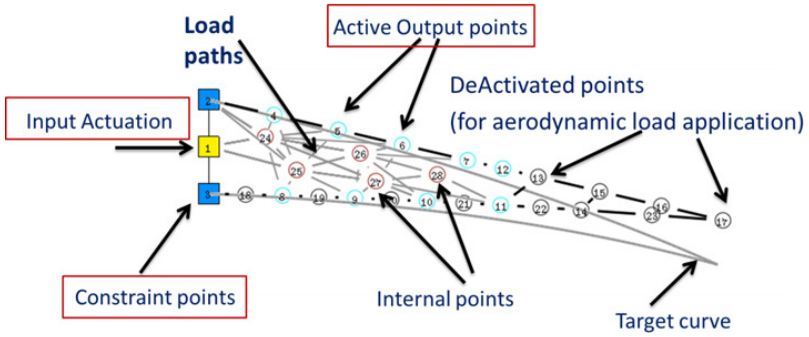

Figure 2.5: A demonstrative connected load path representation of a SIMO compliant mechanism

sizes (Dim), load path output destinations (Dest) and structure boundary sizes (hBound).
Some points placed along the airfoil skin contour, more or equal than those used as active output points, are used to minimize the Least Square Error (LSE) between the deformed shape and the target shape obtained as result of the morphing shape optimization level. The minimization problem is subjected to many constraints: size constraints for the load path beam elements and structure boundary elements, internal point boundaries, two global connectivity equations, stress and buckling constraints and the elastic equilibrium equation. For the analysis of the actuated mechanism, each set of load path is transformed into a sequence of Finite Volume Beams [21].
Non–linear analyses are performed to correctly describe the behavior of mechanisms subject to large displacements; the equilibrium equation is represented by the residual convergence. Moreover, the structural solver includes modal, buckling, static linear, non–linear analysis modules.

2.2.2 Genetic Algorithms based on Multi-objective approach

The deformation of the airfoil skin depends on the topology of the compliant mechanism and also on its dimensions, therefore topology and size design must be simultaneously faced. SPHERA includes a customized Genetic Optimizer where the individuals of the population are composed by mixed–type design variables. The generation of each new population is produced by selection, crossover and mutation strategies, that combine the topology synthesis and the sizing optimization into the same process.

A compliant mechanism must be able to satisfy the kinematic and structural requirements, for all the load conditions corresponding to the considered flight conditions. This is a multi–objective design problem that can be efficiently incorporated into the genetic algorithm.

When multiple objectives are considered, the optimal solution is a trade–off between the different objectives.

The selected approach to solve the multi–objective optimazion problem is the so called Elitist Non-Dominated Sorting Genetic Algorithm (NSGA–II) [16].

2.2.3 Optimization Problem

The design of morphing airfoil consists in the definition of a structure able to transfer the deformation work from an input point (actuator) to the output points placed along the skins. This is the kinematic requirement, but also structural requirements are needed, in order to assure the fulfillment of the undeformed or the deformed shape under the external loads. In general, more than one load conditions corresponding to the undeformed shape and more than one target shapes can be considered.

When SPHERA is applied to the design of morphing leading or trailing edge wing section, two main objectives are considered:

- the minimization of the SE (Strain Energy) in a problem where the input point is fixed and the external aerodynamic loads are those of the structural requirement;

- the minimization of the LSE (Least Square Error) between the deformed and the target shape, under the input actuation load and the external aerodynamic loads corresponding to the kinematic requirement.

The definition of the multi–objective optimization problem consists in two sub–problems. The former is the kinematic design:

Minimize:

$$LSE = \frac{1}{n}\sum_{i=1}^{n}\sqrt{(x_{d,i}-x_{m,i})^2+(y_{d,i}-y_{m,i})^2+(z_{d,i}-z_{m,i})^2} \tag{2.10}$$

such that:

$$Dim_{min} \leq Dim_{i,j} \leq Dim_{max}$$
$$hBound_{min} \leq hBound_k \leq hBound_{max}$$
$$(x_{low},\, y_{low},\, z_{low}) \leq interCoord \leq (x_{up},\, y_{up},\, z_{up})$$
$$\sum_{i \in InOut} Top_i \geq 1$$
$$\sum_{i \in InSpc \cup pathSpcOut} Top_i \geq 1$$
$$\sigma \leq \sigma_{allowable}$$
$$\mathbf{r} = \mathbf{0}$$

where n is the number of control points along the boundary, $(x_d,\, y_d,\, z_d)$ are the grid positions in the deformed condition computed by the structural analysis and $(x_m,\, y_m,\, z_m)$ the corresponding target shape points. $interCoord$ are the coordinates of the internal points. $Dim_{i,j}$ is the cross sectional thickness of the j–th beam of the i–th load path. $hBound_k$ is the thickness of the k–th structure boundary. The optimization problem is subjected to size constraints for the load path beam elements (Dim_{min} and Dim_{max}) and the structure boundary elements ($hBound_{min}$ and $hBound_{max}$) and to constraints for the internal point boundaries ($(x_{low},\, y_{low},\, z_{low})$ and $(x_{up},\, y_{up},\, z_{up})$). Moreover, constraints on the Top_i variables, assure the connectivity of the structural topology. Finally there are a stress limitation and the imposition of the elastic equilibrium equation.

The other problem is the structural design:

$$\min_{\mathbf{u},\, E_e} SE = \min_{\mathbf{u},\, E_e} \mathbf{u}_{out}^T \mathbf{K}(E_e)\mathbf{u}_{out} \tag{2.11}$$

such that:

$$\mathbf{K}(E_e)\mathbf{u}_{out} = -\mathbf{f}_{out}, \quad with\ SPC_{in}$$
$$E_e \in \mathrm{E}_{admissible}$$

where SE is the strain energy, $\mathbf{u}_{out}$ is the nodal output displacement vector due to the force $-\mathbf{f}_{out}$ and $\mathbf{K}$ is the symmetric global stiffness matrix.

It is important to underline that, according to the idea of the new optimization procedure, the stress constraint is optional: it can be included in the constraints during the optimization or it can be considered at the end of the optimization by descarding from the Pareto front all the solutions subjected to a maximum stress higher than a chosen threshold. Anyway, the presence of a stress limitation doesn't invalidate the material-independent character which the new procedure assigns to the solution of the genetic optimization. Indeed, the demand of a stress restriction can be thought as the desire to avoid stress peaks and to uniformly distribute the stress inside the entire structure, whatever is the adopted material. Later, the actual admissible stress value will represent an effective constraint when the actual material will be considered.

2.3 Solution refinement

Starting from the results of the two-level optimization procedure, an improvement of the solution is aimed by implementing two further optimization analyses, with an increasing level of detail. The description of the refinement tools is the subject of chapter 4. Here only one matter is discussed, a clarification about the term *refinement*. The developed procedure is born with the purpose of further enhancing the optimal design of morphing devices previously performed by means of the existing two-levels procedure. However it is capable of doing more than that and the application examples prove this. Indeed, although the design phase has been carried out using the usual isotropic aluminium material, after the definition of the topology the adoption of a different material is possible and this material can reveal itself even more promising. For these reasons in the general framework the material of the first two phases has been defined as fictitious. This fact opens a huge range of opportunities in the applications. Moreover, as it will be shown, the adaptation of the existing topology to a different scale is also possible successfully. This brief foreword suggests the interpretation for the whole work.

Chapter 3

Droop nose

3.1 Reference wing

In the framework of EU funded Clean Sky 2 REG-IADP AG2 project, some morphing concepts have been being developed. One of this concerns the conceptual design of a morphing Leading Edge able to guarantee high lift requirements as well as Natural Laminar Wing (NLF) flow.
The first design phase has consisted in the definition of the optimal shape able to satisfy the aerodynamic requirements. Then a possible structural solution for the skin, the internal compliant structure and an adequate actuation mechanism have been assessed. Thanks to the experience acquired participating into SARISTU and NOVEMOR projects, the work carried out inside CS2-AG2 consortium is trying to adopt the concept of a fully compliant structure for the morphing leading–edge structure [50].
The reference aircraft addressed in the project is a 90 pax, twin prop Regional Aircraft. The reference wing is the NLF optimized wing shown in Figure 3.1, whose aerodynamic design has been provided by ONERA. According to the initial requirements on the layout, the morphing Leading Edge is composed by an inboard and an outboard region, as depicted in Figure 3.2. The adoption of a morphing leading edge is forced by the need to delay the stall of the wing during take-off and landing. In order to achieve this goal a seamless and smoothed surface is required so that no anticipated loss of laminarity occurs. This explains the reason why classical slat can't be employed.

The performance requirements consists in the enhacement of maximum lift coefficient C_{Lmax}: 2.4% in take-off condition and 1.7% in landing condition. These values must be obtained thanks to the considered leading edge

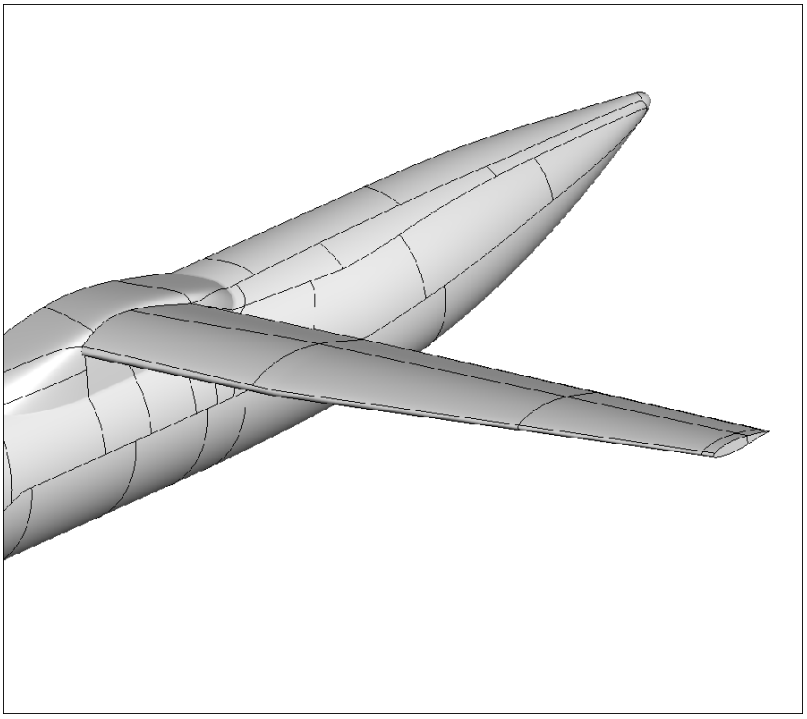

Figure 3.1: NLF optimized wing

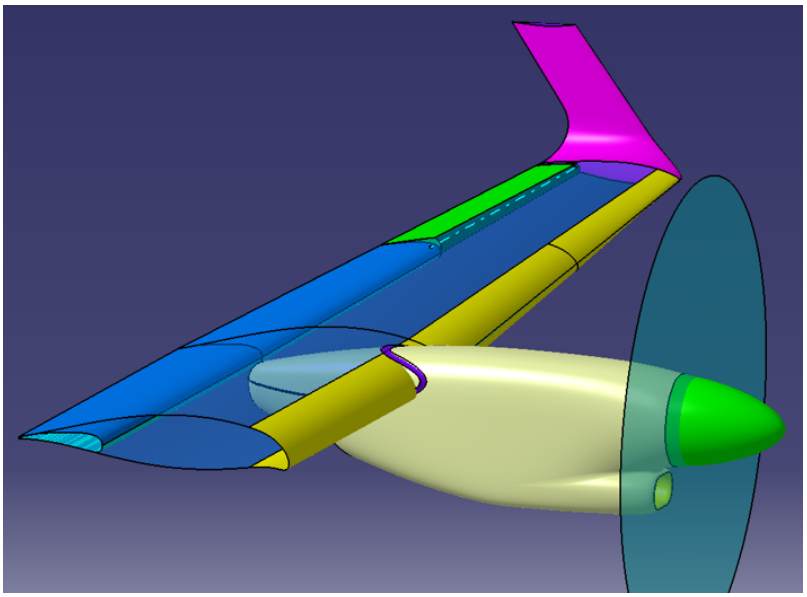

Figure 3.2: Reference Aircraft with morphing leading edge

morphing in cooperation with multi-functional flap designed by University of Naples.
The work already done by Polimi has achieved a structural solution for the leading edge compliant structure. The obtained results represents the starting point for an example of application of the tools specifically developed in this thesis work. The major aim of this application is the validation of the optimization procedure, as well as the demonstration of its potential benefits in terms of solution improvement. Further applications will also show its versatility.

3.2 Topological synthesis results

The morphing shape obtained with PHORMA is used as target shape for the topological synthesis of the compliant ribs. This synthesis is performed by means of the multi-objective genetic algorithm optimization. In principle the most critical flight conditions should be concurrently considered for the design of the internal structure. However, in the preliminary design, only three objective functions are considered:

1. Structural requirement: minimizing the Strain Energy (SE) to preserve NLF wing shape. The morphing mechanism is kept fixed under the aerodynamic loads, at $Mach = 0.48$, corresponding to the Dive Speed at Sea Level;

2. Kinematic requirement: minimizing the Least Square Error (LSE) between Target and Deformed LE shape. The DN mechanism is deployed, under the external aerodynamic loads, at $Mach = 0.197$, corresponding to the Landing flight condition at $\alpha = 10\,^{\circ}$, at Sea Level.

3. Minimizing the maximum value of stress in the mechanism, when it is deployed, under the aerodynamic loads of landing condition.

The aerodynamic loads corresponding to these requirements are shown in Figure 3.3. The results of the genetic algorithm optimization were evaluated looking at the Pareto Front shown in Figure 3.4, in order to select a good compromise between the conflicting kinematic, structural ans stress requirements. The red circle represents the chosen solution. Concerning the kinematic requirement it is characterized by a LSE value of 0.0065 m. The internal structure and its deformation once actuated are shown in Figure 3.5.
Then some manual modifications have been applied, driven by the need of

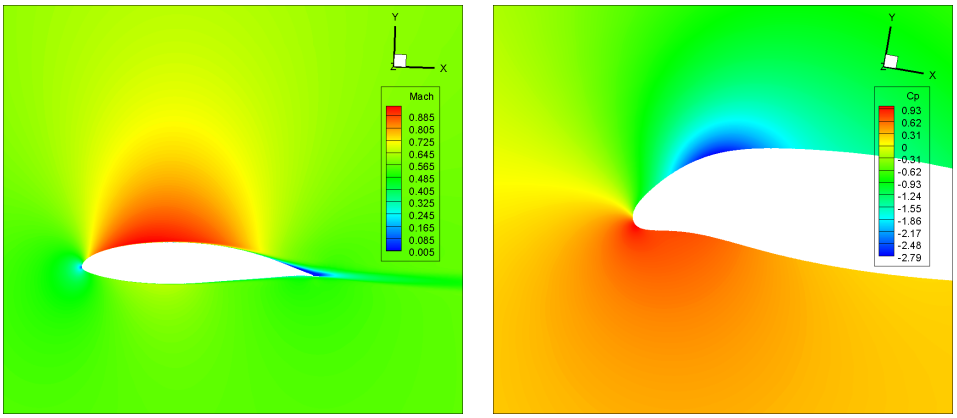

Figure 3.3: Aerodynamic loads for the structural (left) and kinematic (right) requirements

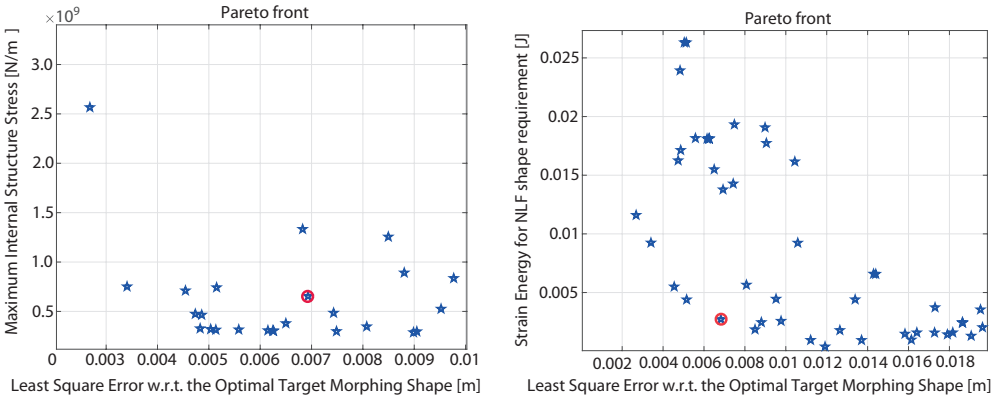

(a) Maximum stress vs LSE (b) Strain energy vs LSE

Figure 3.4: Pareto Front from the genetic algorithm

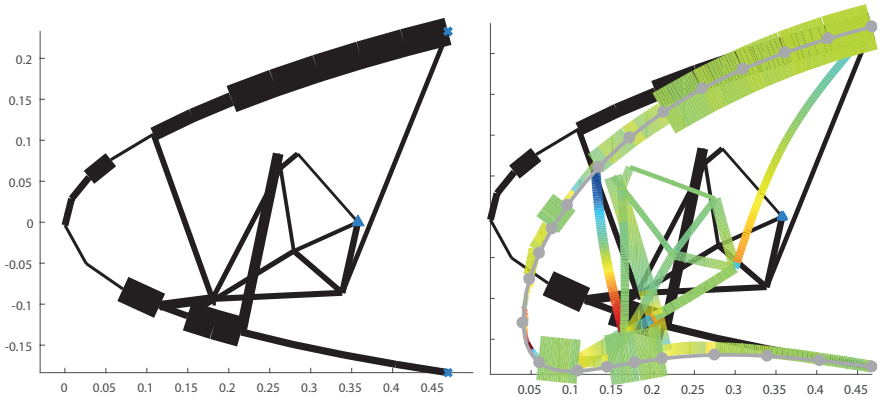

Figure 3.5: Optimal selected solution

less occupied space. The resulting solution is the starting point for all the applications discussed hereafter and it is shown in Figure 3.6.

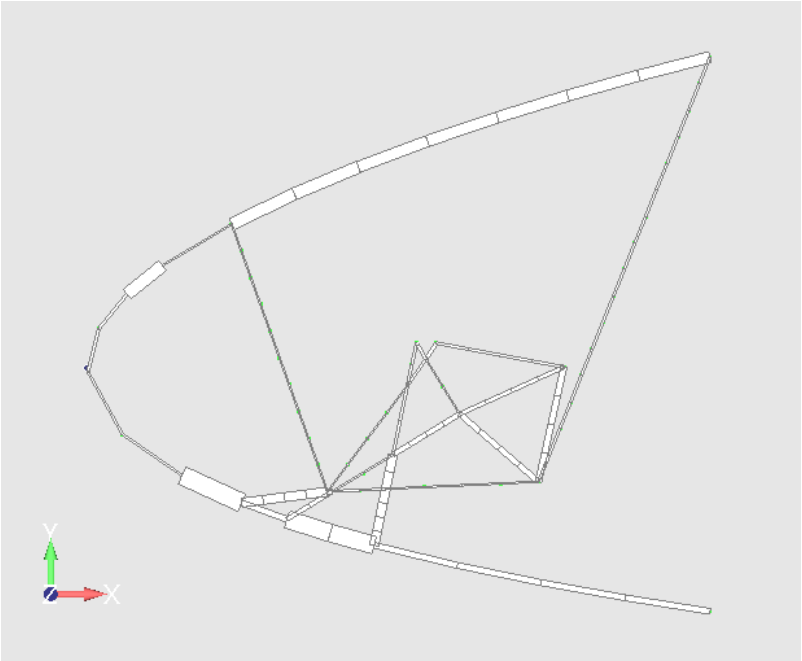

Figure 3.6: Updated selected solution

This model is made of beam elements, both for the skin and the mechanism. In order to account for the effect of the skin stiffness due to its spanwise extension, the link between the presented two-dimensional model and the real three-dimensional configuration is given by the following expression [13]:

$$t_{skin} = \sqrt[3]{\frac{w_{rib}}{p_{rib}}} \cdot t_{beam} \tag{3.1}$$

where t_{skin} and t_{beam} are the thickness of 3D wing skins and the thickness of the equivalent beams representing the skins in the 2D beam model used during the genetic optimization, respectively; w_{rib} and p_{rib} are the rib thickness, in the span-wise direction, and the rib pitch.

The analysis of the model in the droop nose configuration shows a maximum stress in the mechanism equal to 550 MPa, exactly what expected from the selection operated in the Pareto front of Figure 3.4. The choice of accepting a level of stress so high, was dictated by the need of achieving the 16° droop angle, required to be close to the aerodynamic target. Obviously

it is unthinkable to presume the availability of an aluminium alloy with such a yield strength. This aspect is confirmed by the maximum principal strain provided by the finite element analysis, equal to 0.0076, higher than the elongation at yield of a typical aluminium alloy, which can be 0.0065. This result establishes the unfeasibility of the aluminium alloy as material of the compliant mechanism in the considered droop nose device. Moreover it suggests the need to adopt materials able to guarantee high recoverable strains, greater than 1%. This potentiality can be found in the superelastic behaviour of the shape memory alloys, described in section 3.3, and employed in the applications of chapter 5 as material of the mechanism, as an alternative to the aluminium alloy.
Although preliminary computations have assessed the impossibility to satisfactorily use the isotropic elastic material, in any case it will be subjected to the proposed optimization procedure in order to evaluate the result about it.

3.3 Shape memory alloys

Shape memory alloys are materials that exhibit the so-called shape memory effect: once deformed, they are able to recover their original shape thanks to a thermal cycle. This effect was firstly discovered by the swedish researcher Arne Olander which observed it in a gold-cadmium alloy [26]. In the 1960s shape memory materials gained interest with the work of Buehler and Wiley at the U.S. Naval Ordnance Laboratory [10]. The research dealt with nickel titanium alloys, which took the name NiTiNOL (Nickel Titanium Naval Ordnance Laboratory). Also other materials were discovered to present the shape memory behaviour, for instance Cu-Al-Ni and Cu-Zn-Al-Mn alloys, but until today Nitinol is the shape memory alloy most adopted in the applications.
In addition to the shape memory effect, another peculiar property that shape memory alloys do show is the so-called superelasticity. At relatively high temperatures it can happen the recovery of large deformations as a consequence of mechanical stress induced transformation. A representation of the two effects is shown in Figure 3.7 [2].

A brief description of the phase transformations as well as the shape-memory alloy micromechanics behind the material macroscopic behaviour follows.
Shape memory alloys may exist in two state phases: austenite (parent phase) and martensite (product phase). The transformation process be-

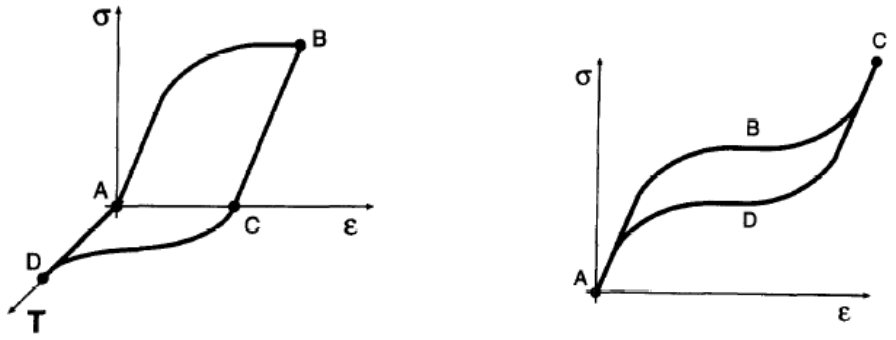

Figure 3.7: Shape-memory effect (left) and superelastic behaviour (right)

tween the two phases is a solid-solid transformation. This kind of process is non-diffusive, it is typical for those materials that present crystalline structure, and consists in small-length ordered displacements of the atoms [33]. In order to transform austenite in martensite, two possibilities there exist. If the transformation is induced by a temperature decrease, twinned (or multi-variant) martensite is obtained. Instead if the transformation is induced by stress increase, detwinned (or single-variant) martensite is the result. The difference between them concerns the crystallographic geometry of the martensite.

The macroscopic behaviour of the shape memory alloys can be described in terms of superelasticity and shape memory effect. Superelastic effect refers to the recovery of very large strains upon unloading, without permanent deformations. Shape memory effect is related to the ability of returning to an initial shape after a temperature variation.

In order to understand the behaviour of shape memory alloys it is essential to refer to their four characteristic transition temperatures, that are M_f, M_s, A_s and A_f, in ascending order. M stands for martensite and A for austenite. Subscripts f and s specify finish and start temperatures of the transformation processes. Martensitic phase is stable at temperatures below M_f. Austenitic phase is stable at temperatures higher than A_f. For temperatures between A_s and M_s, both phases are contemporary present. At a temperature below M_f the application of stress induces the reorientation of the crystals forcing martensite twinned to transform into martensite detwinned. Associated with this transformation there are residuals strains that still remains after the removal of the load. In order to recover them, shape memory effect is exploited: temperature is brought above A_f, the material transforms in austenite, then lowering the temperature single-variant martensite in the original shape is obtained.

The superelastic effect is due to the dependence of the transition temperatures on the stress level. Superelasticity occurs when starting from austenite, at a temperature above A_f and kept constant, a load is applied up to reach a critical stress value, that induces martensite transformation. Continuing to increase the stress level the transformation finishes and then the elastic loading of martensite starts. If the plastic limit is not reached, the described transformation is reversible upon unloading and will return to a zero strain condition. An initial austenite phase is therefore necessary condition of the appearance of superelasticity. However if the temperature is higher than a value indicated as M_d, the material will show an elastic-plastic behaviour. This can be explained looking at Figure 3.8 [44]. Slip is an irreversible process. If the critical stress for slip at a certain temperature is lower than the critical stress to induce martensite at the same temperature, the superelastic behaviour won't occur and irreversible strains will remain.

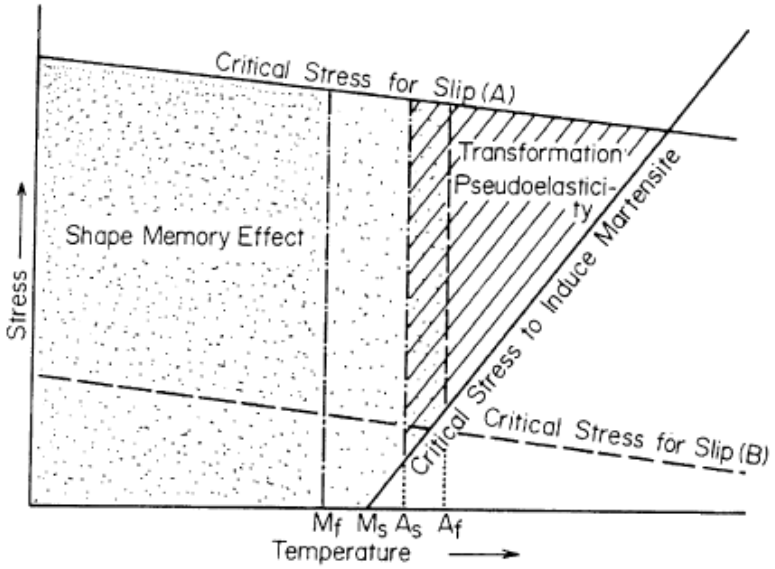

Figure 3.8: Representation for the appearance of superelasticity in temperature-stress space

A review of the kinematics and the kinetics approaches for the description of the martensitic phase transformations occurring in shape-memory alloys can be found in [2].

3.3.1 Superelastic behaviour

Superelastic effect finds application in different fields, such as aerospace, civil, mechanical and biomedical engineering. For instance it can be employed in medical guidewires, cardiovascular stents, orthodontic wires, eyeglass frames. In the aerospace field many examples of shape memory effect applications are available [4, 58]. Superelastic effect is less common, but some applications can be found, as in [62] where nickel titanium superelastic material is used in the manufacturing of a compliant mechanism. The selected manufacturing process was the wire electrical discharge machining (wire-EDM). The choice of using nitinol was lead by its high strain capability, that was confirmed by the strains measured in the experimental tests.
In general, superelasticity-based applications exploit the possibility of recovering large deformations and the existence of the transformation stress plateau, which guarantees near constant stress over large strain intervals [2].

3.3.2 Modeling and numerical simulations

The complexity of shape memory alloys make their modeling very difficult. The fundamental characteristics that numerical simulation should be able to reproduce are those of a very flexible material able to achieve very large strains that are reversible upon unloading. At Hibbitt, Karlsson & Sorensen (West) [47] a user material routine was developed on the basis of the model proposed by Auricchio and Taylor [2]. Starting from the generalized plasticity concept, the mathematical model is based on an additive strain decomposition, where the strain is written as the sum of two terms: a linear elastic component and a transformation component:

$$\Delta\epsilon = \Delta\epsilon^{el} + \Delta\epsilon^{tr} \tag{3.2}$$

Concerning the transformation strain:

$$\Delta\epsilon^{tr} = a\,\Delta\zeta\,\frac{\partial F}{\partial\sigma} \tag{3.3}$$

where F is a transformation potential and ζ is the fraction of martensite. They are related by a stress potential law:

$$\Delta\zeta = f(\sigma,\zeta)\Delta F \tag{3.4}$$

If the stress overcomes the yielding of the material, also plastic strains develop. The transformation strain is of the order of 6%. The elastic strain

is smaller, usually below the 2%. Since the transformation strains are greater than typical elastic strains in a metal, the material behaviour is indicated as superelastic. This constitutive model is available in Abaqus as UMAT user material. It is suitable to simulate the superelastic behavior of shape memory alloys such as Nitinol.
The material data required to set up the numerical model are obtained from uniaxial tests. These data characterize the start and the end of the phase transformation during loading, unloading and reverse loading. The different elastic constants for the austenite and martensite phases are accounted for and temperature dependence is also included. The $\sigma - \epsilon$ curve along with the significant parameters is shown in Figure 3.9. Figure 3.10

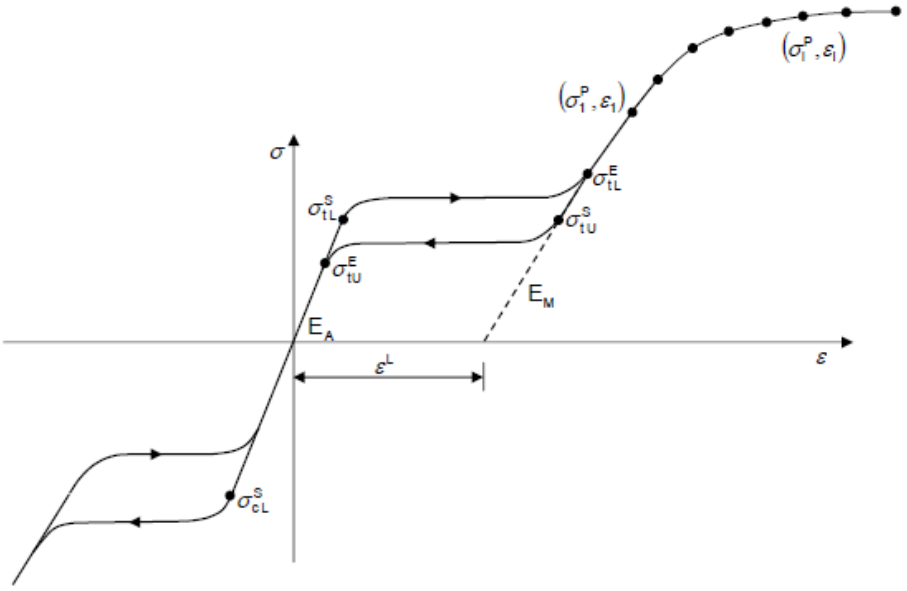

Figure 3.9: Uniaxial stress-strain curve for the superelastic behaviour

shows the dependence of critical stresses on temperature. An example of $\sigma - \epsilon$ curve coming from an experimental test is shown in Figure 3.11.
Concerning the user interface, in order to define the material properties, the *USER MATERIAL option is required. Moreover, the name parameter of the *MATERIAL must start with ABQ_SUPER_ELASTIC. The number of solution-dependent state variables (SDVs) is provided via the *DEPVAR option. The formulation requires 24 SDVs in the elastic case and 31 when also plasticity is considered.
Different behavior in tension and compression can be obtained if σ_{CL}^S is assigned different from σ_L^S. This is usually the case and has many

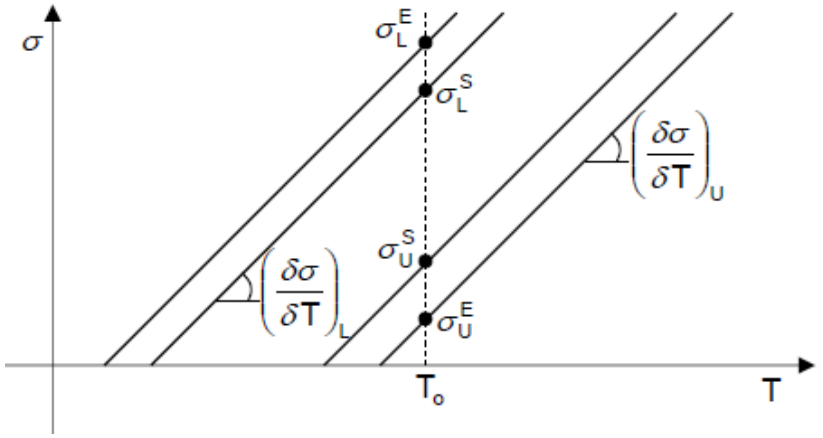

Figure 3.10: Stress-temperature diagram for the superelastic behaviour

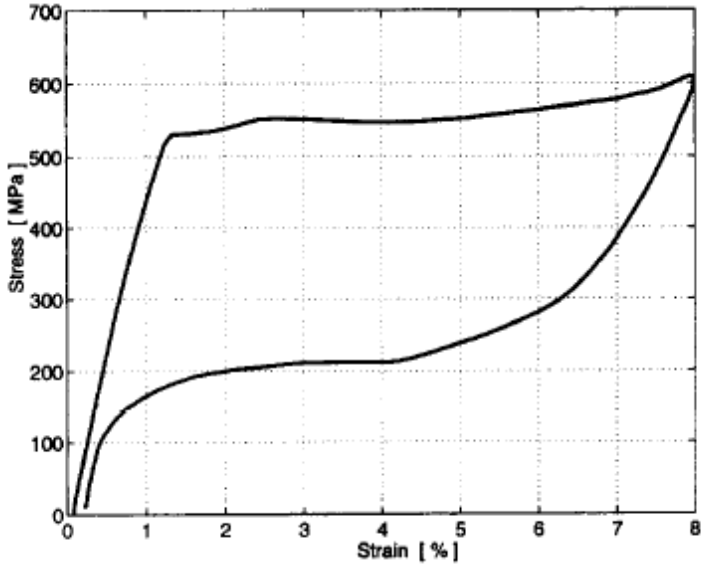

Figure 3.11: Experimental data for the uniaxial tension stress-strain response of a Ni-Ti alloy [2]

consequences, as widely depicted in [48]. For instance, the neutral axis may deviate from the centerline of a symmetric section beam and plane sections may not remain plane. However this asymmetric behaviour, though easily intelligible, won't be taken into account for the sake of simplicity.
In order to define the material model it is necessary to provide $15 + N_A$ material constants on the data lines of the *USER MATERIAL option, where N_A is the number of anneals that are performed. When plastic behaviour is also considered, $16 + N_A + 2N_P$ material constants must be specified, where N_P is the number of stress-strain pairs needed for the definition of the yield curve. Due to the aeronautical application, since no permanent deformations are admitted in the operational cases, superelastic-only behaviour will be considered while plasticity won't be modelled. Neither the possibility to simulate an annealing process will be used; it consists in the resetting of the state variables to zero during an analysis in order to provide a new unloaded configuration. This functionality is of no interest in the present dissertation and will not be considered. Table 3.1 describes the parameters required by the material routine for a superelastic-only use.

Table 3.1: Superelasticity UMAT: list of parameters

Symbol	Definition
E_A	Austenite Young's modulus
ν_A	Austenite Poisson's ratio
E_M	Martensite Young's modulus
ν_m	Martensite Poisson's ratio
ϵ^L	Transformation strain
$\left(\frac{\delta\sigma}{\delta T}\right)_L$	$\delta\sigma/\delta T$ loading
σ_L^S	Start of transformation loading
σ_L^E	End of transformation loading
T_0	Reference temperature
$\left(\frac{\delta\sigma}{\delta T}\right)_U$	$\delta\sigma/\delta T$ unloading
σ_U^S	Start of transformation unloading
σ_U^E	End of transformation unloading
σ_{CL}^S	Start of transformation stress in compression
ϵ_V^L	Volumetric transformation strain

Many elements are supported to be used in conjunction with the Nitinol material: 3D solids, plane strain, axisymmetric, plane stress, 3D shells, 3D membranes, 3D beams. A simple uniaxial loading and unloading of

a beam-like body has been performed in order to compare the results obtained using beam, shell and solid elements. The results do not show significant differences among them, therefore in what follows the more appropriate modeling stategy according to the situation will be preferred.
Concerning the analysis procedure, the material model can be used with all the analysis procedures related to mechanical behavior, hence it is well suitable for the non linear static analysis that will be performed by means of the keyword *STATIC.
Many outputs are provided at the end of the analysis, among which the linear elastic strains, the transformation strains and the fraction of martensite.

3.3.3 Selection of material properties

In absence of detailed information about the material data for superelastic applications, in this section a simple numerical design of the material is carried out in the respect of what explained in the aforementioned discussion on Nitinol. The purpose is to establish a set of parameters that is able to give a material suitable for the specific application here addressed. In particular, the dependence on temperature has to be taken into account and the desired superelastic behaviour must be valid for the wide range of aeronautical operative temperatures. The material coming from this study will be used in the applications as the material of the internal compliant mechanism, in alternative to the usual isotropic aluminum material, and the comparison between them will be shown.
The phase transformations occur in temperature ranges depending on the material composition. Transformation stresses increase linearly with the temperature. The proportionality is described by means of the Clausius-Clapeyron coefficients, typically supposed to be equal for both martensitic and austenitic transformation and constant in the entire temperature range [9]. These coefficients can assume values in the range between 2.5 MPa/K and 15 MPa/K [2]. According to [11], phase transformations don't depend on temperature rates and stress rates.
Some material parameters (elastic modulus, Poisson's ratio, stress influence coefficient, maximum transformation strain) are borrowed from Qidwai and Lagoudas [46], and reported in Table 3.2.
Concerning the transformation temperatures, they can be widely shifted after manufacturing by performing suitable solution annealing and aging treatments [18]. Therefore all the temperatures are chosen according to the desired useful operative range, and it is supposed that the selected values are achievable. Further investigation, prototype fabrication and

Table 3.2: Nitinol characteristics from [46]

Parameter	Value
E_A	72 GPa
ν_A	0.33
E_M	30 GPa
ν_m	0.33
ϵ^L	0.05
$\left(\frac{\delta\sigma}{\delta T}\right)_L$	7 MPa/K
$\left(\frac{\delta\sigma}{\delta T}\right)_U$	7 MPa/K

testing are intended as future work.
It is expected that the material would show the superelastic behaviour for a wide range of temperatures, here selected between $-10\,^{\circ}$C and $40\,^{\circ}$C (263 K and 313 K). This means that austenitic finish temperature must be below the previous minimum temperature (263 K), hence a value of 260 K is chosen. Another fundamental requirement is that up to the maximum temperature (313 K) the stress at the end of the martensite transformation is below the critical stress for slip, here assumed in the order of 800 MPa; therefore a suitable martensite finish temperature may be 220 K.
The reference temperature considered in the analysis is 293 K. According to this, the stress values characterizing the plateaus are shown in Table 3.3. Figure 3.12 shows the relationship between the selected transformation

Table 3.3: Critical stresses at $T_0 = 293\,\mathrm{K}$

Parameter	Value
σ_L^S	441 MPa
σ_L^E	511 MPa
σ_U^S	301 MPa
σ_U^E	231 MPa
σ_{CL}^S	441 MPa

temperatures and stress level. In particular, the reference temperature and the minimum and maximum temperatures are highlighted.

All the computations for the design involving Nitinol will be performed at the reference temperature $T_0 = 293\,\mathrm{K}$. After the design will be completed, verification in terms of deformed shape and internal stress will be performed also using the limit temperatures.

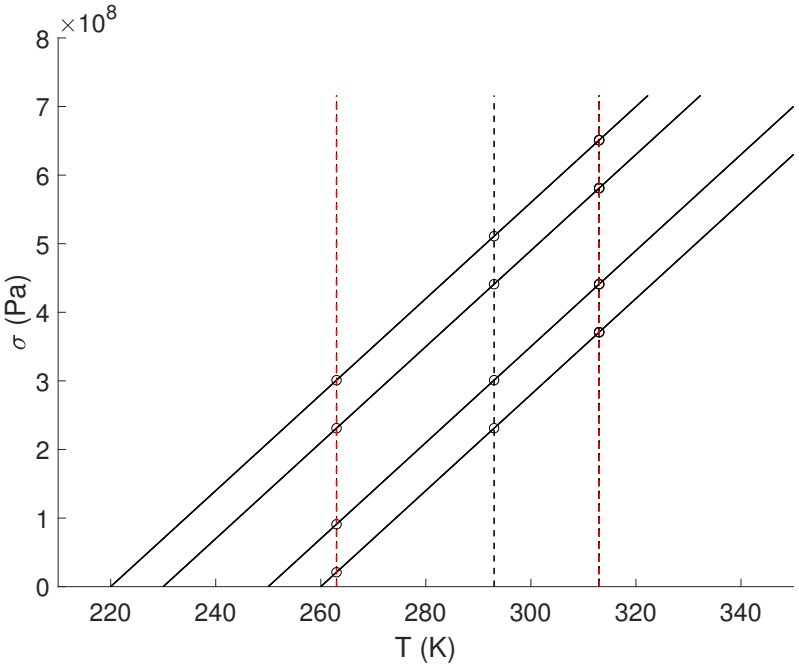

Figure 3.12: Reference and limit temperatures in the stress-temperature diagram for the superelastic behaviour

Chapter 4

Solution refinement tools

This chapter describes the tools specifically developed in this thesis work in order to improve the existing design procedure. These tools are not simply intended for the refinement of the previously found solution. They are conceived to specialize the field of application of the current solution, to enhance its performance in terms of desired requirements and also to get close to the manufacturing.
The main capabilities provided are:

- The possibility to adapt the internal mechanism synthesized topology to:
  - a different wing;
  - different positions in the span of the same wing in case of tapering;
  - a scaled model of the same wing.
- The possibility to change the material both of skin and mechanism even if the topology has already been defined. Several types of material can be implemented, among which isotropic, composite, superelastic.
- The availability of:
  - different strategies of finite element modeling and levels of detail;
  - different types of static analysis;
  - different types of optimization analysis.
- The achievement of a solution almost ready for manufacturing process and experimental testing.

All these potentialities can be allowed only by means of the combined use of a numerical computing environment and a finite element analysis software. The presented approach is very general and various implementative techniques may be used. The detailed description of the above-mentioned features will take place referring to the specific softwares employed in this work, that are Matlab and Abaqus, both of them selected for their respective powerful capabilities.

Section 4.1 describes the specialization of the topology to the actual structural configuration. At this phase, a sizing and geometric optimization is performed. Section 4.2 faces the problem of the transition from a beam-elements model to the actual drawing of the designed device, performing a shape optimization of the compliant mechanism aimed at the minimization of local stresses.

4.1 Gradient-based optimization

4.1.1 Optimization problem definition

The problem that is intended to be solved in this phase can be formulated as:

$$\begin{aligned} \min \quad & LSE \\ \text{such that} \quad & \sigma_{max}^{VM} \leq \bar{\sigma} \\ & LSE_{NLF} \leq tol_{NLF} \\ & t_{LB}^{rib} \leq t_i^{rib} \leq t_{UB}^{rib} \qquad \forall i = 1, \ldots, n_{rib} \\ & t_{LB}^{skin} \leq t_j^{skin} \leq t_{UB}^{skin} \qquad \forall j = 1, \ldots, n_{skin} \\ & x_{LB_k} \leq x_k \leq x_{UB_k} \qquad \forall k = 1, \ldots, n_{intPoints} \\ & y_{LB_k} \leq y_k \leq y_{UB_k} \qquad \forall k = 1, \ldots, n_{intPoints} \end{aligned} \tag{4.1}$$

The scalar objective function is the Least Square Error (LSE) between the deformed shape and the target shape when the mechanism is actuated, computed as:

$$LSE = \frac{1}{n_{cp}} \sum_{i=1}^{n_{cp}} \sqrt{(x_{d,i} - x_{m,i})^2 + (y_{d,i} - y_{m,i})^2} \tag{4.2}$$

where n_{cp} is the number of control points along the skin, (x_d, y_d) are the positions of the control points in the deformed condition obtained by the

structural finite element analysis and (x_m, y_m) the corresponding points on the target shape.
The first constraint is the structural limitation related to the stress inside the mechanism. σ_{max}^{VM} is the maximum Von Mises stress in the compliant rib and $\bar{\sigma}$ is its admissible value. The evaluation of this constraint must be done in the morphing configuration.
LSE_{NLF} is the least square error between the undeformed shape and the deformed shape computed under the aerodynamic loads of a critical condition such as the Dive Speed, while keeping the mechanism fixed. This function represents an index of the deformability of the morphing structure when the device is not actuated. It must be restricted below a selected tolerance. This requirement is needed to guarantee that the structure is able to withstand the aerodynamic loads and that the aerodynamic performances of the conventional configuration are not affected by the presence of an internal compliant structure; the last point is especially critical when the morphing device must be adopted in combination with a Natural Laminar Flow wing.

The variables of the problem are:

- the in-plane dimensions t_i^{rib} of the beam segments of the compliant mechanism;
- the thickness t_j^{skin} of the sectors in which the skin is divided;
- the positions (x_k, y_k) of the internal points of the compliant mechanism.

For each variable, properly lower and upper bounds must be selected.
Subsection 4.1.3 discusses in details the models and the analyses used to evaluate the objective function and the constraints of the optimization problem, whose solution method is explained in subsection 4.1.2.

4.1.2 Gradient-based methods

Gradient-based methods are a family of methods that try to minimize or maximize an objective function with searching directions suggested by the gradient of the function at the current solution point. The optimization problem of interest is set up in Matlab by means of the *fmincon* function, able to deal with the minimization of constrained nonlinear multivariable function [43].

The general formulation of the problem is:

$$\begin{aligned} \min_{x} \quad & f(x) \\ \text{such that} \quad & c(x) \leq 0 \\ & ceq(x) = 0 \\ & A \cdot x \leq b \\ & Aeq \cdot x = beq \\ & lb \leq x \leq ub \end{aligned} \tag{4.3}$$

Among the available optimization algorithms, Sequential Quadratic Programming (SQP) is chosen. At each major iteration of this algorithm, the Hessian of the Lagrangian function is approximated using a quasi-Newton updating method. Then a QP subproblem is generated and solved, giving the search direction of a line search procedure [6].

4.1.3 Automatic model generation

The objective function and the constraints of the optimization problem are evaluated as results of finite element analyses performed by Abaqus. The genetic algorithm optimization discussed in section 2.2 used the PFEM code as finite element solver. The model used to design the compliant mechanism, whose results have been reported in 3.2, employed beam elements both for the mechanism and the skin. In particular, the thickness of the skin was modified in order to take into account its extension in the wing-span direction.
Here a more accurate model for the skin is adopted. The length of the skin in the span-wise direction is chosen equal to the rib pitch and a single rib is modeled at the middle of this length. Concerning the finite element modeling, shell elements are used for the skin and beam elements for the compliant rib. Illustrative examples of the described model, both in case of leading and trailing–edge devices, are shown in Figure 4.1.
The reference system has:

- x-axis parallel to the relative wind, directed from the leading to the trailing edge;
- z-axis along the span, from the root to the tip of the left wing;
- y-axis such that a right-handed frame is obtained.

Concerning the analysis type, since large deformations are expected, static non linear analysis is mandatory. Two different analyses are required:

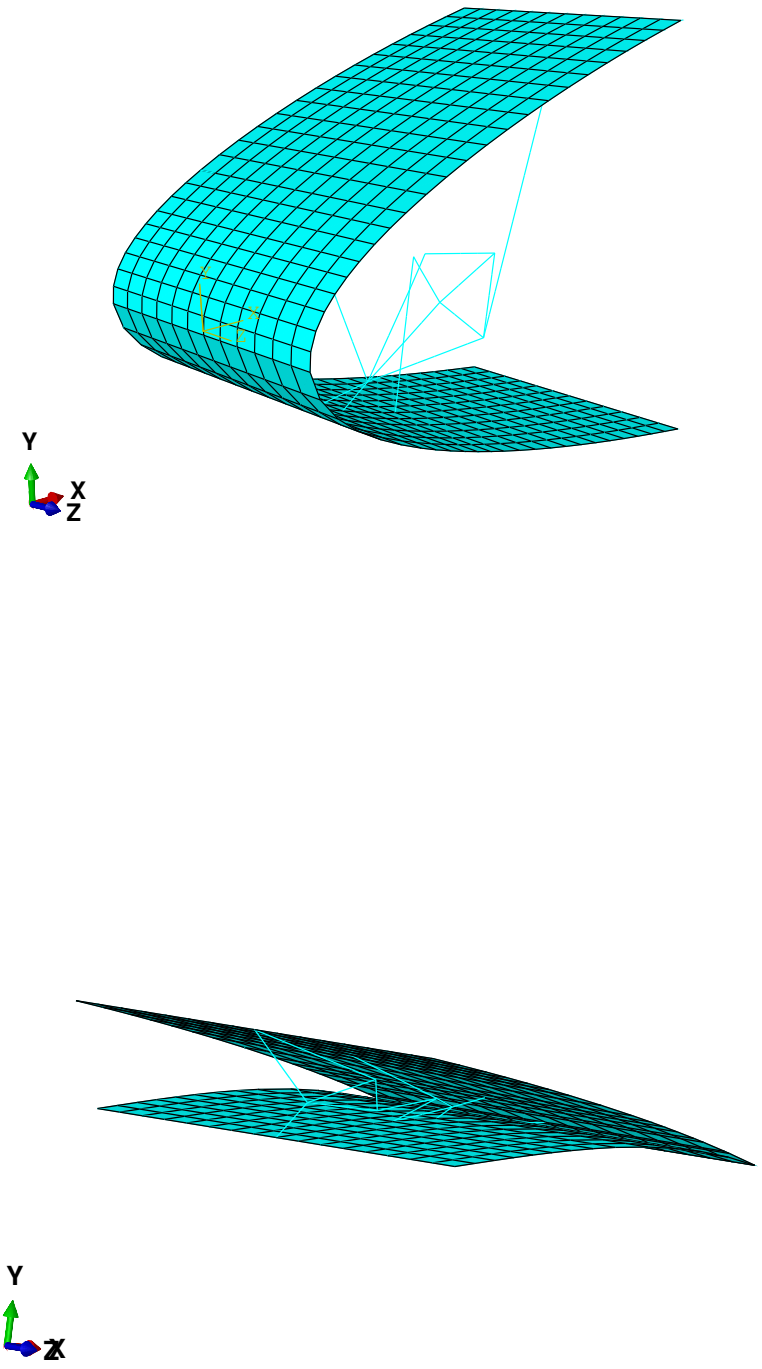

Figure 4.1: Abaqus models for the gradient-based optimization

1. analysis of the model when the compliant mechanism is actuated, while it is subjected to the aerodynamic loads of the morphing condition, for instance take-off or landing;

2. analysis of the model when the compliant mechanism is fixed, under the aerodynamic loads of a critical flight condition, such as Cruise or Dive Speed condition.

The model is the same in the two cases, apart from the loads and the boundary conditions, as better described later.
As already explained, the variables of the optimization problem are the section parameters of skin and rib, but also the position of the internal points of the rib. Therefore each analysis required by the optimization algorithm to evaluate the finite differences needed to compute the gradient has to be performed on a different finite element model. This fact forces the automatization of the model generation as well as its interaction with the optimization solver. Abaqus script capabilities are exploited in order to automatize the generation of the model. The Abaqus Scripting Interface is an application programming interface (API) to the models and data used by Abaqus [1]. It is an extension of the Python object-oriented programming language and it works through Python scripts. The following potentialities of the Interface will be used:

- create the components of an Abaqus model, such as parts, materials, loads, and steps;

- create and submit Abaqus analysis jobs.

These operations are the counterpart of what is usually done by hand using the CAE environment.
A dedicated Python script is written to realize the above-mentioned tasks. It requires the variables of the optimization problem, but also some parameters and data that remain constant throughout the optimization process and that depend on the particular morphing device that is intended to be designed. The required parameters and data are:

- The position of the skin points that define the leading (or trailing) edge airfoil; these points are used to create the skin model and also as control points in which the target shape is known.

- The position of the input actuation point of the mechanism.

- A connectivity matrix to indicate the topology of the compliant mechanism, starting from the identifiers of the internal points and the active output points.

- The rib pitch p_{rib}.
- The rib thickness w_{rib}.
- The characteristics of the materials of the rib and the skin.
- The dimensions of the stringers.
- The actuation force.
- The pressure coefficient distribution and the dynamic pressure for the two aerodynamic configurations.

The sequence of actions performed by the script to implement the modeling strategy is:

1. Create the Sketch of the rib and the Sketch of the skin.
2. Create a Wire Part for the rib and an Extruded Shell Part (with depth equal to p_{rib}) for the skin.
3. Create the sets required to assign the dimensions given by the sizing variables of the problem.
4. Define the materials according to the provided data.
5. Define the rib sections by means of the related variables as well as the rib thickness w_{rib}; define the skin sections by means of the related thickness variables.
6. Create the stringers in the airfoil arc-length position corresponding to the active output points, with an extension equal to the span-wise length of the model.
7. Create a Tie Constraint to connect the rib Part to the skin Part at the points in common.
8. Create a Non-linear analysis Static Step.
9. If the current model is intended for the morphing configuration, apply the actuation force at the actuation point.
10. Apply the aerodynamic loads as Pressure Load providing the pressure coefficient distribution and the dynamic pressure referred to the considered aerodynamic condition.

11. Apply an encastre boundary condition to ground the skin where it would connect to the structural box in correspondence of the spar. If a morphing trailing–edge is under consideration, the lower surface constraint is replaced with an horizontal slider.

12. If the current model is intended for the morphing configuration, apply a planar constraint at the actuation point.

13. If the current model is intended for the configuration with fixed mechanism, apply a pinned constraint at the actuation point.

14. Mesh the rib Part using three-dimensional Timoshenko beam linear elements (B31); mesh the skin Part using 4-node, quadrilateral, stress/displacement shell elements with large-strain formulation (S4).

15. Submit the Job and run the analysis.

This process is carried out every time an analysis run is invoked by the optimization algorithm.
A simplified version of the optimization problem, and as a consequence of the model generation, consists in the exclusion of the internal points position from the optimization variables. This implies a lower computional time at each iteration of the optimization: the search space is smaller and also the required computations. In addition the model generation can be speeded up by observing that now the geometry is kept fixed while only the sizing quantities do change. Therefore the model can be generated once for all, and the operation of changing the section parameters can be simply performed modifying the INP file before each analysis. A consideration about if it is worth implementing the more expensive approach will be discussed in the results of chapter 5.

4.1.4 Optimizer-solver interface and problem set-up

In order to link the optimization process and the finite element solver an appropriate interface between Matlab and Abaqus has been developed. It mainly consists of Matlab functions in charge of writing and reading text files. The fundamental tasks required are:

- pass the current values of the variables to the Python script;

- specify whether the morphing configuration or the conventional one has to be analysed;

- read the outputs from the finite element analysis results. They are the maximum Von Mises stress inside the mechanism and the displacement of the skin points.

In order to set-up the optimization problem and run it in Matlab, the following input data must be supplied:

- maximum admissible stress in the mechanism;
- tolerance for the assessment of deformability;
- bounds for the sizing variables;
- bounds for the internal points position;
- initial solution.

At the end of each iteration, the current solution is saved as well as the corresponding model and the objective function value.

4.2 Compliant mechanism shape optimization

At the end of the previous step, the numerical design phase may have been considered finished since an optimized model has been obtained such that it well satisfies the aerodynamic performances and at same time doesn't violate the structural requirements. However something is still missing, since another step is required to be ready for the subsequent manufacturing process of the designed device. Indeed, the compliant mechanism model addressed until now consists of beam elements. They guarantee a sufficiently accurate estimate of the stress far enough from the element extremities, but they lack of reliability concerning what happens at the constrained regions. Moreover in this zones, the manufacturing detail of the fillets is missing, since it can't be thought to be a simple intersection in a single point. These premises constitute the reason behind the idea of performing the optimization analysis described in the following.

In this section, only the internal compliant mechanism is dealt with. First of all, starting from the beam elements model of the optimal solution, a CAD model of the compliant mechanism is created. In order to do that, the internal and the boundary points of the mechanism of the beam elements model are sketched in the 2D drawing and are connected with lines according to the topology. Then, each line is used as mid line of the corresponding load path, whose in-plane thickness is inherited from

the beam elements and is represented in the drawing by means of two symmetric offsets. Finally, suitable fillets link the lines at their intersection. Later, starting from the CAD model a plane sketch is generated, that exhibits the actual internal points positions and the load path thicknesses of the optimal solution.

In this optimization phase, the selected modeling software is Abaqus again. The created sketch is imported in Abaqus and it is finely meshed with two-dimensional, 4-node bilinear, plane stress solid elements (CPS4). The described sequence is shown in Figure 4.2.

The optimization analysis is implemented by means of a suite of optimization tools, named Tosca Structure. This is a modular system for non-parametric structural optimization able to perform different kinds of optimization analyses coupled with finite element solvers. The integration with CAE environments is straightforward. The optimization process is simulation-based and allows to improve the design in an iterative manner. Among the different tools of optimization offered, *Tosca.shape* is the one that best fits to the desired purpose. Indeed, the shape optimization consists in finding the optimal position of the nodes for the minimization or maximization of a chosen objective function, under some constraints. Shape optimization is typically adopted to modify the component surface in order to reduce local stress: *Tosca.shape* is a tool specifically developed to improve designs for more reliability and durability. The setup of shape optimization problem doesn't require model parameterization; the design area is defined by specifying groups.

According to the previosly described aim of stress reduction, a suitable objective function is the minimization of a stress index inside the structure. In this work the selected objective function is the minimization of the maximum principal stress. Concering the constraints, the volume is not allowed to change. This is a suggested equality constraint that must be satisfied within a tolerance of 10^{-3}. Another constraint that is needed in order to properly lead the analysis is the minimum member size, belonging to the family of the geometric restrictions; the minimum distance between two geometric edges is not allowed to go below a chosen value. The design region, which is modified by the optimization process, includes the surface nodes of the whole model or of a subset of it. In this case of two-dimensional model, the considered nodes are those that lie on the contour of the mechanism. However, also the internal nodes are allowed to move; indeed, a powerful capability provided by Tosca is the mesh smoothing

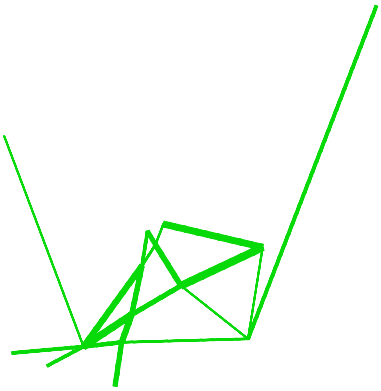

(a) Beam elements model

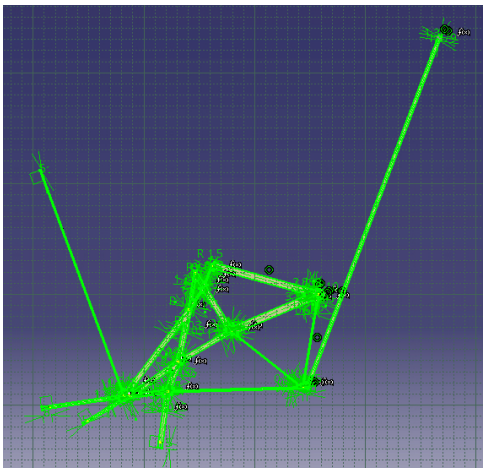

(b) 2D drawing

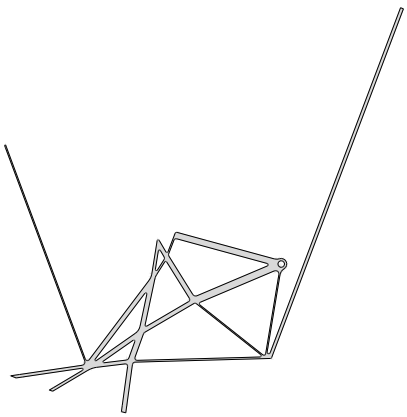

(c) Plane sketch

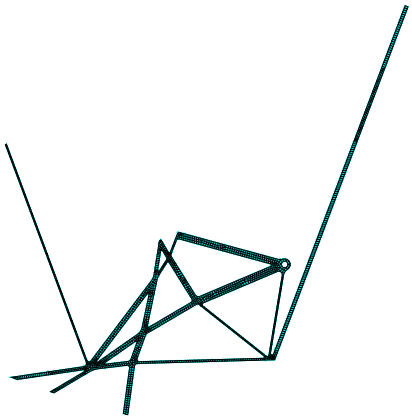

(d) 2D solid elements model

Figure 4.2: Steps from the beam elements model to the 2D solid elements model

in each design cycle in order to keep high quality meshes throughout the optimization process. In other words, the internal nodes displacements are not design variables but they are moved as a consequence of the outer nodes displacement, with the only aim of avoiding the creation of too distorted elements.
An example of nodes belonging to the design area is shown in Figure 4.3.

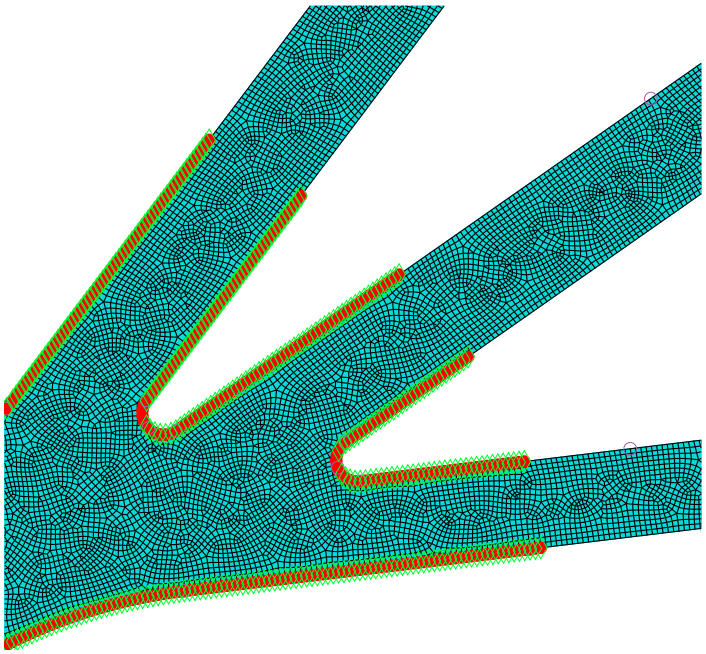

Figure 4.3: Shape optimization: example of design area

The static analysis that is performed in order to evaluate the objective function and the constraints for the optimization analysis consists in imposing the displacements and the in-plane rotation at the points of the rib attached to the skin and applying the actuation force at the actuation point. The displacement history to be imposed is extracted from the outputs of the beams model analysis for the optimum solution of the gradient-based optimization. The major issue faced in performing this kind of analysis comes from the nature of the model, since there are no simple lines and points, but a mesh of solid elements. This means that in order to correctly apply the boundary conditions and the load, some reference points have to be defined. In particular, they are created in correspondence of the external points of the rib and also in the actuation point location. Then they are linked to the rest of the structure by means of the Kinematic Coupling constraint provided by Abaqus. Each reference

point is selected as master point in the connection with the contour of the mechanism in the outer region. An illustrative representation of this interface is shown in Figure 4.4.

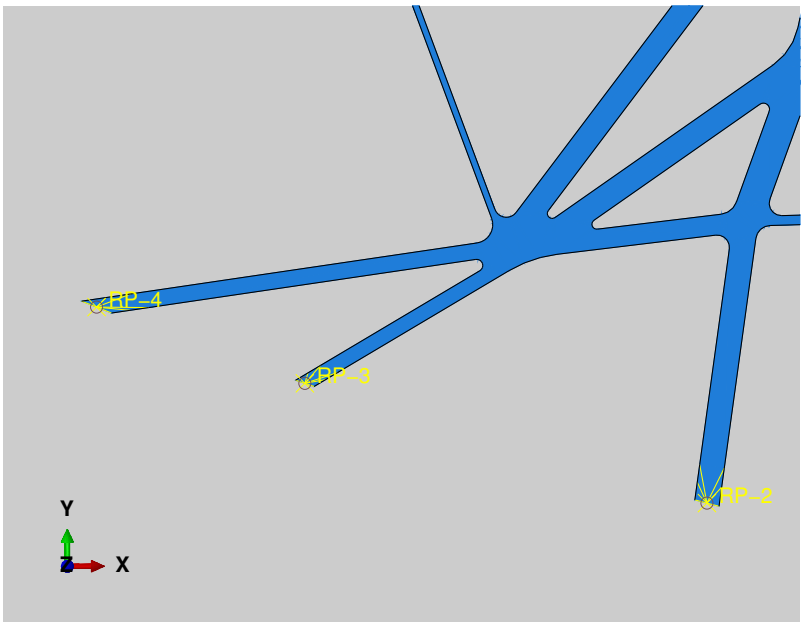

Figure 4.4: Kinematic coupling for the connection of reference points to boundary edges

Chapter 5

Results

In this chapter the refinement process is applied to the results coming from the genetic algorithm optimization shown in section 3.2. Starting from this model, an optimized topology and sizing solution is found by means of the gradient-based optimization performed with the combined used of Matlab and Abaqus. Then, the new optimal solution is transposed in a CAD model used to generate the input for the shape optimization of the compliant mechanism performed by Tosca.
The whole procedure is applied twice, for different materials of the mechanism: the aluminium alloy isotropic material exactly as in the GA topology optimization, and the Nitinol whose characteristics have been discussed in section 3.3.3. Then a comparison between the two sets of results is shown.

5.1 Gradient-based optimization

First of all, the common features of the model and the set-up of the optimization problem are discussed.

- The rib pitch p_{rib} is equal to 130 mm and it is used as span-wise length of the skin.
- The rib thickness w_{rib} is equal to 35 mm.
- The chord of the airfoil is $c = 2.911$ m. Front spar is located at the 16% of the chord, hence the chord extension of the model is 467 mm.
- The actuation force F in the input point has vector components $(-468.21\,\text{N}, -40.96\,\text{N})$.
- The aerodynamic conditions used for the evaluation of the objective function and the NLF constraint are respectively:

- Landing condition at sea level: angle of attack $\alpha = 10°$, dynamic pressure $q_D = 2561\,\text{Pa}$;
- Dive speed condition at sea level: angle of attack $\alpha = 0°$, dynamic pressure $q_D = 5000\,\text{Pa}$.

The pressure coefficient distribution is shown in Figure 5.1.

The model corresponding to the inital solution is depicted in Figure 3.6. It shows the starting design variables, that are the result of the genetic algorithm. Figure 5.3 shows the application of the pressure loads on the model in the two different configurations.

The other required data to set-up the problem are the limit values for the constraints and the bounds. For the NLF LSE tolerance a value of 10^{-3}m is selected.
Concerning the admissible values in terms of stress, they are 550 MPa for the isotropic material and 500 MPa for Nitinol. The value of 550 MPa for the aluminium alloy has already been discussed in section 3.2. The value of 500 MPa for Nitinol is just below the stress level at the end of the loading plateau, for the selected material parameters and reference temperature, as discussed in section 3.3.3.
The bounds for the sizing variables are $1\,\text{mm} \leq t_i^{rib} \leq 7\,\text{mm}$ and $0.5\,\text{mm} \leq t_j^{skin} \leq 7\,\text{mm}$. The internal points position can vary of $\pm 5\,\text{mm}$ both in x and y direction.

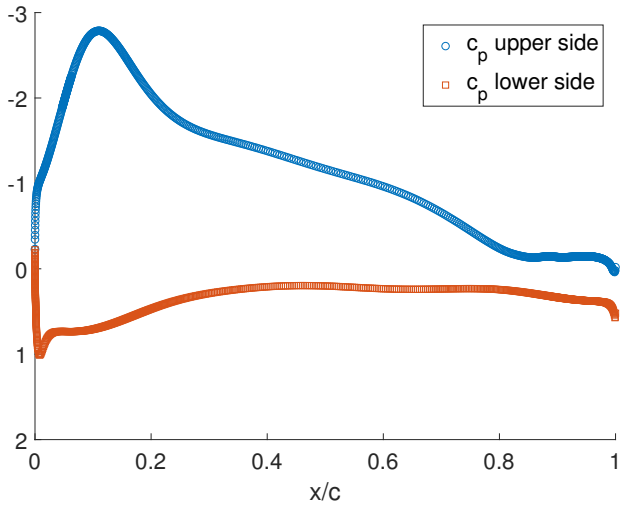

(a) Landing condition ($\alpha = 10°$)

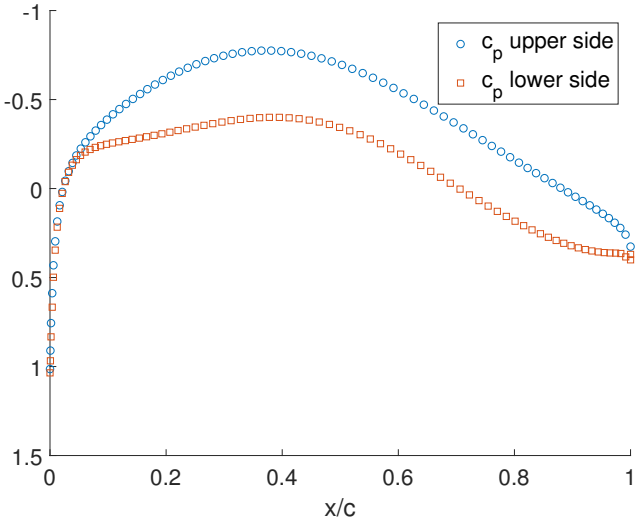

(b) Dive speed condition ($\alpha = 0°$)

Figure 5.1: Pressure coefficient distributions

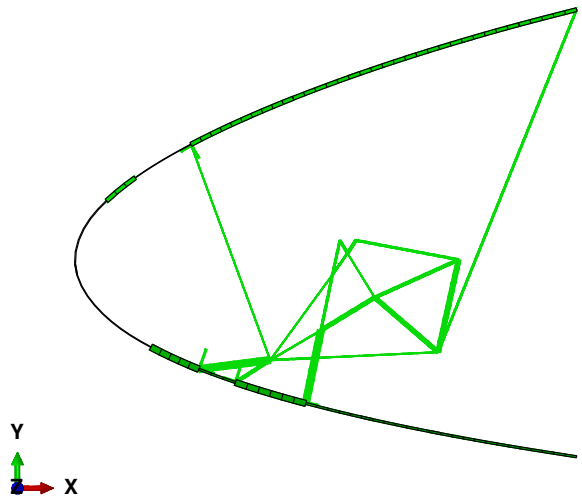

(a)

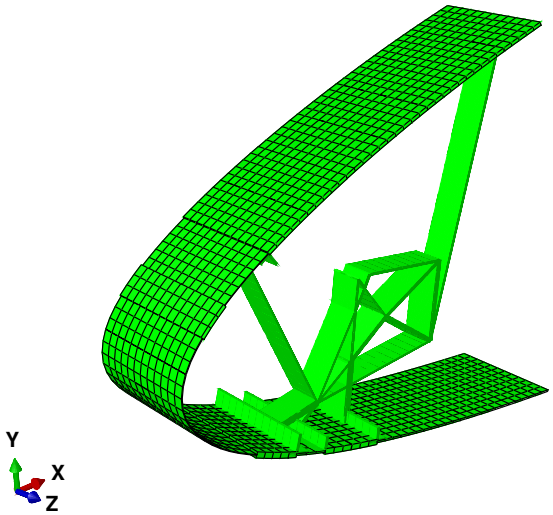

(b)

Figure 5.2: Abaqus model corresponding to the initial variables

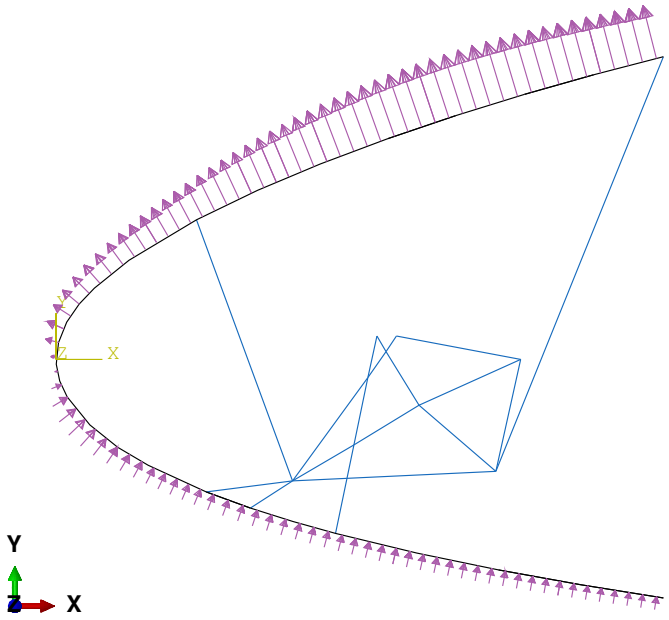

(a) Landing condition ($\alpha = 10°$)

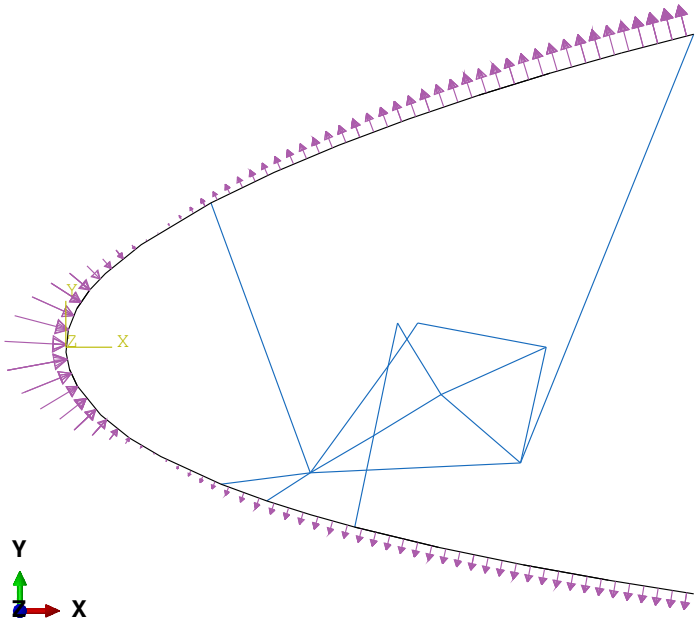

(b) Dive speed condition ($\alpha = 0°$)

Figure 5.3: Pressure loads on the model

5.1.1 Isotropic material

The isotropic material is a typical aluminium alloy, characterized by a Young's modulus $E = 72\,\text{GPa}$ and a Poisson's coefficient $\nu = 0.33$.
Concerning the skin, it is made of composite materials, but here an equivalent isotropic material is selected, as already done with the genetic optimizer. Its characteristics are $E_{skin} = 40\,\text{GPa}$ and $\nu = 0.12$.
At first, a static analysis in the droop nose configuration is performed to evaluate the LSE and the maximum internal stress for the starting solution. The deformed shape is shown in Figure 5.4. Its comparison with the undeformed shape and the target shape is represented in Figure 5.5. The obtained morphed shape is not so good compared to the target one, especially in the lower skin region. The deformed shape is characterized by an LSE value of 10.19 mm. The different value with respect to that given by the genetic algorithm optimization can be explained with the different modeling strategy. The maximum Von Mises stress in the mechanism is 541 MPa, while $LSE_{NLF} = 0.4\,\text{mm}$. Therefore the initial solution is feasible.

The gradient-based optimization is run and it converges to an optimal solution in 50 iterations. The evolution of the objective function with the iteration number is shown in Figure 5.6. The LSE for the optimal solution is 2.23 mm. Maximum stress in the rib is 549.9 MPa.
The comparison between the initial deformed shape and the optimal deformed shape is shown in Figure 5.7. The stress level inside the mechanism is shown in Figure 5.8.
Figure 5.9 illustrates the comparison between the optimal deformed shape and the target one.
Figure 5.10 compares the optimization variables between the starting solution and the optimal solution. For a more clear visualization, thickness values are magnified by a factor 3.

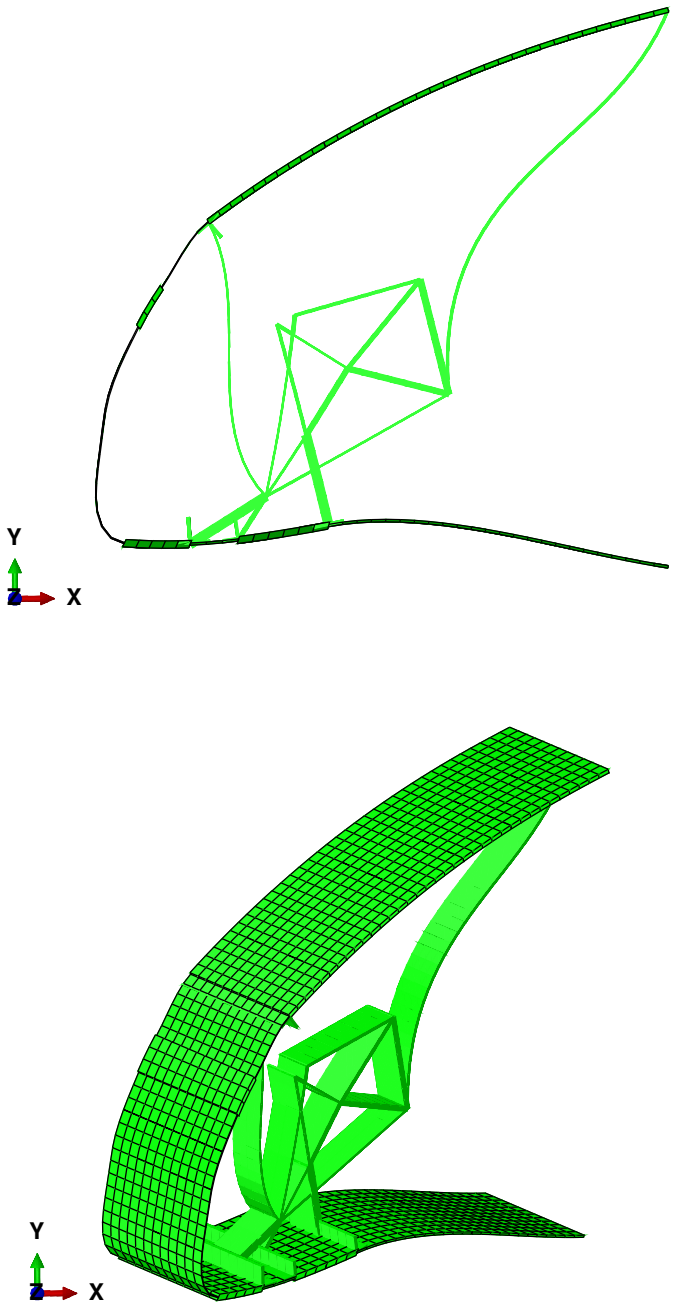

Figure 5.4: Isotropic material: deformed shape of the initial solution

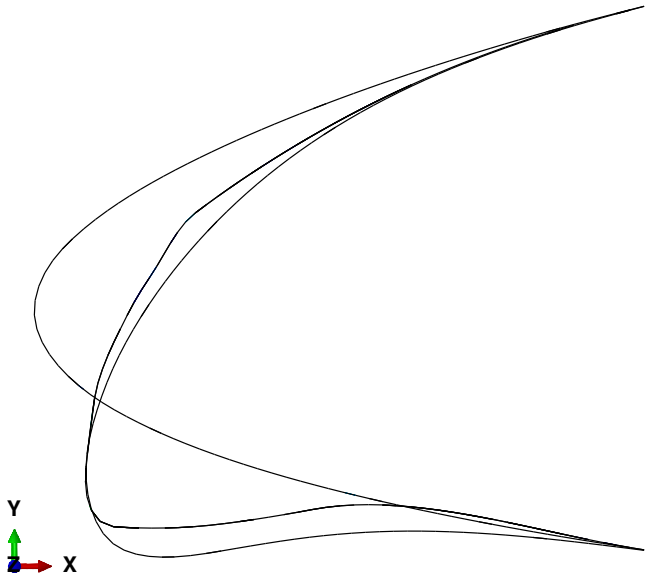

Figure 5.5: Isotropic material: initial solution undeformed/deformed shape and target shape

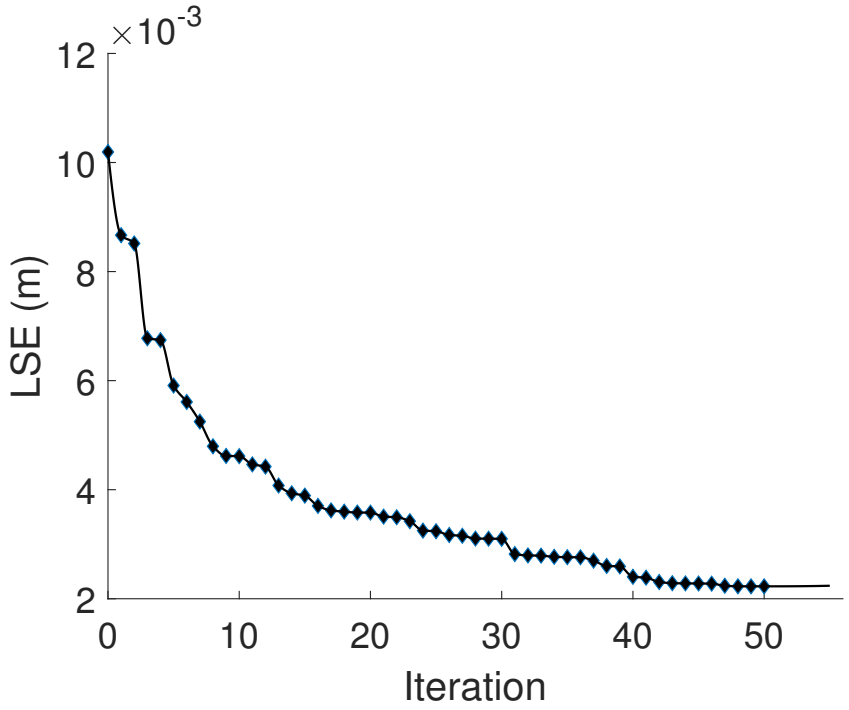

Figure 5.6: Isotropic material: LSE vs iteration

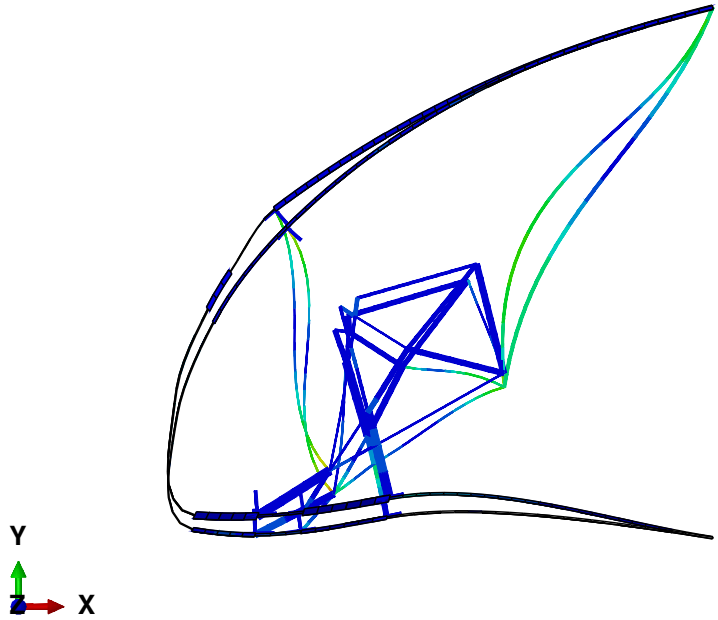

Figure 5.7: Isotropic material: initial solution and optimal solution deformed shapes

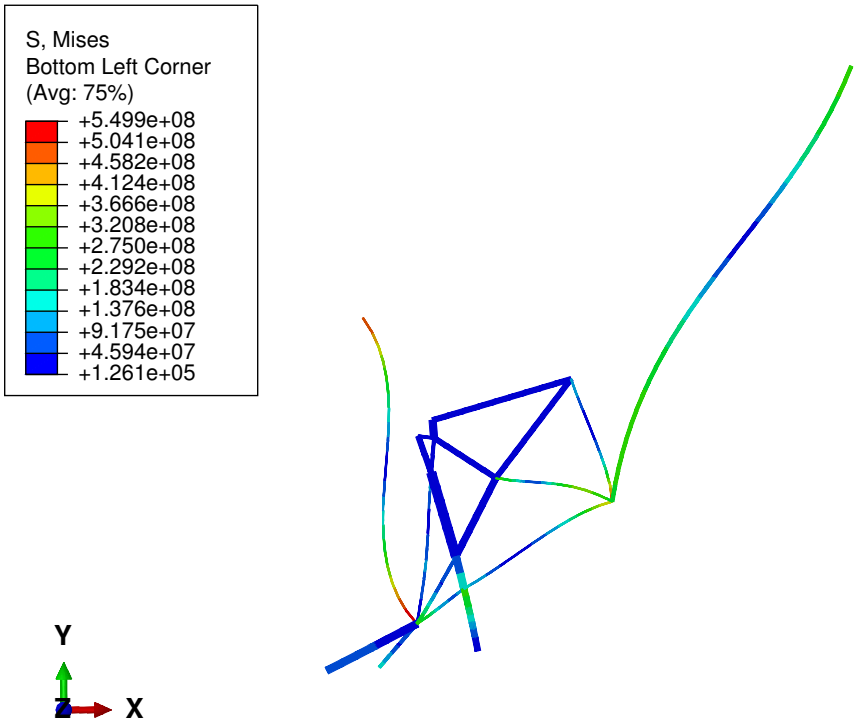

Figure 5.8: Isotropic material: Von Mises stress in the rib

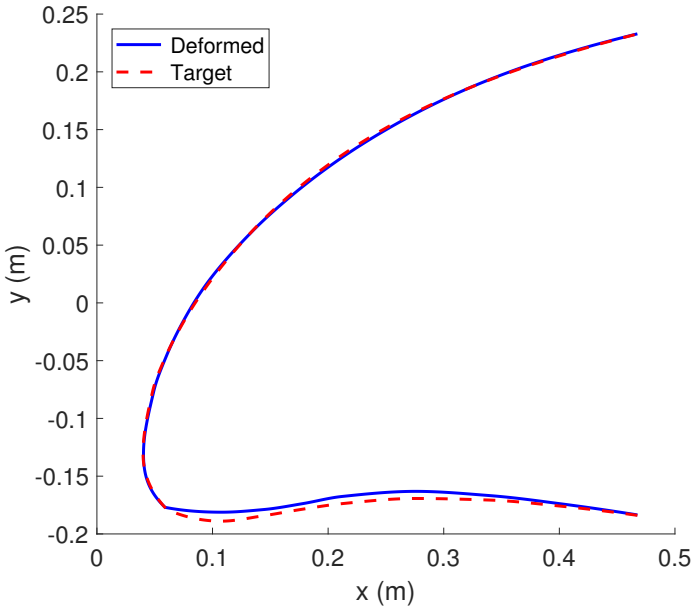

Figure 5.9: Isotropic material: optimal solution deformed shape and target shape

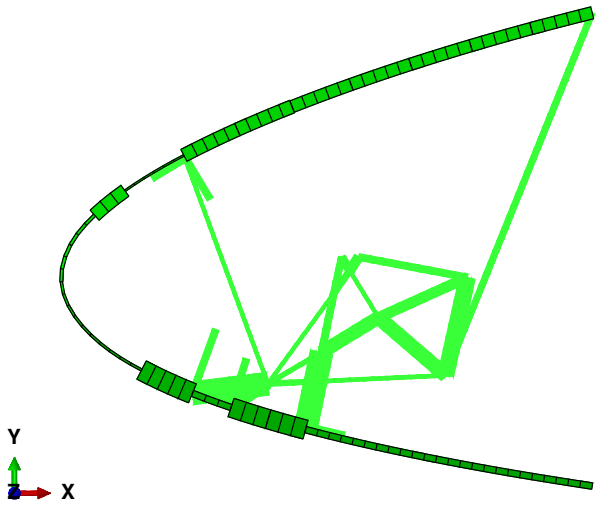

(a) Initial solution

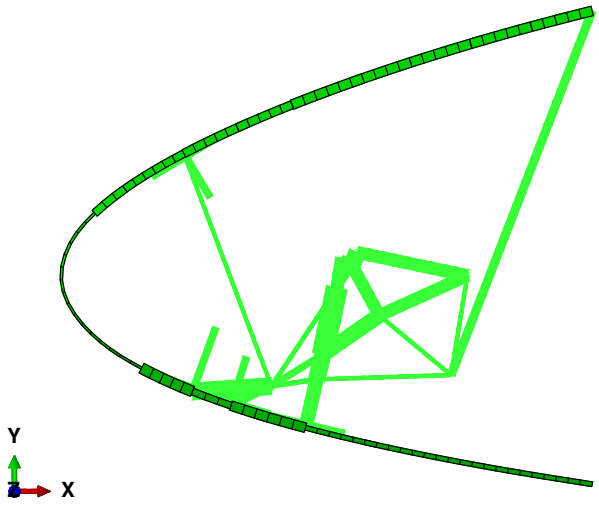

(b) Optimal solution

Figure 5.10: Isotropic material: thicknesses

The results show that the gradient-based optimization, coupling Matlab optimizer and Abaqus finite element solver, is effective in performing the improvement of the kinematic requirement. Indeed, a meaningful reduction of the LSE between the optimal deformed shape and the target shape, with respect to the initial deformed shape, has been achieved. The LSE has been decreased from 10.19 mm to 2.23 mm. The comparison between the initial deformed shape and the optimal deformed shape shows the greater droop angle that characterizes the optimal solution and also its smoother skin surface. Right now, the achieved deformed solution shows a better agreement with the target morphing shape.
Concerning the comparison related to the sizing variables, it can be noted that in order to minimize the objective function with respect to the initial solution, a different arrangement of the internal mechanism in-plane thicknesses is required to allow the desired improvement. Moreover, also the internal points positions are slightly changed.
Concerning the stress limitation, a maximum stress value equal to 549.9 MPa indicates that stress constraint is satisfied within the optimization analysis. However it must be remembered that the selected admissible value is overestimated.
Therefore, the presented results have a purely numerical relevance. They demonstrate the strength of the developed optimization procedure, however the obtained optimal solution can't be considered feasible, in the absence of elastic materials with a sufficiently large elastic range.

In addition to the reported analysis, still from the numerical validation point of view, an optimization analysis without including the position of the internal points has also been performed. This corresponds to a classical sizing optimization. It has got rapidly to convergence, with a minimum LSE value equal to 2.73 mm, slightly higher than the optimum previously obtained. This means that the increased computational cost due to the higher number of variables when the position variation is allowed, may not assure an advantage and hence it would be worthless, at least when the adopted material is the same of the genetic algorithm optimization.
The LSE optimization history is shown in Figure 5.11.

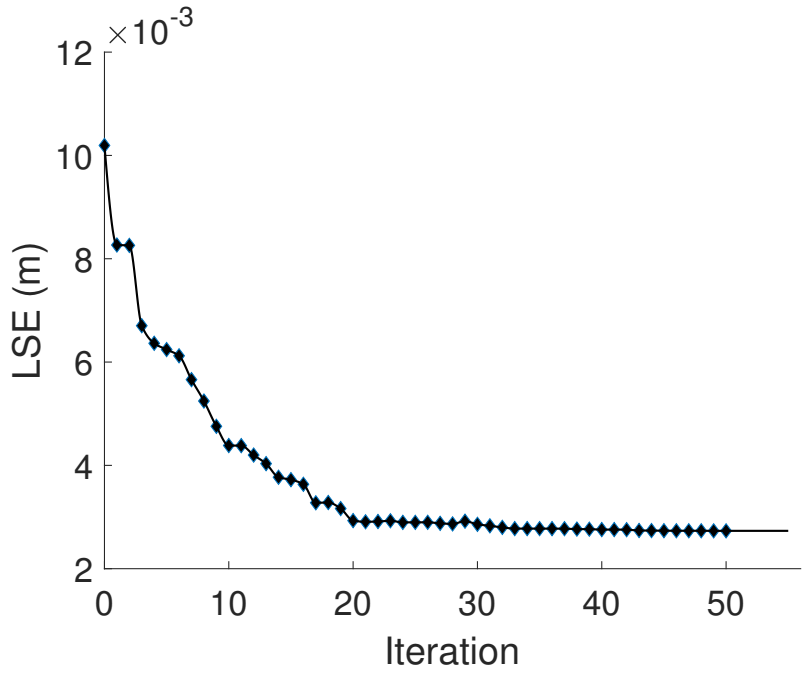

Figure 5.11: Isotropic material: LSE vs iteration (sizing variables only)

5.1.2 Nitinol material

Nitinol behaviour and its properties have been widely described in section 3.3. Here this material is adopted in the same optimization analysis previously performed with the isotropic material.
At first, a static analysis in the droop nose configuration is considered to evaluate the LSE and the maximum internal stress for the starting solution. The deformed shape is shown in Figure 5.12. Its comparison with the undeformed shape and the target shape is represented in Figure 5.13. The deformed shape is characterized by an LSE value of 10.22 mm. Therefore the adoption of a different material with the topology designed using the isotropic material gives no appreciable difference concerning the initial solution. The maximum Von Mises stress in the mechanism is 448 MPa, while $LSE_{NLF} = 0.4$ mm. Therefore the initial solution is feasible. Moreover, the maximum stress is less than that obtained for the isotropic material. This stress reduction, with the same global deformation, is one of the reasons that push in the direction of the use of superelastic materials in the design of compliant structures.
The gradient-based optimization is run and it converges to an optimal solution in 49 iterations. The evolution of the objective function with the iteration number is shown in Figure 5.14. The LSE for the optimal solution is 1.44 mm. Maximum stress in the rib is 462 MPa. The comparison between the initial deformed shape and the optimal deformed shape is shown in Figure 5.15. The stress level inside the mechanism is shown in Figure 5.16.
Figure 5.17 illustrates the comparison between the optimal deformed shape and the target one.
Figure 5.18 compares the optimization variables between the starting solution and the optimal solution. For a more clear visualization, thickness values are magnified by a factor 3.

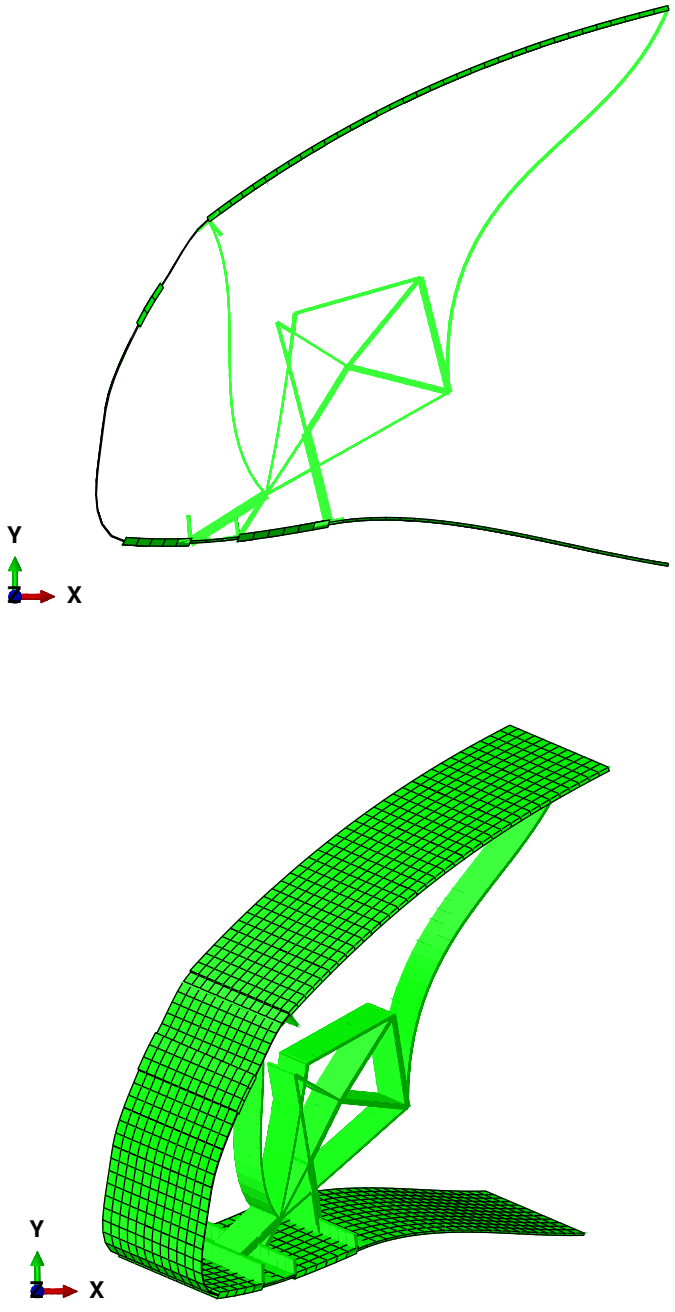

Figure 5.12: Nitinol: deformed shape of the initial solution

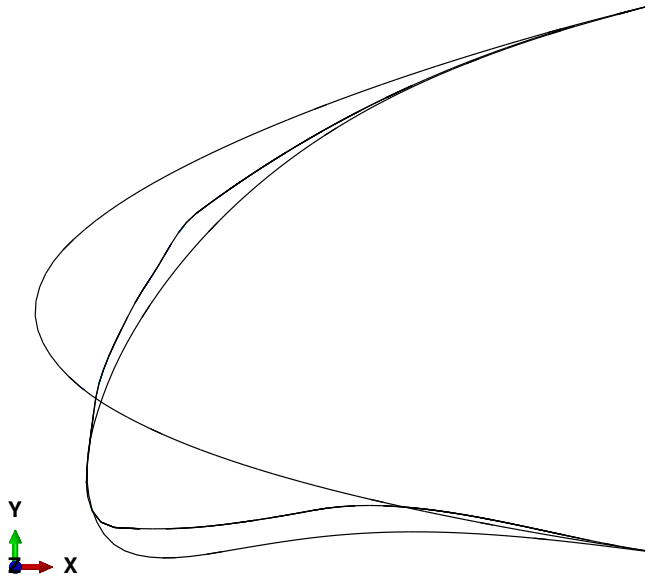

Figure 5.13: Nitinol: initial solution undeformed/deformed shape and target shape

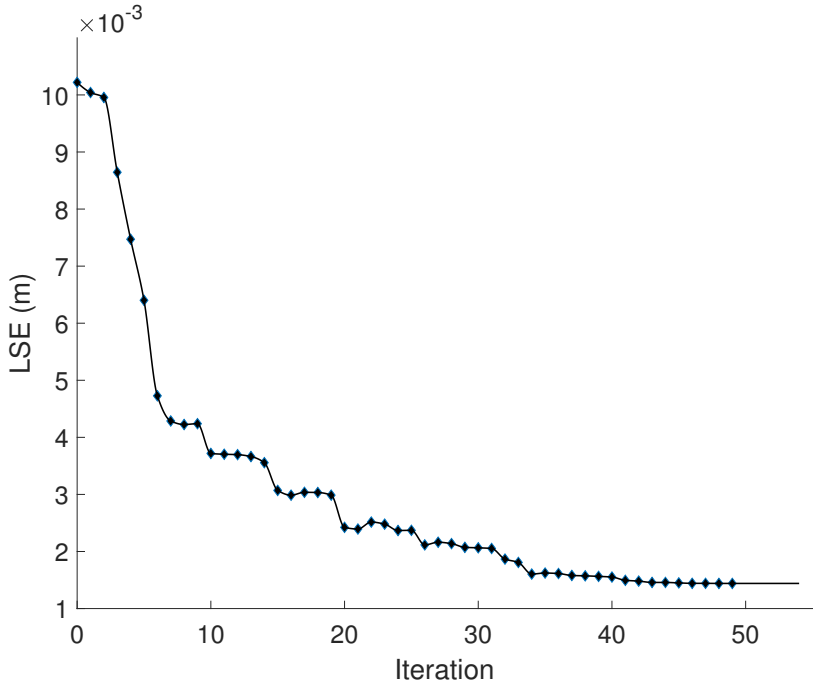

Figure 5.14: Nitinol: LSE vs iteration

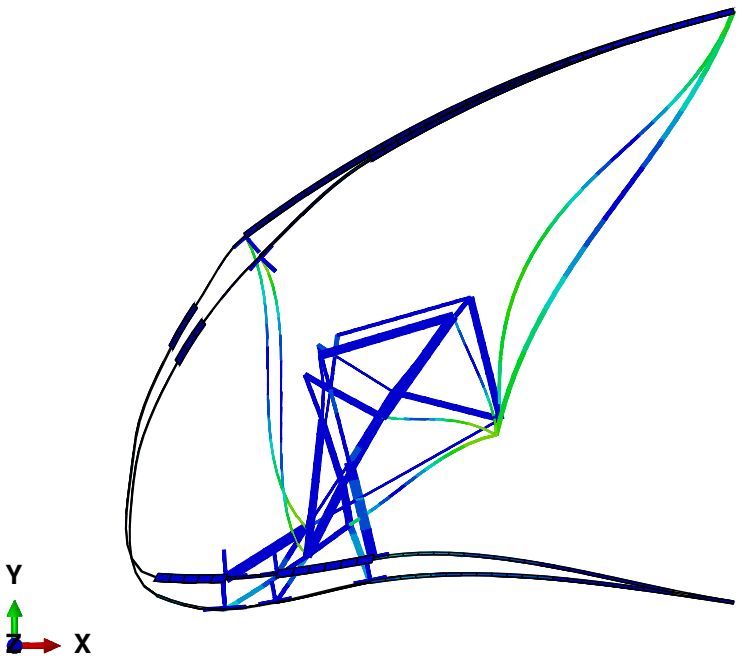

Figure 5.15: Nitinol: initial solution and optimal solution deformed shapes

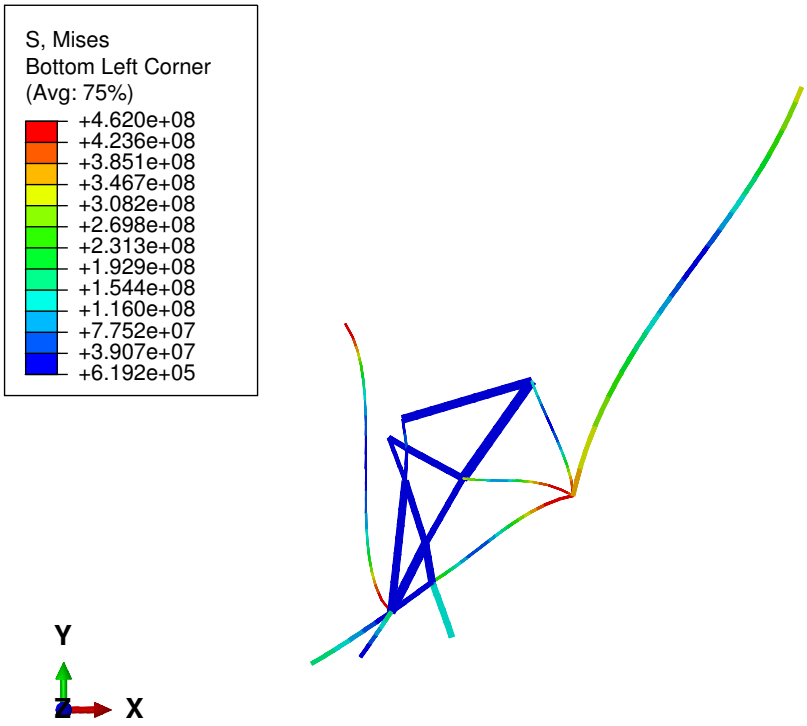

Figure 5.16: Nitinol: Von Mises stress in the rib

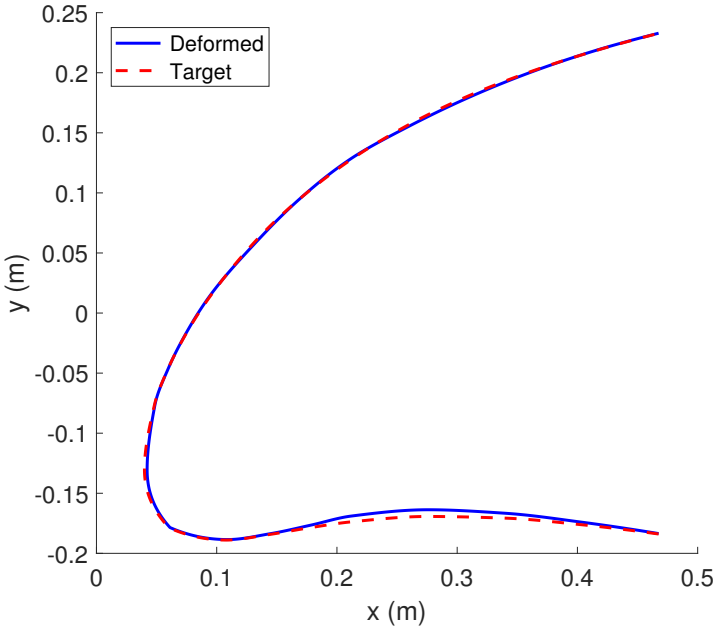

Figure 5.17: Nitinol: optimal solution deformed shape and target shape

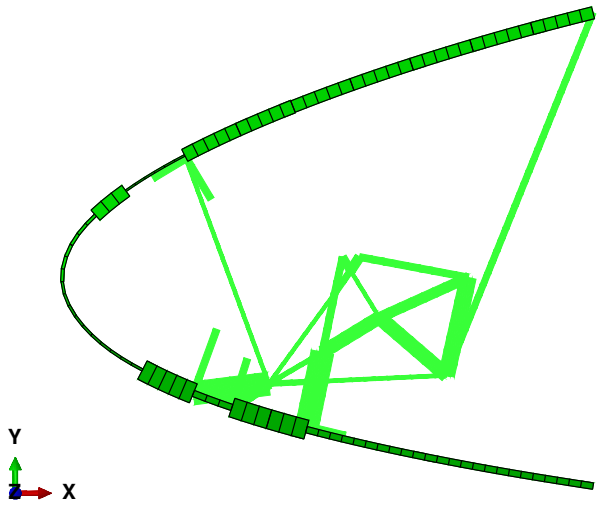

(a) Initial solution

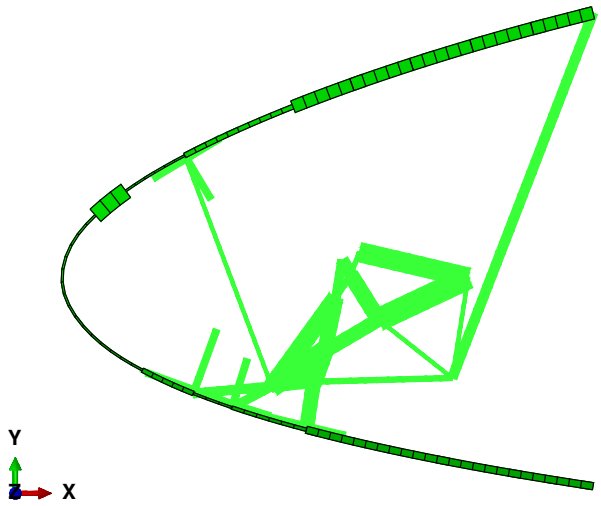

(b) Optimal solution

Figure 5.18: Nitinol: thicknesses

The results show a significative LSE reduction, from 10.22 mm to 1.44 mm, even better than that obtained with the isotropic material (2.23 mm).
Now the agreement between the optimal deformed shape and the target shape is almost perfect. It must be observed that the LSE reduction is again associated with a rearrangement of the thickness distribution inside the compliant mechanism.
The maximum stress in the internal mechanism is 462 MPa. The corresponding maximum strain is 0.018, which is in the range of the recoverable strains. These results reveal that:

- when dealing with compliant structures large strains are expected, hence materials able to provide them are preferred;
- the existence of the stress plateau allows to limit the stress values in the structure;
- the possibility to exploit a large range of deformations allows to achieve a meaningful improvement of the kinematic requirement, more than that a conventional elastic material can provide.

Also in combination with the adoption of Nitinol, an optimization analysis without including the position of the internal points among the optimization variables has been performed. The LSE optimization history is shown in Figure 5.19. The optimization analysis rapidly gets to convergence, however the minimum LSE value is equal to 4.18 mm, significantly worse than the previously obtained optimum value. This means that adapting an existing topology to a different material requires the possibility of slightly moving the internal points of the mechanism, otherwise a sufficient improvement of the objective can't be achieve.

To sum up, the use of Nitinol in combination with the more advance version of the gradient-based optimization here discussed, guarantees a meaningful enhancement of the existing design that uses isotropic material.
Moreover, also the results of section 5.2 will show that Nitinol not only improves the morphing solution from the aerodynamic performance point of view, it may assure the structural feasibility that the isotropic material isn't able to guarantee from the strength requirement point of view.

Finally, the comparison between the optimal isotropic material solution and the optimal Nitinol solution in terms of optimization variables and deformed shape is shown in Figure 5.20 and Figure 5.21, while Figure 5.22 shows the topological differences between the two optimal solutions.

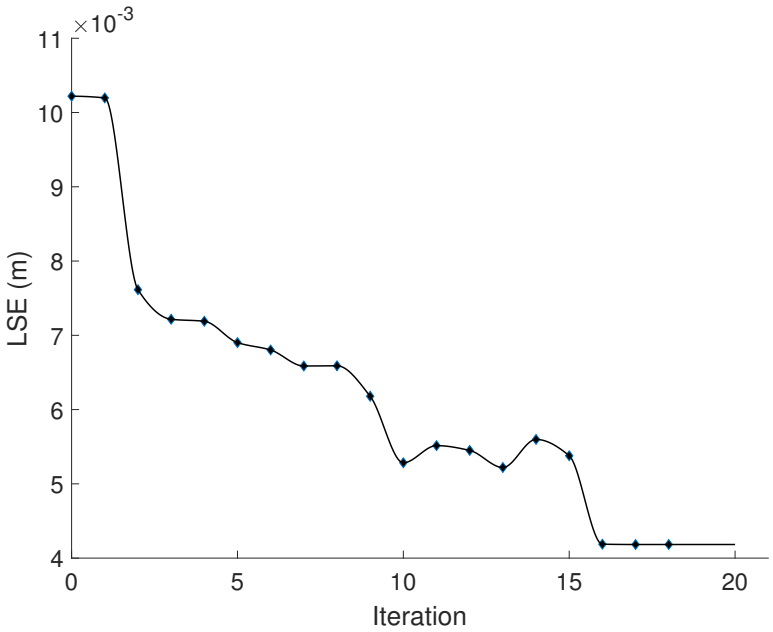

Figure 5.19: Nitinol: LSE vs iteration (sizing variables only)

Apart from the considerations about the kinematic and structural requirements that have been already discussed, here the focus is on the values which the optimization variables assume for the two materials. It is evident, as expected, that different materials are characterized by different values of optimization variables that minimize the objective function.

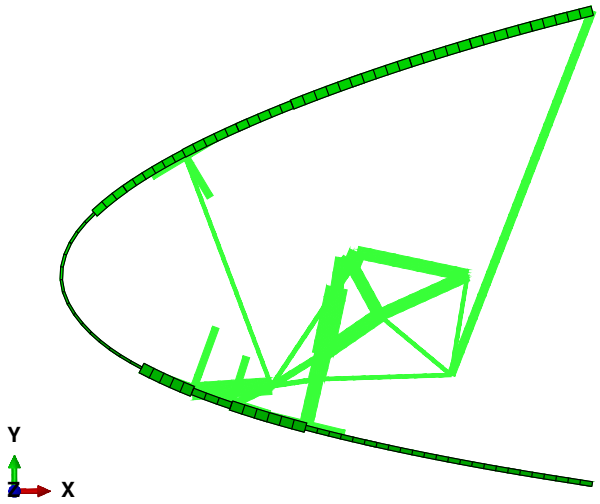

(a) Isotropic material

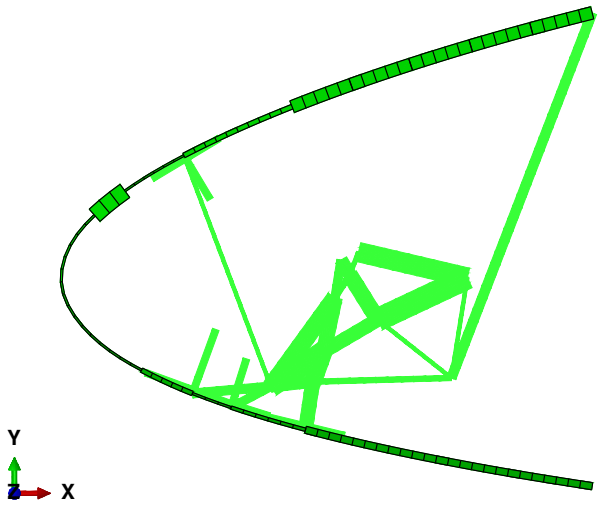

(b) Nitinol

Figure 5.20: Optimal solutions: thicknesses

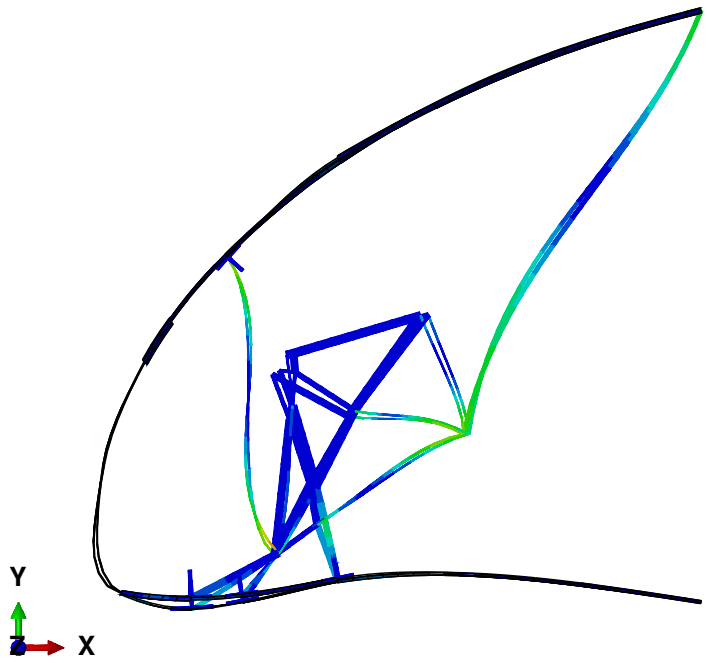

Figure 5.21: Optimal solutions: isotropic material and nitinol deformed shapes

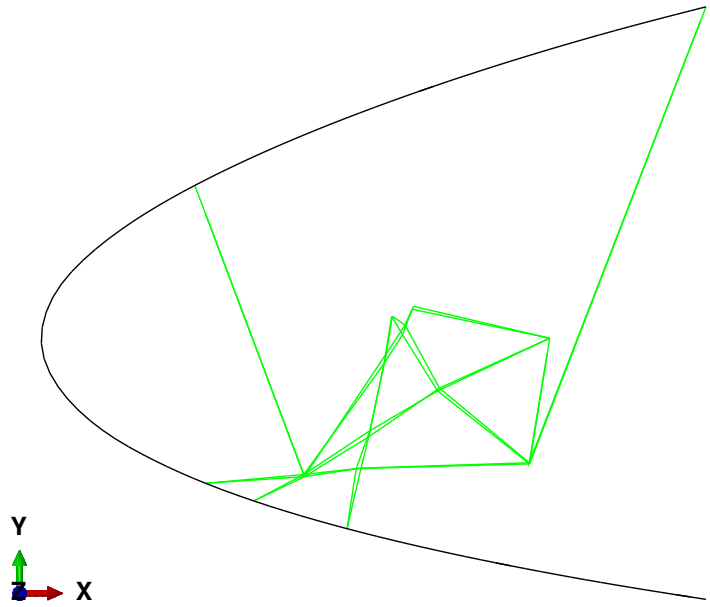

Figure 5.22: Optimal solutions: isotropic material and nitinol undeformed shapes

5.2 Compliant mechanism shape optimization

In this section the results of the shape optimization of the compliant mechanism are presented and discussed. The procedure is applied to the optimal solutions previously found by means of the gradient-based optimization, both in case of isotropic material and Nitinol, leading to different results and conclusions.
Starting from the beam model of the optimal solution, a CAD model is generated. It represents the optimal internal compliant mechanism, featuring the actual internal points position and the thicknesses of the optimal solution. Moreover adequate hypothesis for the fillets radiuses are done. Their improvement is one of the aim of the current optimization step.
The sketch is imported in Abaqus and a two-dimensional solid mesh is generated. At first a static analysis is performed in order to observe the behaviour of the mechanism and to identify the most critical regions. Then the same static analysis is included in the optimization analysis in order to evaluate the objective function and the constraints.

5.2.1 Isotropic material

The two-dimensional solid elements model of the compliant mechanism made of isotropic material is shown in Figure 5.23.
The result of the static analysis with imposed displacements at the boundary is shown in Figure 5.24. In addition to the global deformation, the most stressed regions are highlighted. It can be noted a maximum Von Mises stress of 1200 MPa, higher than the value obtained from the beam model. This can be explained by the fact that a beam model can't give an accurate estimate of the stress in singular points like its extremities or the intersections. The aim of the shape optimization is to try to reduce these localized stress peaks.
Shape optimization is firstly applied to the region depicted in Figure 5.24(c) where the maximum stress is 877 MPa. The design area is shown in Figure 5.25. The objective function is the minimization of the maximum principal stress evaluated in the surroundings of the optimization region. The optimization performs ten iterations, providing a redistribution of the stress and a reduction of its maximum peak. The comparison between the initial solution and the optimized solution is shown in Figure 5.26. The stress is decreased at a value of 598 MPa, however it is still too high for an aluminium material. A similar optimization procedure is carried out on the region of Figure 5.24(b), but failing.

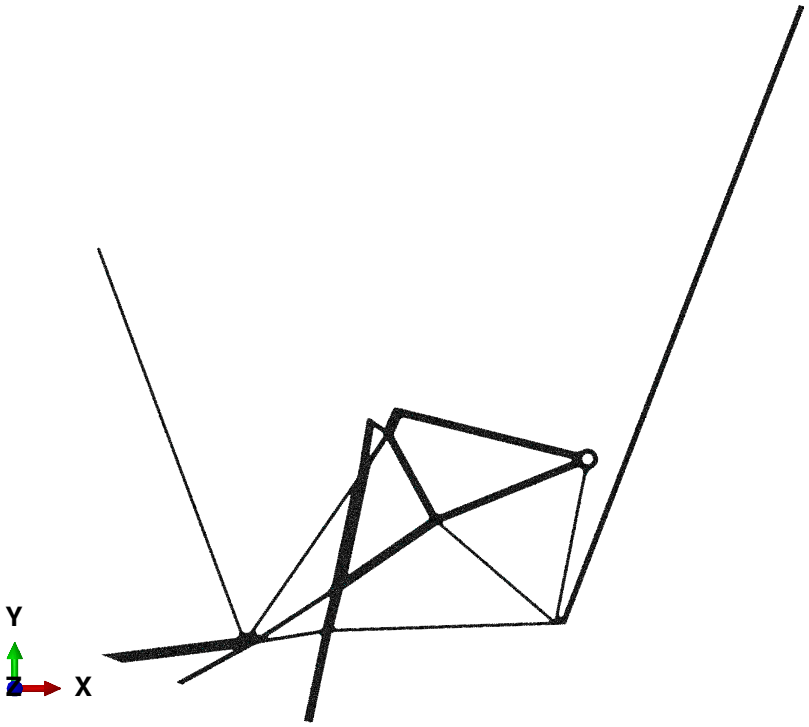

Figure 5.23: Isotropic material: 2D model of the compliant mechanism

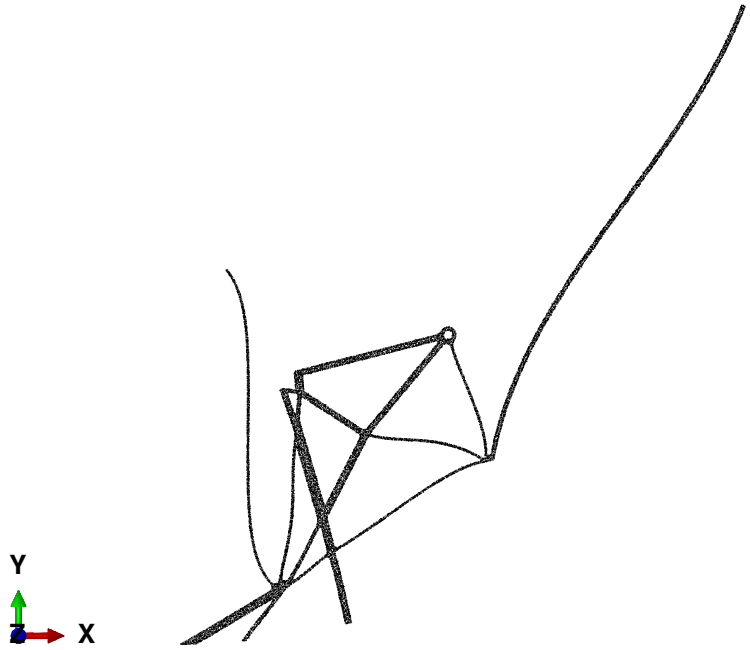

(a)

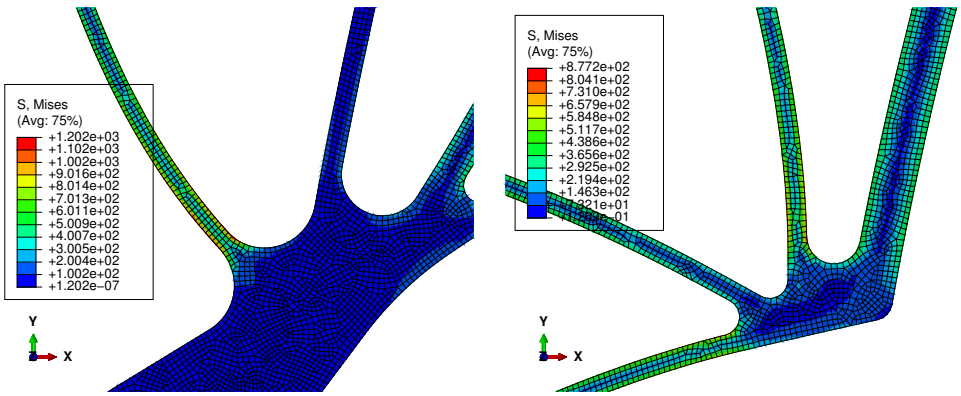

(b) (c)

Figure 5.24: Isotropic material: static analysis of the compliant mechanism

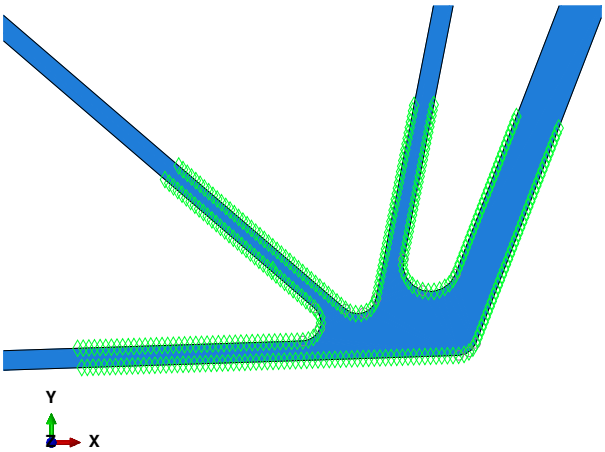

Figure 5.25: Isotropic material: optimization region

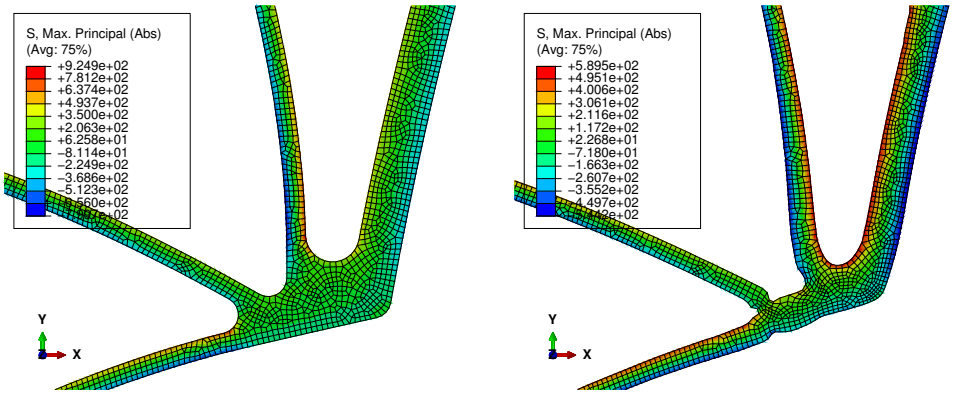

(a) Initial solution (b) Optimum solution

Figure 5.26: Isotropic material: shape optimization

Therefore the first application demonstrates that the procedure is able to modify the junction region in such a way to reduce the stress, however it can't overcome the intrinsic limitation of using a conventional linear material for compliant mechanism devices.

5.2.2 Nitinol material

The two-dimensional solid elements model of the compliant mechanism made of Nitinol is shown in Figure 5.27.

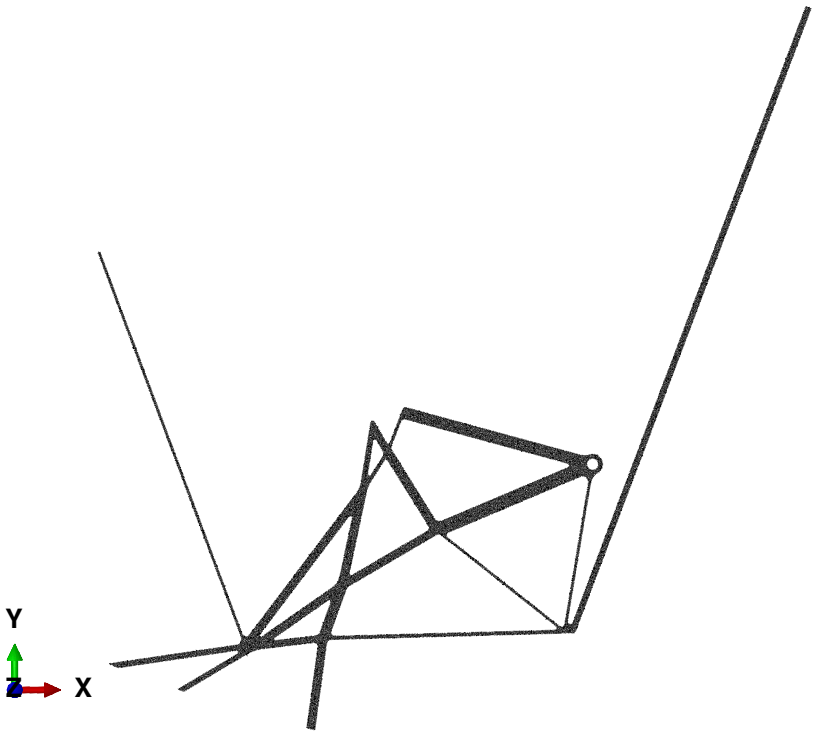

Figure 5.27: Nitinol: 2D model of the compliant mechanism

The result of the static analysis with imposed displacements at the boundary is shown in Figure 5.28. In addition to the global deformation, the most stressed regions are highlighted, the same of the previous case. Also in case of Nitinol the adoption of a more refined finite element model shows stress concentrations, hence shape optimization is needed.
Shape optimization is firstly applied to the region depicted in Figure 5.28(c) where the maximum stress is 549 MPa. The objective function is the minimization of the maximum principal stress evaluated in the surroundings of the optimization region. After eight iterations the maximum stress value is reduced to 525 MPa. The comparison between the initial solution and the optimized solution is shown in Figure 5.29.

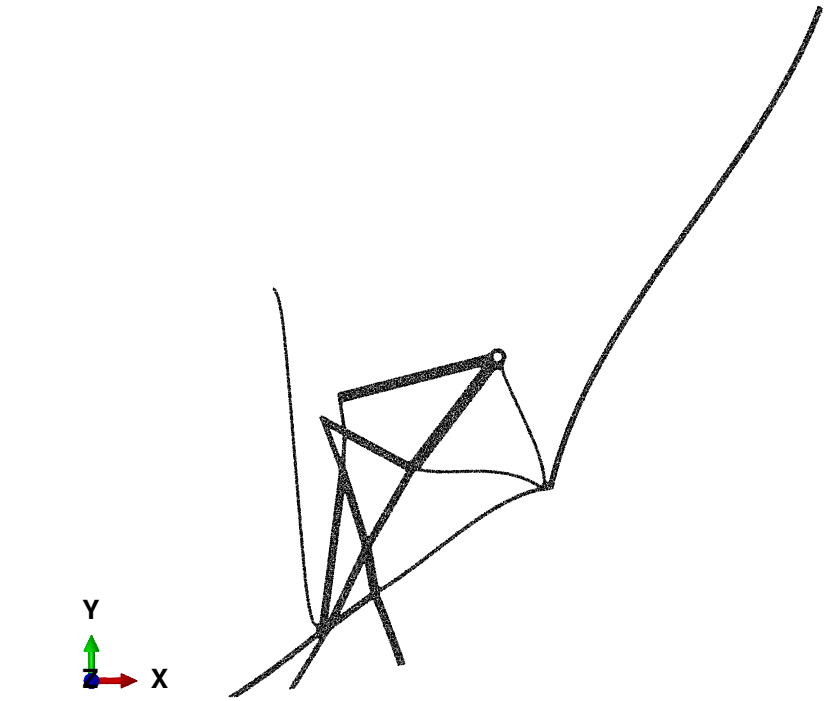

(a)

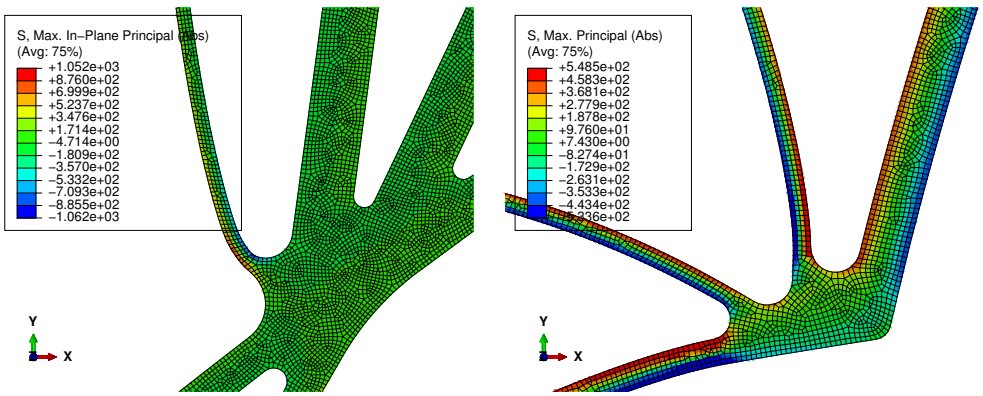

(b) (c)

Figure 5.28: Nitinol: static analysis of the compliant mechanism

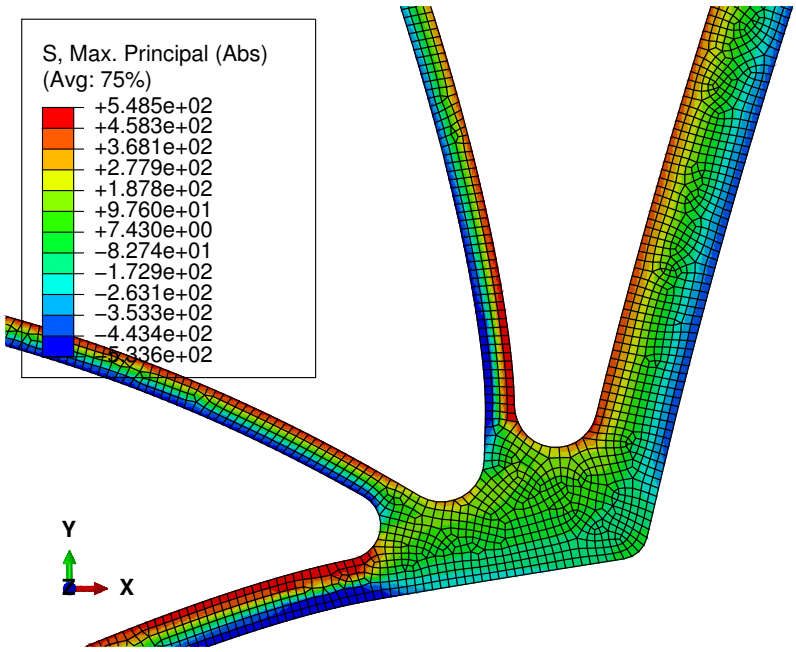

(a) Initial solution

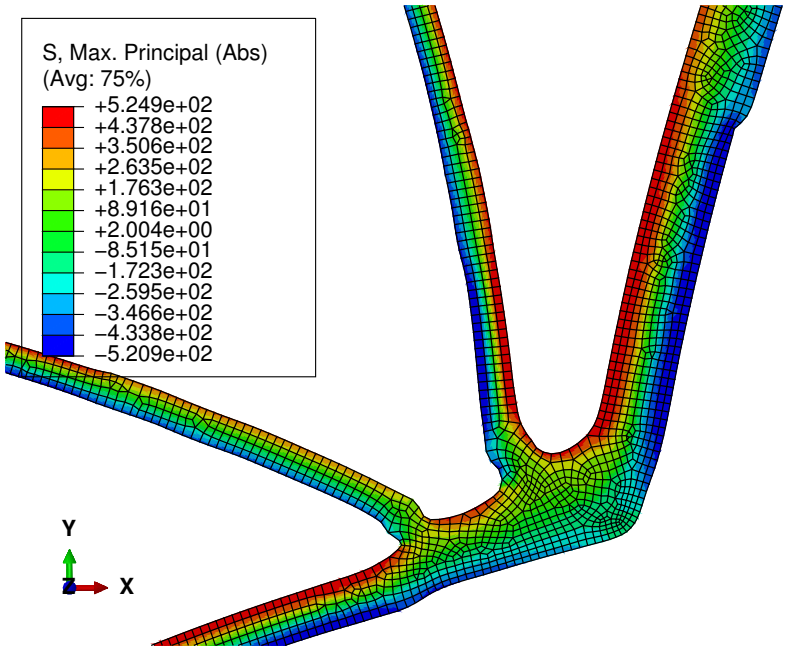

(b) Optimum solution

Figure 5.29: Nitinol: shape optimization for the right region

It can be seen that the redistribution of stress is more effective when a superelastic material is used. Moreover, the transformation strains are significantly reduced, from a maximum value of 0.0427 to a maximum value of 0.0157. The stress-strain relationship for the loading history in the two cases is reported in Figure 5.30.
A similar optimization procedure is carried out on the region of Figure 5.28(b). After seven iterations the maximum stress value is reduced to 541 MPa. The comparison between the initial solution and the optimized solution is shown in Figure 5.31.
Also in this case the shape optimization achieves the stress reduction. Concerning the strains, Figure 5.32 shows that the initial solution is not acceptable since the plateau is fully exploited and then the stress reaches the critical value for slip: permanent deformations will remain upon unloading. Differently, the optimized solution shows an acceptable behaviour: the plateau is not fully exploited and deformations can be recovered. Therefore shape optimization is crucial in the achievement of a feasible structural solution, as well as the adoption of a superelastic material such as Nitinol.
Obviously the situation must be examined more deeply, manufacturing and testing are mandatory, however these preliminary numerical results give confidence to the developed optimization procedure and its tools, as well as the introduction of the superelastic material.
Moreover, also from a numerical point of view a verification is needed, in order to assess if the shape optimization phase decreases the performance in terms of LSE with respect to what has been estimated by the gradient-based optimization.

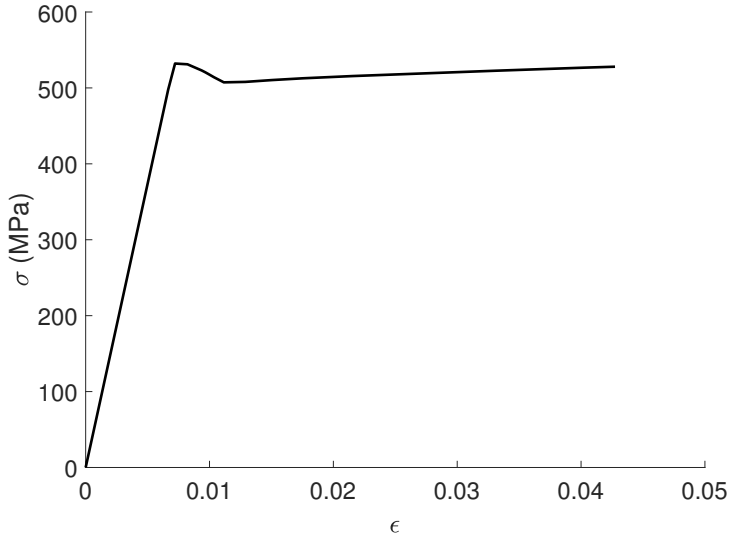

(a) Initial solution

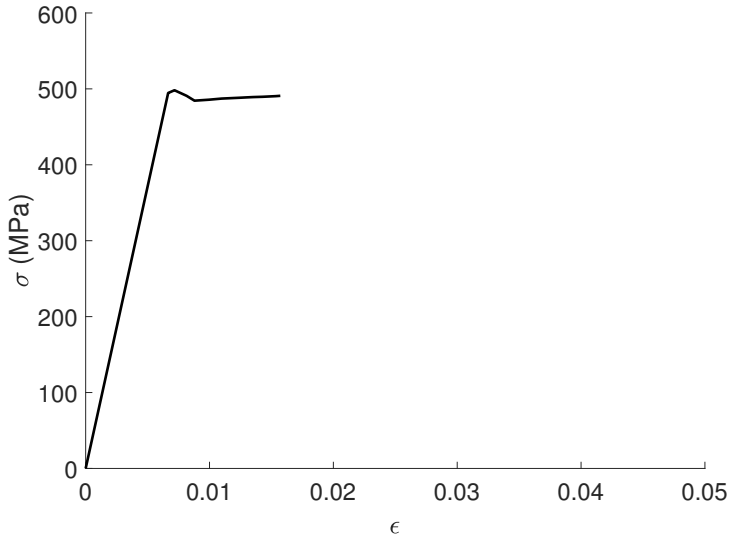

(b) Optimum solution

Figure 5.30: Nitinol: stress-strain curve in the right region

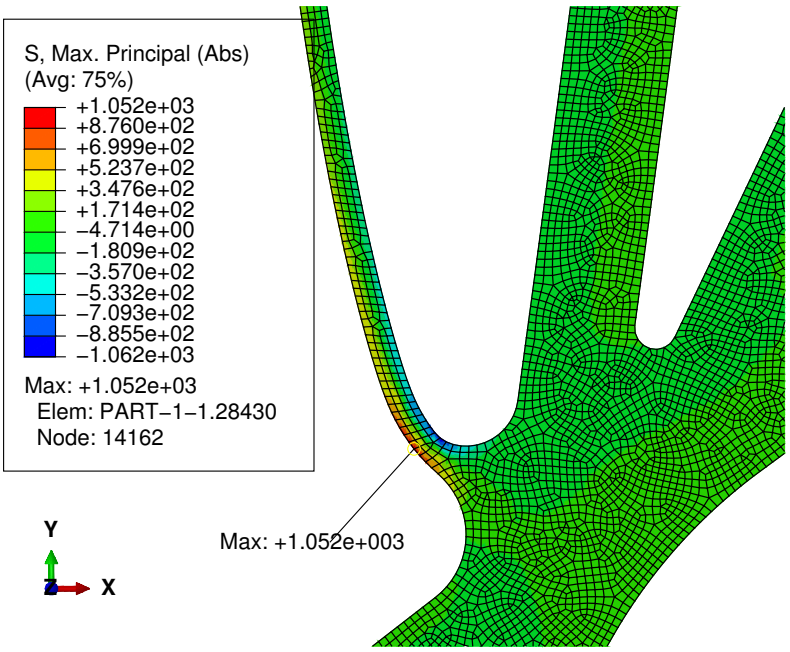

(a) Initial solution

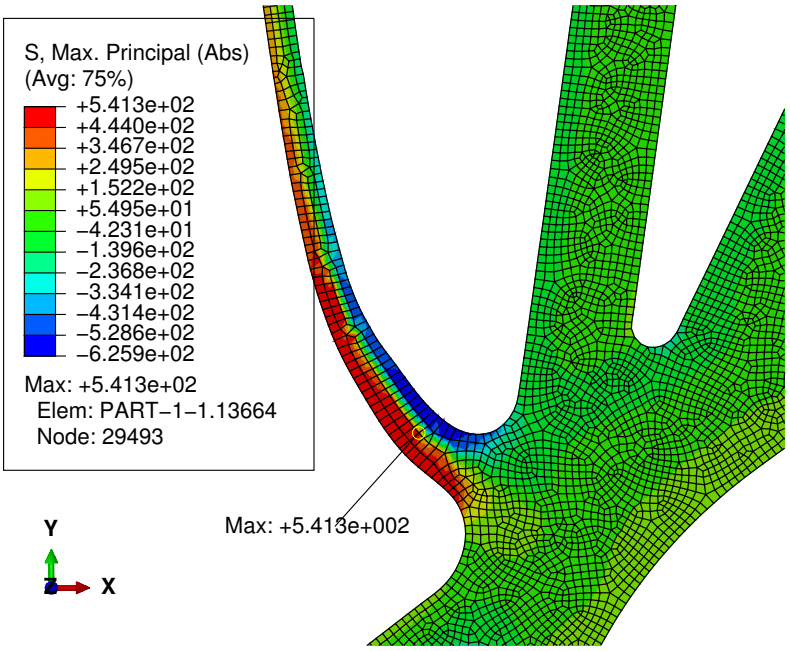

(b) Optimum solution

Figure 5.31: Nitinol: shape optimization for the left region

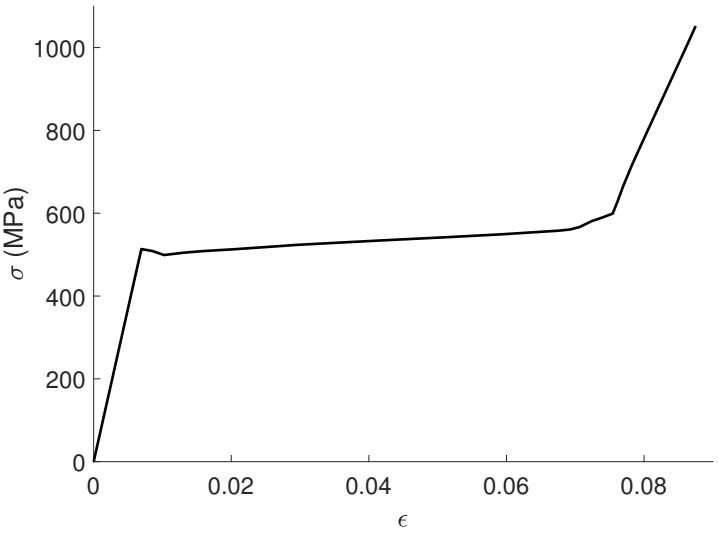

(a) Initial solution

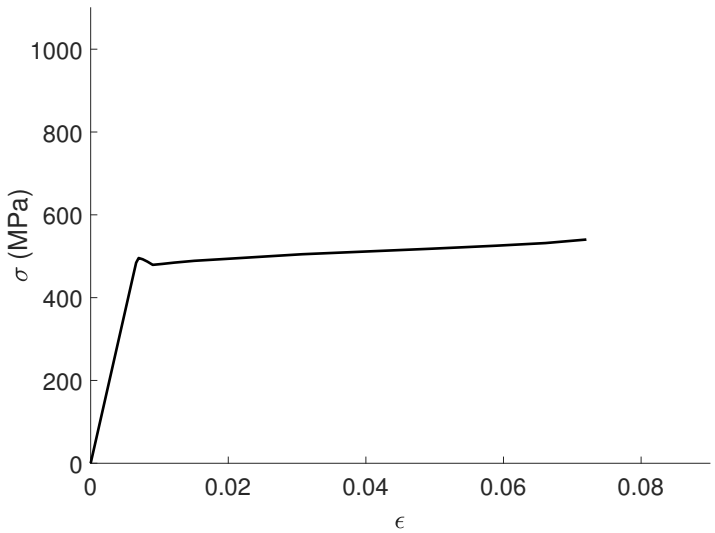

(b) Optimum solution

Figure 5.32: Nitinol: stress-strain curve in the left region

5.3 Considerations about the use of Nitinol

The results of sections 5.1 and 5.2 have shown the comparison between Nitinol and the isotropic aluminum alloy as material for the internal compliant mechanism, highlighting the advantages of the adoption of the superelastic material, both in terms of aerodynamic requirements (LSE) and structural feasibility. Anyway, it must be remembered the dependence of superelastic behaviour from the transition temperatures in relation with the application temperature. The previously shown results were referred to a design temperature $T_0 = 293\,\mathrm{K}$, but the choice of the parameters was done aiming to achieve a wide range of possible application temperatures. In this section the optimal solution of the gradient-based optimization using Nitinol, is verified at the limit temperatures, $T_{min} = 263\,\mathrm{K}$ and $T_{max} = 313\,\mathrm{K}$. Once the optimal solution has been obtained, a kinematic chain able to guarantee the desired displacement of the actuation point must be designed. Therefore, analyses with imposed displacements at the actuation point are performed. The displacement history is extracted from the results obtained at the design temperature. The results of these analyses in terms of deformed shape are shown in Figure 5.33. Table 5.1 compares the achieved LSE values at the different temperatures. Moreover it reports the magnitude of the actuation force required to accomplish the imposed displacement in each case.

Table 5.1: Nitinol: optimal solution at different temperatures

Temperature (K)	LSE (mm)	Actuation Force (N)
263	1.77	422
293	1.44	470
313	1.57	498

As expected, the smaller LSE is obtained at the design temperature, but the values in the off-design conditions do not worsen considerably. The different actuation force required is due to the different stress level at which the plateau starts changing the operative temperature. The comparison of the maximum principal stress-strain relationships in the most critical point of the structure is shown in Figure 5.34. In addition to the usual loading phase, it reports the unloading of the structure and the recovery of the transformation strains. Lower the temperature, lower the plateau stress and higher the transformation strain.

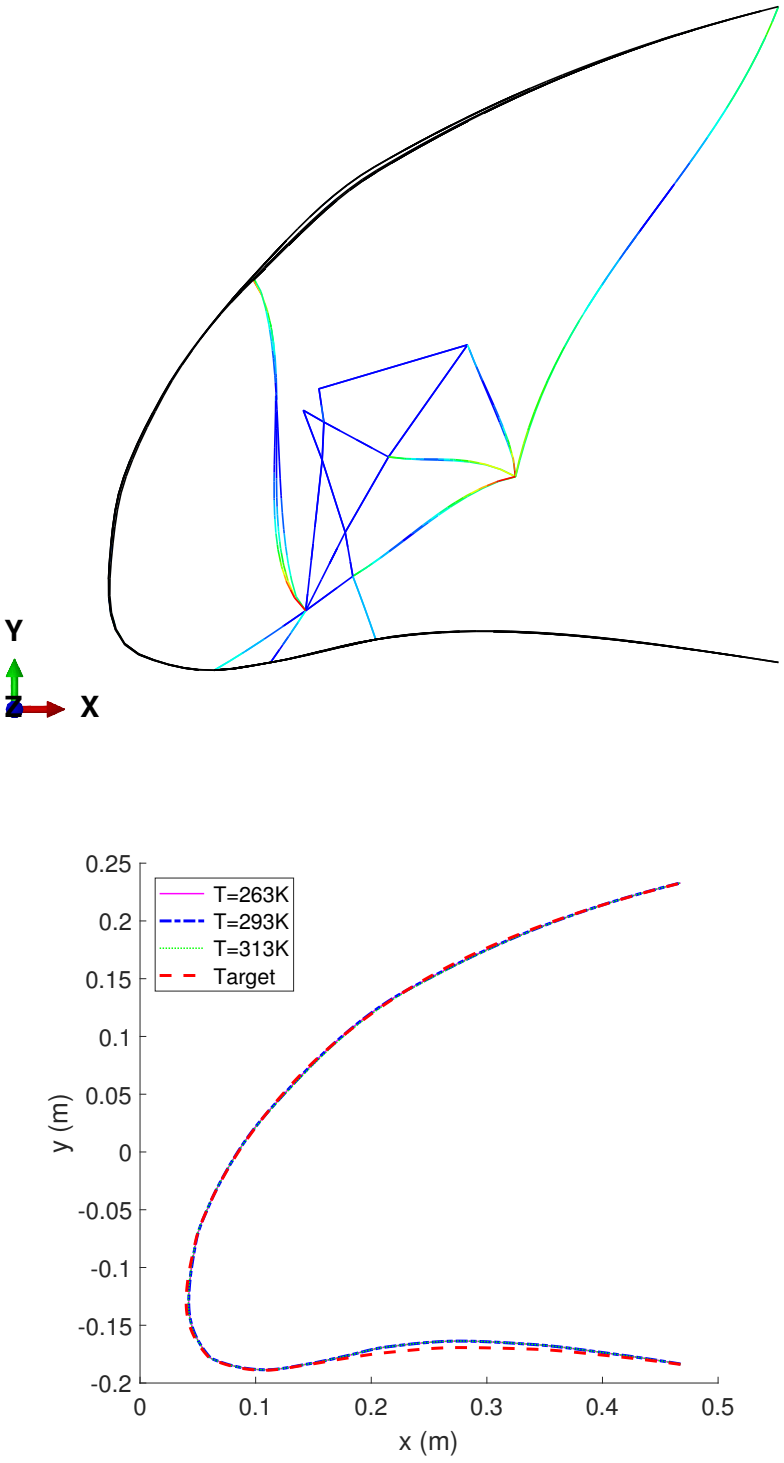

Figure 5.33: Nitinol: deformed shape of optimal solution at different temperatures

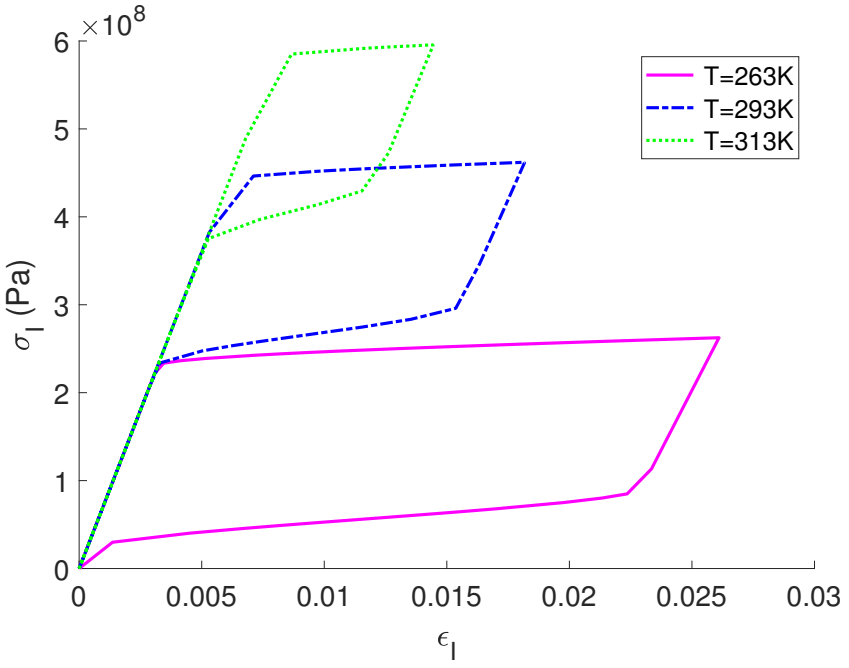

Figure 5.34: Nitinol: stress-strain relationship at different temperatures

5.4 Considerations about the optimization procedure

The results of the present chapter have shown the application of the optimization procedure and its benefits in terms of fulfillment of the requirements. A local refinement of the solution obtained from the genetic algorithm optimization allows a substancial improvement of the morphing device. Moreover, even adopting the same topology, the application of a different material is possible and the results demonstrate a further enhancement if Nitinol is selected. Indeed, it has permitted the achievement of a better kinematic requirement, as well as the withstanding of the loads within the material strength limits. This confirms the suitability of superelastic materials for compliant mechanisms application in the morphing field. The overall procedure can be considered validated since it is able to improve the starting solution, decreasing the LSE at the first step and reducing the stresses at the second step.
The proposed procedure is general for the application to morphing wings devices. Even though only an example of droop nose has been analyzed, the procedure can be straightforwardly extended to the optimization refinement of a trailing-edge morphing device.

Moreover, the optimization procedure allows to adapt a given topology to different airfoil shapes and also to different geometric scale of the same airfoil. An example of this is the scaling process performed when a scaled wind tunnel model has to be designed. This usually requires a complete redesign of the structure. However the application of the procedure to the 1:3 scaled model of the droop nose suggests the possibility to scale down the topology provided that the sizing variables and also the internal points position are re-optimized according to the requirements of the new model. The results are discussed in chapter 6.

Chapter 6

Applications

6.1 Preliminary design of a scaled wind tunnel model

In the framework of EU funded Clean Sky 2 REG-IADP AG2 project, one of the activity is related to the construction and testing of a wind tunnel model at scale 1:3 (WTT2). Its main purpose is the characterization and validation of NLF technology, but also the study of high lift conditions. The model is equipped with many features, among which the deployable morphing leading–edge. In this section a preliminary approach to the design of the scaled droop nose is presented, aimed at a further confirmation of the validity of the optimization procedure.
The design of scaled wind tunnel models represents a challenging problem since the scaling law for the stiffness is different from the geometric one. Therefore there is usually the need of changing the materials and the topology of the structure in order to reproduce the required characteristics. As already explained, the proposed optimization procedure is here applied to readapt the full scale topology to the scaled model, changing the sizing variables and the internal points position according to the optimization analysis in order to fulfill the requirements. Concerning the material of the mechanism, it must be inevitably changed. In order to identify material data for the design of the internal structure, based on previous experience at POLIMI [49], 3D printing technology can be selected for the manufacturing of the scaled model; a possibile technique is the Stereolithography (SLA) in combination with a fine powder on the basis of polyamide 12 (PA 2200), whose mechanical characteristics are reported in Table 6.1. This technique allows to realize morphing devices in a single piece with good accuracy in terms of thickness distribution (0.5 mm).

Table 6.1: Mechanical parameters of PA 2200

Parameter	Value
Flexural Modulus	1.4 GPa
Poisson's ratio	0.35
Flexural Strength	76 MPa

Concerning the skin, glass fibers composite material can be selected, whose mechanical properties are shown in Table 6.2.

Table 6.2: Mechanical parameters of glass

Parameter	Value
E_{11}	25 GPa
E_{22}	25 GPa
ν	0.20
G_{12}	4 GPa
G_{13}	4 GPa
G_{23}	4 GPa

6.1.1 Results

First of all, the geometry of the model and the set-up of the optimization problem are discussed. The airfoil shape, the internal mechanism topology, rib pitch and rib thickness are scaled down of a factor 3.

- The rib pitch p_{rib} is equal to 43.3 mm and it is used as span-wise length of the skin.
- The rib thickness w_{rib} is equal to 11.7 mm.
- The chord extension of the model is 155.7 mm.
- The actuation force F in the input point has vector components $(-31\,\text{N}, -2\,\text{N})$.
- The aerodynamic conditions taken into account are both at $Mach = 0.148$, Sea Level, corresponding to a dynamic pressure $q_D = 1550\,\text{Pa}$;

an angle of attack $\alpha = 10°$ is considered for the evaluation of the objective function while $\alpha = 0°$ for the deformability constraint. The pressure coefficient distributions are the same shown in Figure 5.1.

The scaled model corresponding to the inital solution is depicted in Figure 6.1 together with the original model.

Concerning the starting design variables, the thicknesses of the skin are

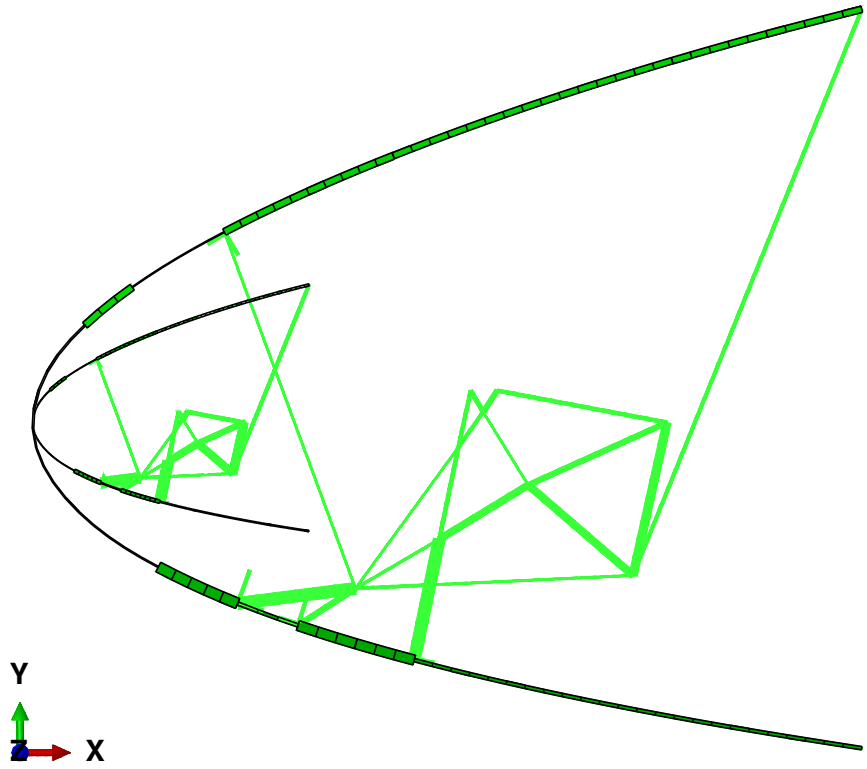

Figure 6.1: Scaled model and full scale model

reduced by the scaling factor, while the dimensions of the rib paths are preserved.

The other required data to set-up the problem are the limit values for the constraints and the bounds. For the deformability LSE tolerance a value of 10^{-4}m is selected. The admissible value in terms of stress is 76 MPa. The bounds for the sizing variables are $1\,\text{mm} \leq t_i^{rib} \leq 6\,\text{mm}$ and $0.2\,\text{mm} \leq t_j^{skin} \leq 4\,\text{mm}$. The internal points position can vary of $\pm 5\,\text{mm}$ both in x and y direction.

At first, a static analysis in the droop nose configuration is performed to evaluate the LSE and the maximum internal stress for the starting solution. The deformed shape is shown in Figure 6.2. It is characterized by an LSE value of 3.56 mm. The maximum Von Mises stress in the mechanism is 31 MPa, while $LSE_{NLF} = 0.06$ mm. Therefore the initial solution is feasible.
The gradient-based optimization is run and it converges to an optimal solution in 21 iterations. The evolution of the objective function with the iteration number is shown in Figure 6.3. The LSE for the optimal solution is 0.84 mm. Maximum stress in the rib is 31 MPa. The comparison between the initial deformed shape and the optimal deformed shape is shown in Figure 6.4. The stress level inside the mechanism is shown in Figure 6.5.
Figure 6.6 illustrates the comparison between the optimal deformed shape and the target one.
Figure 6.7 compares the sizing variables between the starting solution and the optimal solution. Moreover, Figure 6.8 shows the topological differences between the two solutions.

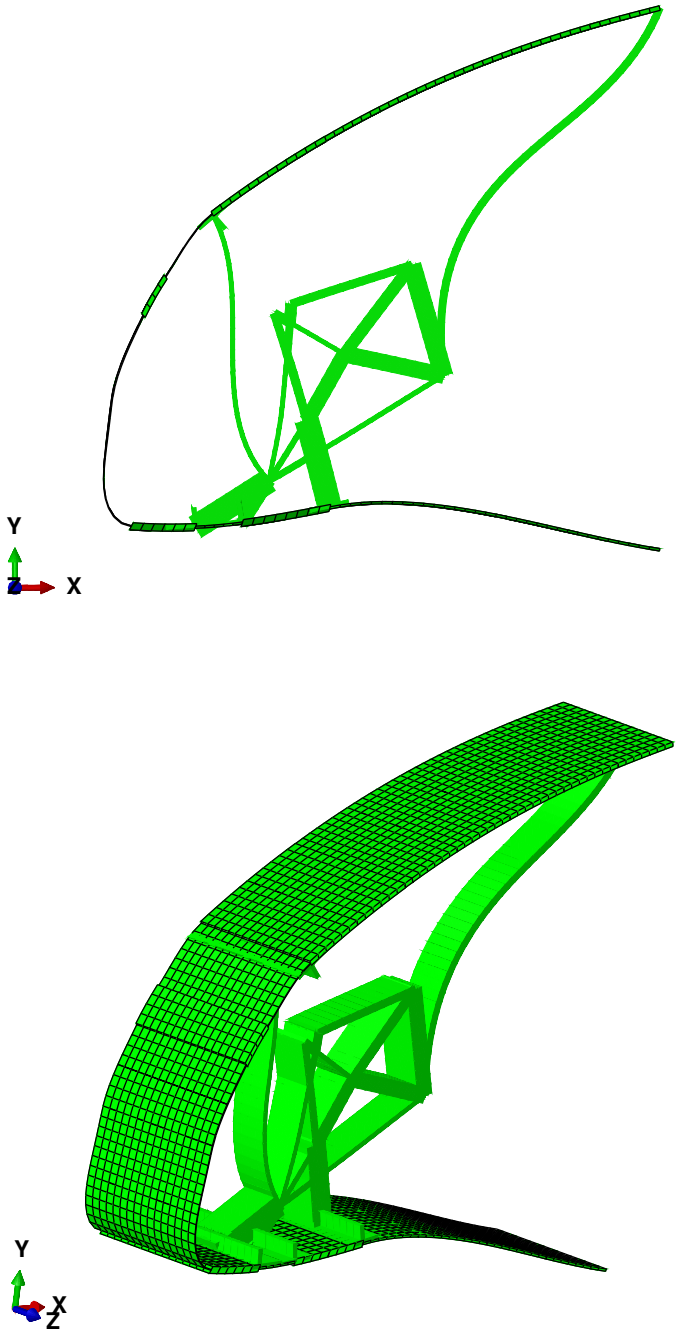

Figure 6.2: Scaled model: deformed shape of the initial solution

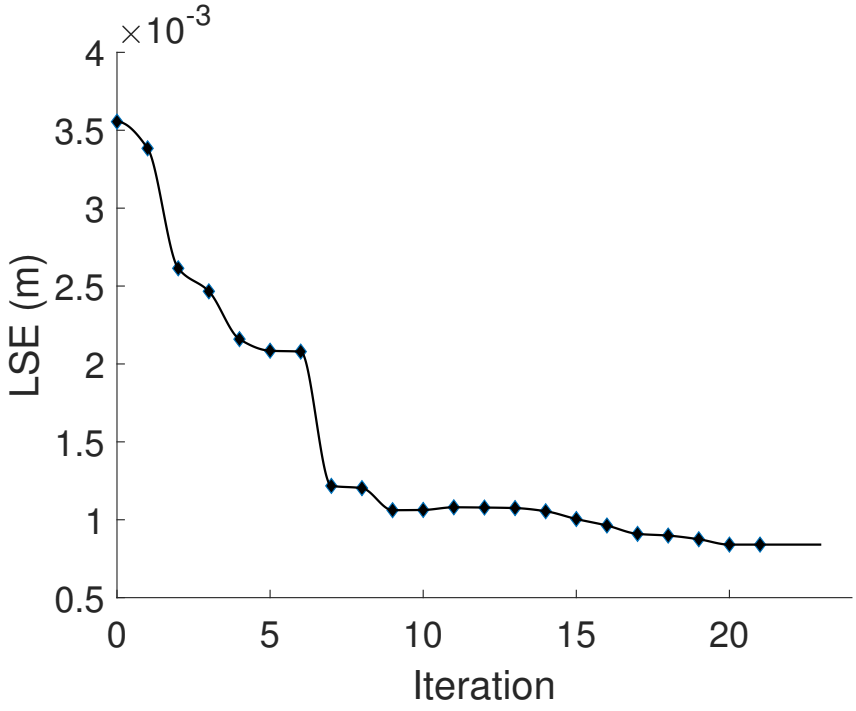

Figure 6.3: Scaled model: LSE vs iteration

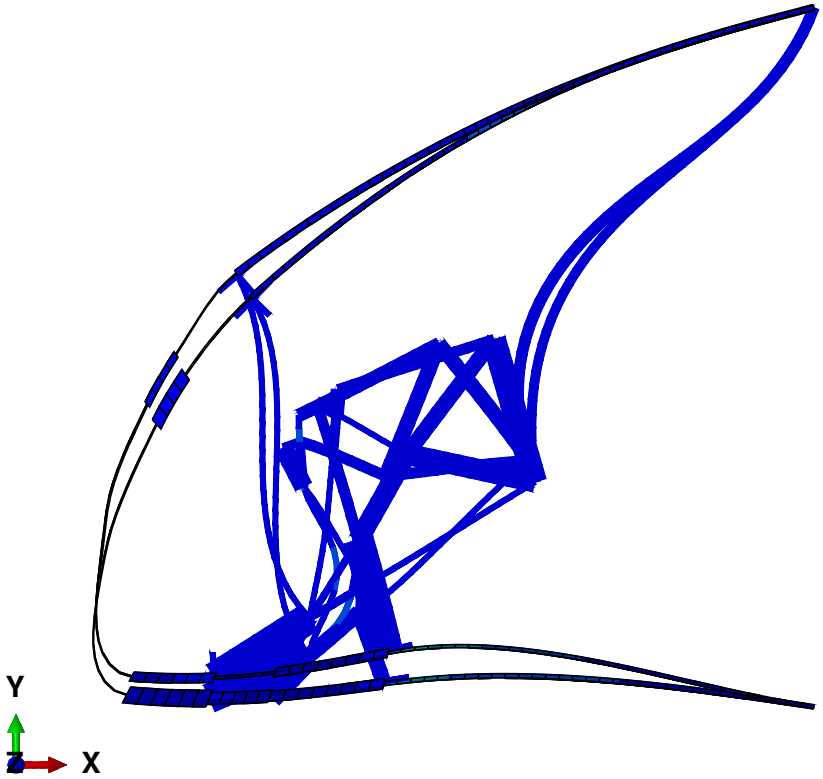

Figure 6.4: Scaled model: initial solution and optimal solution deformed shapes

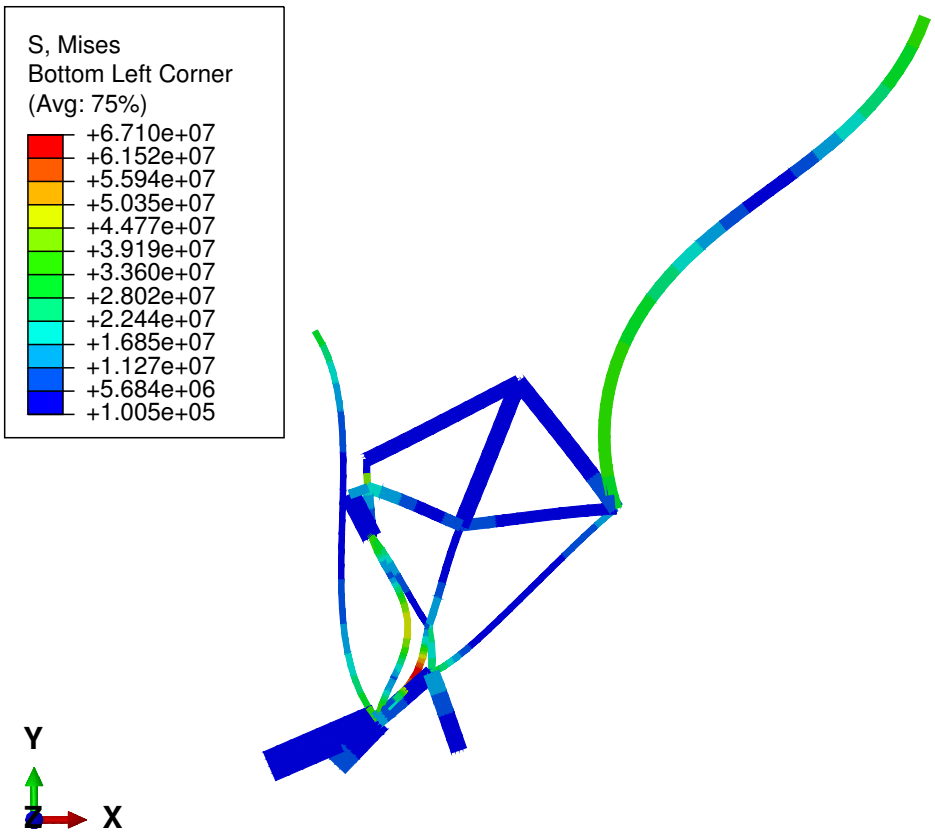

Figure 6.5: Scaled model: Von Mises stress in the rib

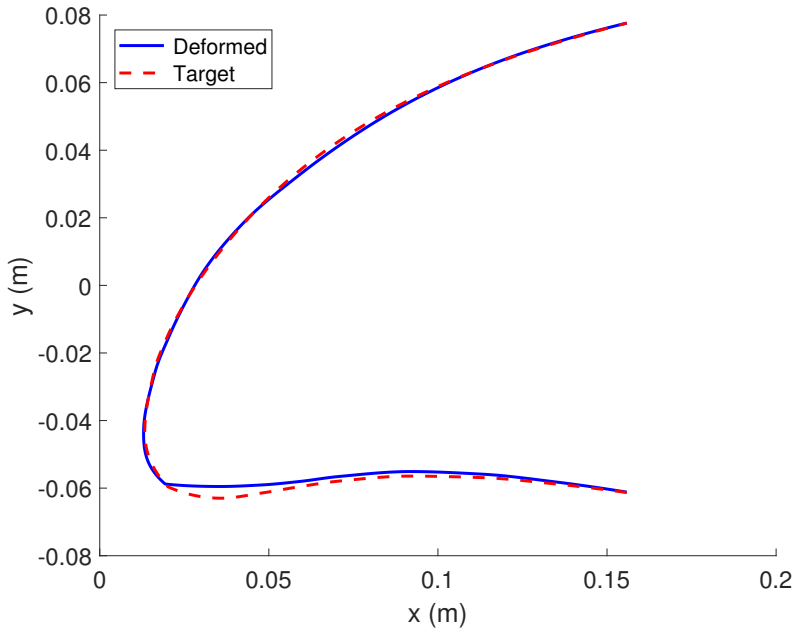

Figure 6.6: Scaled model: optimal solution deformed shape and target shape

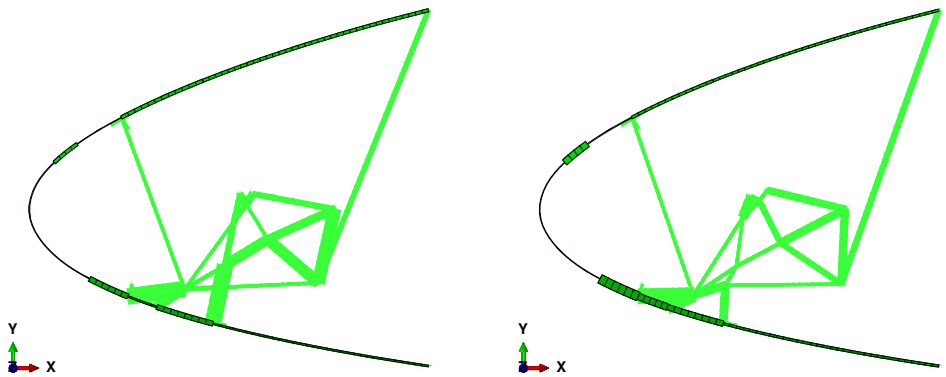

(a) Initial solution (b) Optimal solution

Figure 6.7: Scaled model: thicknesses

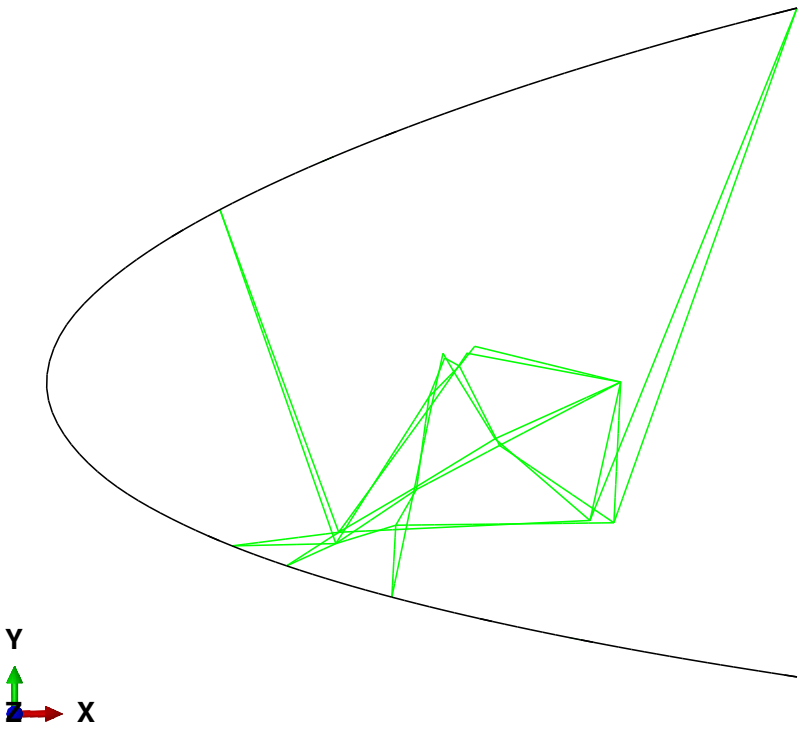

Figure 6.8: Scaled model: initial solution and optimal solution undeformed shapes

The preliminary design of the scaled droop nose has been performed. The results can be considered acceptable, since the optimal deformed shape shows a good enough adherence with the desired target shape, both in terms of droop nose angle and smoothness of the skin surface. This achievement has been allowed by an appropriate distribution of thicknesses, quite different from that of the inital guess solution, whose performance was not very satisfactory. Also a considerable displacement of the internal points with respect to the initial solution contributes to the enhancement of the result.
Once again, the developed gradient-based optimization turns out to be efficient for the improvement of the kinematic requirement of a morphing design problem. Moreover, the optimal solution satisfies the structural requirements related to the stress level in the actuated mechanism and the sufficient stiffness under the aerodynamic loads of a conventional unmorphed configuration.

It must be remembered that the topology of the internal mechanism had been designed as the result of an optimization process related to the full scale geometry of the reference wing. The presented preliminary results prove the validity of the proposed approach, also when dealing with a geometric scaling. In order to further improve the solution, different materials of the compliant mechanism could be taken into account, looking for the one that is able to guarantee the best performances. Moreover, additional constraints can be included in the optimization analysis, depending on specific requirements needed for the wind tunnel tests.
Once an adequate solution in terms of beam elements model has been obtained, shape optimization can be performed in order to finalize the design in view of the manufacturing process.
Finally, manufacturing and testing are mandatory for the assessment of the numerical solution and to study the overall behaviour of the morphing device.

Chapter 7

Conclusions

In this work an optimization procedure to improve the design of morphing devices has been proposed. The field of morphing in which it is located is the active camber morphing, limited to leading and trailing edges. The resulting concept is that of hybrid wings, where the wing-box structure is not affected by morphing while the performance enhancement is due to the leading and trailing edge conformable devices.
The selected approach for the design of the internal structure is based on the distributed compliance concept. Instead of using rigid levers connected by joints, the desired shape change is accomplished by efficiently distributing the flexibility into the structure. This choice should avoid the high stress concentrations encountered in mechanisms based on rigid kinematics.
In order to satisfactorily deal with the design problem, conflicting requirements must be simultaneously fulfilled, therefore specific optimization tools are needed to assist the engineer in the definition of morphing solutions representing an optimal compromise between the expected performances and the imposed restrictions.

An existing optimization procedure based on a two-levels approach is the starting point for the whole work. The first level is an aerodynamic shape optimization aimed at obtaining the best morphing shape able to guarantee the aerodynamic requirements under skin structural constraints. The second level regards the design of an internal compliant structure able to realize, once actuated, the desired target shape previously found.
In this thesis, the existing tools have been included in a wider procedure, whose main purpose is the improvement of the second level solution, from both the perfomance and the structural feasibility points of view. This last point is especially critical, since it has been noted that for droop nose applications a conventional aeronautical aluminium alloy isn't able to

provide, limited to the elastic range, the high strains required to achieve the target aerodynamic shape. Therefore the need of large recoverable strains has suggested to exploit the superelastic behaviour, characteristic of shape memory alloys such as Nitinol.
The use of a different material with respect to that employed in the optimization for the definition of the internal mechanism topology represents the main added value of the proposed procedure. A previously obtained topology can be later readapted including various materials. To do this, a dedicated optimization tool has been specifically developed in this work in order to find the optimal design variables according to the selected material. It is a gradient-based optimization whose variables are the sizing in-plane dimensions of both the mechanism and the skin and also the local position of the internal points of the mechanism. The objective of the optimization analysis is the improvement of the kinematic requirement under structural constraints. The beam elements model of the mechanism used in this analysis is later translated into a more detailed two-dimensional solid elements model in order to assess the stress concentrations at the load path intersections. Then a shape optimization is performed on this model to reduce the stress peaks by modifying the design of the critical regions, bringing to a final solution almost ready for the manufacturing process.

The entire procedure has been applied to the droop nose device of a regional aircraft in the framework of an European project. First of all the internal compliant structure made of isotropic aluminum alloy has been assessed. The results have shown an improvement of the aerodynamic requirement in terms of deformed target shape, however the violation of the structural constraints establishes the unfeasibility of the solution. As already explained, the unsuitability of the traditional aeronautical material for the considered application leads to its replacement with the Nitinol superelastic material. The same procedure has been repeated with the new material giving a satisfactory outcome. Indeed, the exploitation of the stress plateau typical of the superelastic behaviour has allowed the limitation of the maximum stress and as a consequence the achievement of better performances in obtaining the desired morphed shape. Very large strains can appear in the morphing configuration but the superelastic effect assures their recovery. Later, the dependence of the material behaviour on the operative temperature is assessed by comparing the optimal solution at the design temperature and at the selected limit temperatures. The results show good performances also in the off-design conditions.
All these results demonstrate the validity of the procedure according to its

purposes of performance improvement, structural feasibility, versatility of applications.
In addition to the refinement of existing solutions and the possibility to adopt new materials, another potentiality of the procedure concerns the application of available optimal topologies to a different geometric scaling of the wing. This has been practically shown by facing the preliminary design of a 1:3 scaled wind tunnel model of the same droop nose device previously addressed. The results have well confirmed the eligibility of the procedure in dealing with this particular task. The topology has been reduced according to the scaling factor and the starting optimization variables have been selected in a suitable manner. Concerning the material, three dimensional printing technology has been selected for its manufacturing. The results have proved once again the effectiveness of the optimization in the achievement of a solution characterized by valuable performances in terms of deformed shape and also the structural feasibility of the device.

Concerning the future work needed to further improve the proposed procedure, the next required step is the numerical verification of the designed optimal morphing device. This is needed since the last step of the procedure optimizes the internal mechanism only, with boundary conditions inherited from the deformed shape. Therefore it is essential to verify that the final result doesn't exhibit a worsening of the performances. The last step from the numerical point of view is the realization of complete three-dimensional models of the morphing devices and the assessment of their overall behaviour, as well as the interaction with the wing-box structure. This is essential in view of the future integration of morphing devices inside a real wing structure.
Once the numerical design phase is completed, manufacturing and testing are required to establish the real feasibility of the conceived solution. This includes in-depth studies of characterisation for the materials and also the investigation of the related manufacturing technologies. This is especially crucial in case of Nitinol. Due to the dependence of its mechanical characteristics on the alloy composition, the manufacturing process, the thermal treatments and the operative temperatures, a lot of work is required to better understand what is needed to achieve the actual application of Nitinol in the aeronautical structures.
Finally, the acquisition of a strong experience in the design of morphing devices by means of dedicated procedures is fundamental to undertake the difficult certification process of unconventional aircraft.

Bibliography

[1] *Abaqus Scripting User's Guide*. Dassault Systemes Simulia Corporation. 2016.

[2] Ferdinando Auricchio, Robert L. Taylor, and Jacob Lubliner. "Shape-memory alloys: macromodelling and numerical simulations of the superelastic behavior". In: *Computer methods in applied mechanics and engineering* 146.3-4 (1997), pp. 281–312.

[3] S. Barbarino et al. "Airfoil structural morphing based on SMA actuator series: numerical and experimental studies". In: *Journal of Intelligent Material Systems and Structures* 22.10 (2011), pp. 987–1004.

[4] Silvestro Barbarino, Wulf G. Dettmer, and Michael I. Friswell. "Morphing trailing edges with shape memory alloy rods". In: *Proceeding of*. 2010.

[5] Silvestro Barbarino et al. "A review of morphing aircraft". In: *Journal of intelligent material systems and structures* 22.9 (2011), pp. 823–877.

[6] M.C. Biggs. "Constrained minimization using recursive quadratic programming". In: *Towards global optimization* (1975).

[7] Kenneth Bonnema and Stephen Smith. "AFTI/F-111 mission adaptive wing flight research program". In: *4th Flight Test Conference*. 1988, p. 2118.

[8] Jason Bowman et al. "Development of next generation morphing aircraft structures". In: *48th AIAA/ASME/ASCE/AHS/ASC Structures, Structural Dynamics, and Materials Conference*. 2007, p. 1730.

[9] L. Catherine Brinson. "One-dimensional constitutive behavior of shape memory alloys: thermomechanical derivation with non-constant material functions and redefined martensite internal variable". In: *Journal of intelligent material systems and structures* 4.2 (1993), pp. 229–242.

[10] W.J. Buehler and R.C. Wiley. "Nickel-based alloys Technical Report". In: (1965).

[11] A. Chrysochoos, M. Lobel, and O. Maisonneuve. "Thermomechanical coupling of pseudoelastic behavior of CuZnAl and NiTi alloys". In: *Comptes Rendus De L Academie des sciences serie II* 320.5 (1995), pp. 217–223.

[12] Monroe Conner. *F-111 Advanced Fighter Technology Integration.* 2017. URL: `https://www.nasa.gov/centers/dryden/multimedia/imagegallery/F-111AFTI/EC85-33205-07.html`.

[13] Alessandro De Gaspari and Sergio Ricci. "A two-level approach for the optimal design of morphing wings based on compliant structures". In: *Journal of Intelligent Material Systems and Structures* 22.10 (2011), pp. 1091–1111.

[14] Alessandro De Gaspari and Sergio Ricci. "Application of the active camber morphing concept based on compliant structures to a regional aircraft". In: *Industrial and Commercial Applications of Smart Structures Technologies 2014*. Vol. 9059. International Society for Optics and Photonics. 2014, p. 90590D.

[15] Alessandro De Gaspari and Sergio Ricci. "Knowledge-based shape optimization of morphing wing for more efficient aircraft". In: *International Journal of Aerospace Engineering* 2015 (2015).

[16] Kalyanmoy Deb. *Multi-objective optimization using evolutionary algorithms*. Wiley, 2005.

[17] R. Decamp and Richard Hardy. "Mission adaptive wing advanced research concepts". In: *11th Atmospheric Flight Mechanics Conference*. 1984, p. 2088.

[18] Mohammad Elahinia et al. "Fabrication of NiTi through additive manufacturing: A review". In: *Progress in Materials Science* 83 (2016), pp. 630–663.

[19] M. Frecker, Noboru Kikuchi, and S. Kota. "Topology optimization of compliant mechanisms with multiple outputs". In: *Structural Optimization* 17.4 (1999), pp. 269–278.

[20] M.I. Frecker et al. "Topological synthesis of compliant mechanisms using multi-criteria optimization". In: *Journal of Mechanical design* 119.2 (1997), pp. 238–245.

[21] Gian Luca Ghiringhelli, Pierangelo Masarati, and Paolo Mantegazza. "Multibody implementation of finite volume C^0 beams". In: *AIAA journal* 38.1 (2000), pp. 131–138.

[22] Douglas K. Gould. *Final Report, Variable Camber Wing/ Phase I*. Tech. rep. D180-17606-1 (Contract No. N00014-73-C-0244), Research & Engineering Div., Boeing Aerospace Co, 1973.

[23] J.A. Hetrick and S. Kota. "An energy formulation for parametric size and shape optimization of compliant mechanisms". In: *Journal of Mechanical Design* 121.2 (1999), pp. 229–234.

[24] FlexSys Inc. 2018. URL: `https://www.flxsys.com/`.

[25] Markus Kintscher, Hans Peter Monner, and Olaf Heintze. "Experimental testing of a smart leading edge high lift device for commercial transportation aircrafts". In: *27th International Congress of the Aeronautical Sciences (ICAS), Nice, France*. 2010.

[26] Kyle Kirkland. *Chemistry: Notable Research and Discoveries*. Vol. 2. Infobase Publishing, 2010.

[27] Johannes Kirn and Stefan Storm. "Kinematic solution for a highly adaptive droop nose". In: *ICAST2014: 25th international conference on adaptive structures and technologies*. 2014, pp. 6–8.

[28] Sridhar Kota, Peter Flick, and Fayette S. Collier. "Flight Testing of FlexFloilTM Adaptive Compliant Trailing Edge". In: *54th AIAA Aerospace Sciences Meeting*. 2016, p. 0036.

[29] Sridhar Kota et al. "Design of compliant mechanisms: applications to MEMS". In: *Analog integrated circuits and signal processing* 29.1-2 (2001), pp. 7–15.

[30] Sridhar Kota et al. "Mission adaptive compliant wing–design, fabrication and flight test". In: *RTO Applied Vehicle Technology Panel (AVT) Symposium*. 2009.

[31] Brenda M. Kulfan. "Universal parametric geometry representation method". In: *Journal of Aircraft* 45.1 (2008), pp. 142–158.

[32] Daochun Li et al. "A review of modelling and analysis of morphing wings". In: *Progress in Aerospace Sciences* (2018).

[33] Paulo Silva Lobo, João Almeida, and Lús Guerreiro. "Shape memory alloys behaviour: A review". In: *Procedia Engineering* 114 (2015), pp. 776–783.

[34] Kerr-Jia Lu and Sridhar Kota. "An effective method of synthesizing compliant adaptive structures using load path representation". In: *Journal of Intelligent Material Systems and Structures* 16.4 (2005), pp. 307–317.

[35] Kerr-Jia Lu and Sridhar Kota. "Parameterization strategy for optimization of shape morphing compliant mechanisms using load path representation". In: *ASME 2003 International Design Engineering Technical Conferences and Computers and Information in Engineering Conference*. American Society of Mechanical Engineers. 2003, pp. 693–702.

[36] Kerr-Jia Lu and Sridhar Kota. "Topology and dimensional synthesis of compliant mechanisms using discrete optimization". In: *Journal of Mechanical Design* 128.5 (2006), pp. 1080–1091.

[37] Anna-Maria R. McGowan et al. "Perspectives on Highly adaptive or morphing aircraft". In: (2009).

[38] Ashok Midha, Tony W. Norton, and Larry L. Howell. "On the Nomenclature and Classification of Compliant Mechanisms. the Components of Mechanisms". In: (1992).

[39] Giulio Molinari, Andres F. Arrieta, and Paolo Ermanni. "Aerostructural optimization of 3-D adaptive wings with embedded smart actuators". In: *54th AIAA/ASME/ASCE/AHS/ASC Structures, Structural Dynamics, and Materials Conference*. 2013, p. 1528.

[40] H.P. Monner et al. "Design aspects of the adaptive wing—the elastic trailing edge and the local spoiler bump". In: *The Aeronautical Journal* 104.1032 (2000), pp. 89–95.

[41] Gabriel Murray, Farhan Gandhi, and Charles Bakis. "Flexible matrix composite skins for one-dimensional wing morphing". In: *Journal of Intelligent Material Systems and Structures* 21.17 (2010), pp. 1771–1781.

[42] Shinji Nishiwaki et al. "Topology optimization of compliant mechanisms using the homogenization method". In: *International journal for numerical methods in engineering* 42.3 (1998), pp. 535–559.

[43] *Optimization Toolbox User's Guide*. Matlab The Mathworks Inc. 2017.

[44] Kazuhiro Otsuka and Xiabing Ren. "Physical metallurgy of Ti–Ni-based shape memory alloys". In: *Progress in materials science* 50.5 (2005), pp. 511–678.

[45] Larry D. Peel et al. "Development of a simple morphing wing using elastomeric composites as skins and actuators". In: *Journal of Mechanical Design* 131.9 (2009), p. 091003.

[46] M.A. Qidwai and D.C. Lagoudas. "On thermomechanics and transformation surfaces of polycrystalline NiTi shape memory alloy material". In: *International journal of plasticity* 16.10-11 (2000), pp. 1309–1343.

[47] Nuno Rebelo, N. Walker, and H. Foadian. "Simulation of implantable nitinol stents". In: *Abaqus user's conference*. 2001, pp. 1–14.

[48] Benjamin Reedlunn et al. "Tension, compression, and bending of superelastic shape memory alloy tubes". In: *Journal of the Mechanics and Physics of Solids* 63 (2014), pp. 506–537.

[49] Sergio Ricci, Alessandro De Gaspari, and Luca Riccobene. "Design, manufacturing and wind tunnel test of a morphing wing based on compliant structures". In: *24th AIAA/AHS Adaptive Structures Conference*. 2016, p. 1316.

[50] Sergio Ricci et al. "Design of a Leading Edge Morphing Based on Compliant Structures for a Twin-Prop Regional Aircraft". In: *2018 AIAA/AHS Adaptive Structures Conference*. 2018, p. 1063.

[51] Anton Rudenko et al. "Extremely deformable morphing leading edge: Optimization, design and structural testing". In: *Journal of Intelligent Material Systems and Structures* 29.5 (2018), pp. 764–773.

[52] Laxminarayana Saggere and Sridhar Kota. "Static shape control of smart structures using compliant mechanisms". In: *AIAA journal* 37.5 (1999), pp. 572–578.

[53] M. Santer and S. Pellegrino. "Topological optimization of compliant adaptive wing structure". In: *AIAA journal* 47.3 (2009), pp. 523–534.

[54] Ole Sigmund. "On the design of compliant mechanisms using topology optimization". In: *Journal of Structural Mechanics* 25.4 (1997), pp. 493–524.

[55] Clean Sky. 2018. URL: `http://www.cleansky.eu/`.

[56] John W. Smith, Wilton P. Lock, and Gordon A. Payne. "Variable-camber systems integration and operational performance of the AFTI/F-111 mission adaptive wing". In: (1992).

[57] Stephen B. Smith and David W. Nelson. "Determination of the aerodynamic characteristics of the mission adaptive wing". In: *Journal of Aircraft* 27.11 (1990), pp. 950–958.

[58] A.Y.N. Sofla, D.M. Elzey, and H.N.G. Wadley. "Two-way antagonistic shape actuation based on the one-way shape memory effect". In: *Journal of Intelligent Material Systems and Structures* 19.9 (2008), pp. 1017–1027.

[59] J. Szodruch and R. Hilbig. "Variable wing camber for transport aircraft". In: *Progress in Aerospace Sciences* 25.3 (1988), pp. 297–328.

[60] Joachim Szodruch. "The influence of camber variation on the aerodynamics of civil transport aircraft". In: *23rd Aerospace Sciences Meeting*. 1985, p. 353.

[61] C. Thill et al. "Composite corrugated structures for morphing wing skin applications". In: *Smart Materials and Structures* 19.12 (2010), p. 124009.

[62] Srinivas Vasista et al. "Evaluation of a compliant droop-nose morphing wing tip via experimental tests". In: *Journal of Aircraft* 54.2 (2016), pp. 519–534.

[63] Terrence A. Weisshaar. *Morphing aircraft technology-new shapes for aircraft design*. Tech. rep. PURDUE UNIV LAFAYETTE IN, 2006.

[64] R. Wlezien et al. "The aircraft morphing program". In: *39th AIAA/ASME/ASCE/AHS/ASC Structures, Structural Dynamics, and Materials Conference and Exhibit*. 1998, p. 1927.